Advanced Methods for Small Signal Stability Analysis and Control in Modern Power Systems

by

Zhao Yang Dong

B. E.

A thesis submitted in partial fulfillment
of the requirements for the degree of

Doctor of Philosophy

in

Electrical and Information Engineering

The University of Sydney
New South Wales 2006
Australia

August 28, 1998

The author hereby acknowledges that the work embodied in this thesis is the result of original research and has not been submitted for a higher degree to any other University of Institution.

Zhao Yang Dong

Acknowledgments

The work for this thesis was completed in the Dynamical Systems and Control Laboratory of the School of Electrical and Information Engineering at Sydney University.

The author would like to thank Professor David J. Hill for his excellent supervision, and his generous help in providing research funds for my PhD research work.

Many thanks for Dr Yuri V. Makarov for his continuous, patient and excellent associate supervision through out my PhD research.

Also thanks to those who have given me their help and advice throughout my studies. Only a few of them can be mentioned here. Thanks for Dr Dragana H. Popović for her helpful advice on voltage stability and load modeling. Also my thanks to Dr Yash Shrivastava for his informative hints in numerical methods. Special thanks to fellow students in the Laboratory for their helpful discussions and collaborative research work.

Thanks to my family for their love and support all the time during my study.

This work is supported by a Sydney University Electrical Engineering Postgraduate Scholarship.

In Sydney, Australia, August 1998

Zhao Yang Dong

Abstract

This thesis is aimed at exploring issues relating to power system security analysis particularly arising under an open access deregulated environment. Numerical methods and computation algorithms locating the critical security condition points and visualizing the security hyperplane in the parameter space are proposed.

The power industry is undergoing changes leading to restructuring and privatizing in many countries. This restructuring consists in changing the power industry from a regulated and vertically integrated form into regional, competitive and functionally separate entities. This is done with the prospect of increasing efficiency by better management and better usage of existing equipment and lower price of electricity to all types of customers while maintaining a reliable system. As a result of deregulation and restructuring, power suppliers will increasingly try to deliver more energy to customers using existing system facilities, thereby putting the system under heavy stress. Accordingly, many technical and economic issues have arisen, for example, all or some of transient instability, aperiodic and oscillatory instability, insufficient reactive power supply, and even voltage collapse problems may coexist. This situation introduces the requirement for comprehensive analytical tools to assess the system security conditions, as well as to provide optimal control strategies to overcome these problems.

There are computational techniques for assessing the power system stability critical conditions in given loading directions, but it is not enough to just have a few critical points in the parameter space to formulate an optimal control to avoid insecurity. A boundary or hyperplane containing all such critical and subcritical security condition points will provide a comprehensive understanding of the power system operational situation and therefore can be used to provide a global optimal control action to enhance the system security. With the security boundary or hyperplane available, the system operators can place the power system inside the security boundaries, away from instability, and enhance its security in an optimal way.

Based on proper power system modeling, a general method is proposed to locate the power system small signal stability characteristic points, which include load flow feasibility points, aperiodic and oscillatory stability points, minimum and max-

imum damping points. Numerical methods for tracing the power system bifurcation boundaries are proposed to overcome nonconvexity and provide an efficient parameter continuation approach to trace stability boundaries of interest. A Δ-plane method for visualizing the power system load flow feasibility and bifurcation boundaries is proposed. The optimization problem defined by assessing the minimal distance from an operating point to the boundaries is considered. In particular, emphasis is placed on computing all locally minimal and the global minimum distances. Due to the complexity of any power system, traditional optimization techniques sometimes fail to locate the global optimal solutions which are essential to power system security analysis. However, genetic algorithms, due to their robustness and loose problem pre-requisites, are shown to fulfill the task rather satisfactorily.

Finally, a toolbox is described which incorporates all these proposed techniques, and is being developed for power system stability assessment and enhancement analysis.

Contents

Chapter 1

Introduction

1.1 Open Access and Power System Stability

Nowadays, power systems are undergoing dramatic changes leading to deregulation and open access. Under this situation, the traditional centralized power system generation, transmission and distribution decision making processes are being changed into decentralized form with more feedback and modification from the market. Under the deregulated power market, the power producers will tend to send more electricity to the users using existing transmission system facilities.

One of the most important planning and control issues, for competitive and deregulated open-access power grids, is maximization of contractual energy transfers from the power producers to consumers over long electrical distances in increasingly complicated networks (due to more interconnection) [77]. These power transfers are subject to limitations of different sorts including the thermal limits for all transmission facilities, restrictions on voltage levels and frequency, power flow feasibility constraints, and stability boundaries. They determine whether it is possible to accommodate a contractual power transfer in view of significant deviations of load demands and power inputs so characteristic of the open-access power grids [77]. The transmission limits must be defined and taken into account by the pool operator in power flow planning and control as well as by consumers and producers and in their private bilateral and multilateral trades [148].

Power systems are large nonlinear systems with rich dynamics which may lead to instability under certain conditions. With the load demands increasing rapidly, modern power grids are becoming more and more stressed. This has already resulted in many stability problems caused by such reasons as high (real) power transfer and/or insufficient reactive power supply. The voltage collapses which have occurred recently have again drawn much attention to the issue of stability security margins in power systems [2]. The small signal stability margins in particular are highly dependent upon such system features as load flow feasibility boundaries, minimum and maximum damping conditions, saddle node and Hopf bifurcations, and limit induced bifurcations. Unfortunately, it is very difficult to say in advance which of these features will make a decisive contribution to instability. Also it is a feature of stressed systems that traditional problems of angle, voltage and oscillatory instability can coexist so that all need to be considered together. Despite the progress achieved recently, the existing approaches deal with these (physical and mathemat-

ical) features independently - see [42, 107] for example- and additional attempts are needed to get a more comprehensive view on the small-signal stability problem. Before introducing the specific techniques involved, we look at the fundamentals of power system stability issues with which the thesis will deal.

A power system is said to be stable if it has the property that it retains a state of equilibrium under normal operating conditions and regains an acceptable state of equilibrium after being subjected to a disturbance [95]. Small signal (or small disturbance) stability is usually regarded as the ability of the power system to maintain synchronism under small disturbances. Such disturbances occur continually on the system because of small variations in loads and generation. The disturbances are considered sufficiently small for linearization of system equations to be permissible for the purpose of analysis. Physically, instability is usually thought of in two forms:

- Steady increase in generator rotor angle and/or decrease of voltages;
- Oscillations of increasing amplitude due to lack of sufficient damping.

In dynamical terms, instability is traditionally viewed in terms of angles and frequency. Small signal analysis using linear techniques, eigenvalue analysis, provides valuable information about the inherent dynamic characteristics of the power system and assists in its design. In terms of eigenvalue analysis, the system is said to be stable if all eigenvalues of the system Jacobian have negative real parts. Otherwise, the system may be expected to undergo either instability of different kinds or oscillatory behavior.

Since small signal stability is based on a linearized model of the system around its equilibrium operation points, formulation of the problem is very important. The formulation of the state equations for small signal analysis involves the development of linearized equations about an operating point and elimination of all variables other than the state variables. The need to allow for the representation of extensive transmission networks, loads, a variety of excitation systems and prime mover models, HVDC links, and Static VAR Compensators (SVCs) requires a systematic procedure for treating the wide range of devices [95]. Modeling of these power system devices can be found in [8, 9, 38, 78, 120].

Among all small signal stability issues, voltage stability has been of particular interest lately. Voltage stability is the ability of a power system to maintain steady

acceptable voltages at all buses in the system under normal operating conditions and after being subjected to a disturbance. Also, voltage stability has been defined as the ability of a system to maintain voltage such that load demand increase is met by increase in power [31, 76, 115]. Traditional theory implies that a system is voltage stable if voltage sensitivity is positive for every bus voltage. Small signal (or small-disturbance) voltage stability is concerned with a system's voltage dynamics following small perturbations.

The aim of this thesis is to explore the techniques capable of finding the region in which the system is small signal stable allowing simultaneously for all kinds of (small signal) instability. This region is used to define the so called system security boundaries which allow for appropriate operating margins.

The tendency to higher system stress increases the probability of problems caused by small signal instability. Advanced techniques, which are aimed at solving these problems, are required, so as to ensure maximum profits for the utilities by supplying more electricity while keeping the system reasonably stable.

1.2 State of Art of Power System Stability and Numerical Methods

In this section, we give a brief overview of some existing approaches dealing with power system small signal stability problems. This is useful background for Chapters 3, 4 and 5.

1.2.1 Terms and Definitions

We first clarify the terms and definitions in the area of power system stability. As mentioned above, small signal stability belongs to the family of power system stability properties, which generally refer to the ability of a power system to remain in a state of equilibrium under normal operating conditions, and to regain an acceptable state of equilibrium after a disturbance [95]. There are many definitions in this area; at the time of writing, there is an effort to achieve standardization by IEEE and CIGRE. For purposes of this thesis, the book by Kundur [95] gives a

complete presentation. According to this reference, small signal stability (or small disturbance stability) is the ability of the power system to maintain synchronism under small disturbances. The power system small signal stability problem is handled by linearized analysis because the disturbance is small enough. Although, it is commonly in terms of angle stability, here we use it in the general sense of any relevant variables.

In papers by Hill et al. [64, 65] it is emphasized that power system stability refers to both static and dynamic concepts, and the stability issue generally includes system, angle and voltage stability respectively. The proposals on stability were made as follows:

- Static properties, where algebraic models and quasi-static disturbances are studied, be defined separately;
- Steady state stability refers to stability of a power system in steady state, except for the influence of small disturbances which may be slow or random;
- Stability as a general mathematical term refers to where differential equations (and possible algebraic equations) and time-varying disturbances are studied;

The authors of [64, 65] indicated that more attention should be paid to broader concepts of system stability than specific definitions for angle and voltage stability. Also, in many respects, angle stability and voltage stability are used more as a time-scale decoupling than a variable decoupling. Angle stability is normally considered as a short term phenomenon, while voltage stability is a long term one because slower devices are involved. In situations where no obvious angle/voltage decoupling is involved, it would be more appropriate to talk of system stability in terms of short term or long term behavior [65].

From a static point of view, voltages are described in terms of their level and sensitivity. The voltages are *viable* if they all lie in their accepted operating ranges. Another important concept is *voltage regularity* which demands that the bus voltages have appropriate sensitivity to reactive demand. These voltage sensitivity $\frac{dV}{dQ_d}$ is acceptable if $0 > \frac{dV}{dQ_d} \geq -R$, where $R > 0$. Assuming independent consistent power loads, this sensitivity becomes infinite when the operating point approaches the so-called Point of Collapse (PoC) [25]. More specifically, the definition says: a

power system is at a *locally voltage regular* operating point if (i) for any PQ bus, $\Delta Q_j > 0$ gives $\Delta V_j > 0$; ii) for any PV bus, $\Delta E_j > 0$ gives $\Delta Q_j > 0$. Moreover, the system is at a *voltage regular operating point* if, in addition to being locally regular, the system satisfies $\Delta V \leq 0$ for any $\Delta Q \leq 0$ and any $\Delta E \leq 0$ gives $\Delta V \leq 0$.

While considering dynamic concepts where the variation is fast relative to the system dynamics, the quasi-static assumption is not valid any more. Several important definitions are given below [64, 65]:

- A power system at a given operating state, and subject to a given large disturbance is *large disturbance stable* if the system approaches post-disturbance equilibrium values. Note that acceptable behavior in practice could also include holding synchronism for several swings until stabilizer damping arrives and/or a maximum voltage dip criterion is reached.
- A power system at a given operating state is *small disturbance voltage stable* if, following any small disturbance, its voltages are identical or close to the pre-disturbance values.
- A power system undergoes *voltage collapse* if, at a given operating point and subject to a given disturbance, the voltage is unstable or the post-disturbance equilibrium values are non-viable.

These definitions require precise mathematical interpretation before embarking on analysis.

According to Kundur [95], power system stability can be categorized into the following families:

- Angle stability, which is the ability to maintain synchronism and torque balance of synchronous machines in the power system.
  - Small signal stability
    - Non-oscillatory Instability
    - Oscillatory Instability
  - Transient Stability, which is the ability of power system to maintain synchronism when subjected to a large disturbance. It will result in

large excursion of generator angle and is affected by nonlinear power-angle relationship. The period of interest is limited up to 10 seconds.

- Voltage stability, which is the ability of the power system to maintain steady acceptable voltage at all buses in the system under normal operating conditions and after disturbances. Or in other words, the system voltages approach post-disturbance equilibrium values both at a given operating condition and after being subjected to given disturbances [64]. It is mainly a problem of keeping reactive power balance, even though active power balance is also important in this case. Industrial practices to judge voltage stability include analysis of Q-V curves [95, 114, 115] and modal analysis [53].

  - Large disturbance voltage stability, which is caused by large disturbances including system faults, loss of generation, circuit contingencies, system switching events, dynamics of ULTC, loads, etc. It requires coordination of protection and controls, and usually lasts about several seconds to several minutes. Long term dynamic simulation is necessary for analysis.
  - Small disturbance voltage stability indicates the situation that, for a power system, the system voltages recover to the value close to or the same as the original value before disturbance at a given operating condition [64]. This kind of instability is usually caused by slow changes in system loads. Static analysis techniques are used for analytical purposes.

- Mid-term stability, which is caused by severe upsets, large voltage and frequency excursions, and involves fast and slow dynamics. The period of time-of-interest usually lasts up to several minutes.

- Long-term stability, which is also a result of severe upsets and large voltage and frequency excursions. It involves slow dynamics, and will last up to tens of minutes for study purposes.

- Voltage Collapse, stands for the situation that for a given operating point, the system voltage is unstable or the post disturbance values are nonviable after a given disturbance [64].

There are also many other concepts concerning the classification of power system stability problems [39].

1.2.2 Numerical Methods for Power System Stability Analysis

Now, let us take a look at the general techniques for analyzing power system stability problems.

Static and Dynamic Point of View of Stability

Based on the definitions of the stability problem, there are two approaches, namely, the static approach and dynamic approach. To start with numerical methods dealing with these stability problems, it is necessary to give a general model for the power system including all its dynamics as well as algebraic constraints. Generally, a power system with all its static and dynamic aspects can be described by the following form of differential and algebraic equations (DAEs):

$$\dot{x} = f(x, z, u, p) \tag{1.1}$$

$$0 = g(x, z, u, p) \tag{1.2}$$

where x is the vector of state variables such as machine angles, dynamic load variables; z is the vector of remaining system variables without dynamic consideration; u is vector of system controls, and p is the vector of system parameters. In the sequel, we sometimes use λ to denote a parameter which may be varied slowly. (The assumption is that this variation is slow enough such that the system behavior can retain its equilibrium conditions.) In the following analysis, variable λ may be chosen as a bifurcation variable with the meaning that when λ slowly approaches some specific value, the system undergoes dramatic changes in its states, corresponding to the occurrence of bifurcations. As a special case, where there are no algebraic equations or controls to be selected, the above system can be simplified into the form:

$$\dot{x} = f(x, \lambda) \tag{1.3}$$

$$0 = g(x, \lambda) \tag{1.4}$$

Usually, the differential equations describe the system dynamics and the algebraic equations represent the system load flow equations.

Static stability deals with static properties corresponding to properties of angle and voltage changes for certain small parametric changes. Specific illustrations are the $Q-V$ and $E-Q$ variation relationships given in the definitions set by Hill et al. [65]. A comprehensive approach for static stability analysis can be developed in load flow studies by evaluating Jacobian sensitivities [68, 133]. To study this property in detail, the general form load flow equations are given as:

$$f(\delta, V; p) = 0 \qquad \text{active power balance} \tag{1.5}$$

$$g(\delta, V; p) = 0 \qquad \text{reactive power balance} \tag{1.6}$$

where δ and V stand for dependent angles and voltages, and p consists of the variable parameters, e.g. $p = (E, P, Q)$ [E is the vector of controllable voltages.] The load flow Jacobian is:

$$J = \begin{bmatrix} F_\delta & F_v \\ G_\delta & G_v \end{bmatrix} \tag{1.7}$$

where F_δ denotes the derivative $\frac{\partial f}{\partial \delta}$ and similarly for the other terms F_v, G_δ and G_v. The following form can be easily derived [68]:

$$G_v^* dV = dQ - G_\delta F_\delta^{-1} dP - G_l^* dE \tag{1.8}$$

where * denotes the Schur complement:

$$G_v^* = G_V - G_\delta F_\delta^{-1} F_v G_l^* = G_l - G_\delta F_\delta^{-1} F_l \tag{1.9}$$

When considering the angle and voltage stability together, regularity should be checked with entries of J^{-1}. There are two major concepts regarding the stability, i.e. the *Points of Maximum Loadability (PML)*, where dV/DQ or dV/dP becomes infinite; and *Points of Collapse (PoC)* where dV_j/dp_k becomes unbounded as Δp_k tends to zero. Analytical study of PoC and PML corresponds to the singularity of load flow Jacobians. PoC and PML are two different concepts, however they could refer to the same point depending on the power flow and steady-state models used. PoC was first proposed by F. Alvarado and was first associated with another important stability concept, saddle node bifurcation point, by C.A. Canizares. It can be shown that, if $detF_a \neq 0$, since $detJ = detF_\delta detG_v^*$, then $detJ = 0$ corresponds to $detG_v^* = 0$. This approach measures proximity to the PoC as the system stability limit. However, if $detG_v \neq 0$, since $detJ = detG_v detF_\delta^*$, then singularity

of J corresponds to the singularity of F_δ^*, which indicates a break down in active power and angle stability.

Dynamic analysis of power system stability considers time-varying disturbances where the variation is fast relative to the system dynamics. In such cases, the quasi-static assumption is no longer valid. Small and large disturbance stability (steady-state or transient stability) are the major cases of dynamic analysis. Definitions of small and large disturbance stability given above are used. As compared with the analytical static view, the dynamic view of system voltage stability, especially allowing for voltage collapse, also includes the possibility that voltages may not stay near equilibrium values. Analytically, the voltage collapse analysis involves two steps, including both static and dynamic point of views [65]:
(1). Determine the post-disturbance equilibrium by power flow calculations. If none exist or they are voltage non-viable, then collapse has occurred [traditional static view].
(2). Determine the region of attraction for any voltage viable equilibria. If the disturbed state lies in this region, then collapse is avoided. Otherwise, collapse may occur [dynamic part of the definition].
In step (2), because of the conservative nature of the nonlinear analysis, the stability regions are only estimated. So, simulation is needed to check if collapse is to occur if the disturbed state lies outside the estimated region.

The key idea from these two points of view is that a system may be well behaved in a static sense, but unstable in a dynamic sense, and vice versa.

Numerical Methods

There are many numerical methods for power system stability analysis based on the concepts introduced above. Basically, a power system when subjected to a slow parametric variation may undergo an instability caused by a bifurcation (including reaching the PoC). For small signal stability analysis, the system equation is first linearized and then studied for its stability property. It is convenient to change the general model of a power system into the form below:

$$\dot{x} = f(x, z, \lambda) \tag{1.10}$$

$$0 = g(x, z, \lambda) \tag{1.11}$$

The system can be linearized around an equilibrium point which is the solution of the system: $0 = f(x, z, \lambda)$ and $0 = g(x, z, \lambda)$. The linearized system takes the form:

$$\Delta \dot{x} = F_x \Delta x + F_z \Delta z \tag{1.12}$$

$$0 = G_x \Delta x + G_z \Delta z \tag{1.13}$$

Eigenvalues of the linearized system provide the time domain characteristics of a system mode. The following eigenvalue characteristics provide the analytical basis for this approach:

- Real eigenvalues represent non-oscillatory modes; a negative one corresponds to decaying mode, while a positive one relates to aperiodic instability;
- Complex eigenvalues are associated with system oscillatory modes; the pair of complex eigenvalues with negative real parts indicate a decreasing oscillatory behavior, and those with positive real parts result in an increasing oscillatory behavior.

Other eigenproperties such as eigenvectors and participation factors also provide useful information about the system stability analysis [7, 11, 12, 13, 17, 18, 95, 111, 136, 146]. See *Appendices* for detailed eigenanalysis techniques. Upon obtaining the linearized system equations, and therefore the Jacobian or state matrix, eigenanalysis techniques can be used to explore the small signal stability of the system under consideration. In particular, it is valuable to study movement of modes as parameters λ vary.

Numerical methods revealing the system stability properties are aimed to locate conditions where eigenvalues of the system Jacobian correspond to special stability issues. These numerical methods can be applied to find PoC points, aperiodic and oscillatory instability points.

The relationship between system stability and eigenvalues as well as numerical methods needed will be summarized in the following chapters. Here only a brief general description is given, as follows:

(1) PoC calculation is aimed at locating the points where the power flow Jacobian is singular by the following equation [21, 25, 26, 142]

$$f(x, \lambda) \;=\; 0 \tag{1.14}$$

$$g(x,\lambda) = 0 \quad (1.15)$$

$$J_{lf}^{t}(x,\lambda)l = 0 \quad (1.16)$$

$$||l|| = 1 \quad (1.17)$$

where l is the left eigenvector corresponding to a zero eigenvalue of the load flow Jacobian matrix, J_{lf}. The first two equations ensure that the solution points are equilibrium points. The last equation merely ensures a nontrivial solution of (1.16).

(2) Aperiodic and oscillatory stability condition (saddle node and Hopf bifurcation, see definitions in the following chapter) calculation: [21, 25, 26, 42, 142]

$$f(x,\lambda) = 0 \quad (1.18)$$

$$g(x,\lambda) = 0 \quad (1.19)$$

$$\tilde{J}^{t}(x,\lambda)l' + \omega l'' = 0 \quad (1.20)$$

$$\tilde{J}^{t}(x,\lambda)l'' - \omega l' = 0 \quad (1.21)$$

$$||l|| = 1 \quad (1.22)$$

where ω is the imaginary part of a system eigenvalue; l' and l'' are real and imaginary parts of the corresponding left eigenvector l;$\tilde{J}$ stands for the state matrix obtained from the linearized model. Note that aperiodic instability, or saddle node bifurcation happens when the imaginary part of the critical eigenvalue is zero, i.e., $\omega = 0$; oscillatory instability or Hopf bifurcation happens when $\omega \neq 0$.

These formulations are useful for determining load flow feasibility and various stability boundaries and their dependence on parameters λ.

1.3 Aims of The Thesis

This thesis is aimed at giving a comprehensive framework to analyze small signal stability conditions together with numerical methods for special tasks.

As seen from Section 1.2 of this chapter, there are already many approaches to the small signal stability issue. However, each of these is generally focused on one aspect of the stability problem.

It would be helpful to have a comprehensive approach, which could consider such properties of the power system as saddle node and Hopf bifurcations, load flow feasi-

bility boundaries, minimum and maximum damping conditions, singularity induced bifurcations, and limit induced bifurcations within one framework.

Moreover, besides locating particular critical instability conditions, visualization of the hypersurface containing all such instability condition points will provide more understanding of the system security and help develop optimal control strategies to enhance the power system secure operation. We aim to develop techniques to allow more flexible viewing of stability surfaces.

These numerical methods are to locate the stability conditions not only in a given parametric variation direction, but also those conditions from different view points in the whole parameter space, so as to enable visualization of the security boundaries defined by different stability related characteristic points.

Special techniques dealing with computational difficulties will be also considered. One idea is to exploit the special structure of power system equations in order to reduce computation. Another to be attempted is use of genetic algorithms to carry out the complex optimization.

1.4 Contributions and Structure of the Thesis

The techniques proposed in the thesis are based on modal analysis, optimization techniques, knowledge of bifurcations, quadratic programming approaches, and other basic knowledge on power system computation and control, such as load flow computation and power system modeling. The major contributions of the thesis can be categorized as:

- High order numerical method and eigenvalue sensitivity approach to locate the critical stability conditions;
- Techniques for tracing the aperiodic and oscillatory stability boundaries;
- A Δ-plane method to locate and visualize the load flow feasibility boundaries in a chosen cut plane of the parameter space;
- A general method capable of locating all small signal stability characteristic points in one parametric variation direction;

- Genetic algorithms improvement and their application in small signal stability analysis, including location of the critical as well as subcritical stability characteristic points, and searching for optimal system planning results.

- A software toolbox which incorporates these techniques into a modern security assessment package.

The structure of the thesis is as follows:

Chapter 1. Introduction of power system stability, which includes terms and definitions of stability problems, and basic numerical approaches to solve such problems. Also aims, contributions, and structure of thesis is given in this chapter.

Chapter 2. Power system modeling and bifurcation analysis are reviewed. This chapter forms the foundation for further analysis. The power system models used through out the thesis and several important stability related bifurcations are discussed.

Chapter 3. Methods to reveal the critical stability conditions of power systems are addressed. These methods include a review of traditional approaches, initial value approximation techniques, and a comprehensive general method which analyses saddle node, Hopf bifurcations, load flow feasibility boundaries, minimum and maximum damping points within the one formulation.

Chapter 4. Techniques for the visualization of the critical conditions within parameter spaces are studied. A review of current state of art approaches as well as a new Δ-plane method for visualizing the stability boundaries in a chosen parameter space are addressed.

Chapter 5. Genetic algorithms are proposed to overcome solution difficulties associated with most traditional optimization and searching techniques. Their novel application in small signal stability as well as system planning are also proposed.

Chapter 6. A computer software package - power system small signal stability toolbox - is discussed. This toolbox incorporates all the algorithms and techniques involved from the thesis, and is aimed to assess as well as provide information for optimal global control of the power system for better system security.

Chapter 7. This chapter gives concluding remarks on the thesis, as well as prospects for further development.

Appendices. Matrix analysis fundamentals, numerical methods in optimization, and proof of quadratic system properties are given in Appendices A-C.

The results of this thesis have been partially presented already in publications. A list of publications arising from the thesis is given in Appendix D at the end of the thesis.

Chapter 2

Power System Modeling and Bifurcation Analysis

2.1 Introduction

Power system small signal stability analysis relies heavily on proper modeling techniques. Power systems are large interconnected systems, which consist of generation units, transmission grids, distribution systems, and consumption units. There are numerous dynamics associated with the system which may affect the system small signal stability and other kinds of stability problems. The small signal stability technique analyzes the system stability by studying the linearized models of the system dynamics. Load flow computation, state matrix and/or system Jacobian formulation and eigenanalysis are among the common tasks required by small signal stability studies. The traditional aim is to investigate system electro-mechanical oscillatory behavior.

Different approaches to system modeling lead to different analytical results and accuracy. Improper models may result in over-estimated stability margins, which can be disastrous to system operation control. Redundant models will increase computation costs largely, and could be impractical for industrial application. To study the problem of modeling, all components of the power system should be considered for their performance. Based on the stability study requirements, different modeling schemes for the same device will have to be used. For example, three kinds of models of a system/device are necessary to study the power system long term, midterm and transient stabilities.

The power system is modeled as a set of nonlinear differential and algebraic equations. For small signal stability analysis, all the models developed will be linearized around equilibrium points. Under such conditions, the system nonlinearity is being considered as close to linear. The linearized model also include linearized load models for interactive studies.

Traditional system modeling is based on generators and their controls, as well as the transmission system components. Load modeling has received more and more attention for stability analysis purposes. In this chapter, these detailed modeling issues will be discussed. Also a review of the bifurcation analysis interpretation of stability problems will be given.

2.2 Generator Modeling

A power system is composed of generators, generator control systems including excitation control, automatic voltage regulators, PSS, transmission lines, transformers, HVDC links, reactive power compensate devices, newly developed FACTS devices, and loads of different kinds. Every piece of equipment has its own dynamic properties, that may need to be modeled for a stability study. In order to study small signal stability, the generator system modeling is firstly reviewed.

2.2.1 Synchronous Machine Model

Generally, the well established Parks model for the synchronous machine is used in system analysis. However, some modifications of the original Park's model can be employed to simplify the model for stability analysis.

Throughout this thesis, the following two types of generator models are used, i.e., one-axis and two-axis model [6, 121, 129]. Equations of the one axis synchronous machine model, where the damping coil and equation entries of $\dot{\lambda}_d$ and $\dot{\lambda}_q$ are ignored, become

$$\begin{aligned} \tau'_{do}\dot{E}'_q &= E_{FD} - [E'_q - (x_d - x'_d)I_d && (2.1)\\ E'_d &= V_d + x'_q I_q + rI_d && (2.2)\\ \tau\dot{\omega} &= T_M - [E'_q I_q - (L_q - L'_d)I_d I_q] - D\omega && (2.3)\\ \dot{\delta} &= \omega - 1 && (2.4) \end{aligned}$$

For analysis of large scale power systems, often only the angle-speed equation (2.4), voltage/potential equations, and the swing equation (2.3) are considered.

Equations of the two axis synchronous machine model, where the effects of transient resistance are considered and the sub-transient effects are neglected, has the form

$$\begin{aligned} \tau'_{qo}\dot{E}'_d &= -E'_d - (x_q - x'_q)I_q && (2.5)\\ E'_d &= E_d + (x_q - x'_q)I_q && (2.6)\\ \tau'_{do}\dot{E}'_q &= E_{FD} - E'_q + (x_d - x'_d)I_d && (2.7)\\ \tau\dot{\omega} &= T_M - D\omega - [I_d E'_d + I_q E'_q - (L'_q - L'_d)I_d I_q] && (2.8)\\ \dot{\delta} &= \omega - 1 && (2.9) \end{aligned}$$

The notations for the above equations are

E_d, E_q - EMF of the d-axis and q-axis respectively, p.u.

E'_d, E'_q - transient EMF of the d-axis and q-axis respectively, p.u.

E_{FD} - equivalent EMF in the excitation coil, p.u.

V_d - d-axis voltage, p.u.

δ - generator power angle, rad.

ω - generator rotor speed, rad./s.

I_d, I_q - d-axis and q-axis current respectively, p.u.

r - resistance, p.u.

x_d, x_q - d-axis and q-axis synchronous reactance respectively, p.u.

x'_d, x'_q - d-axis and q-axis transient reactance respectively, p.u.

x''_q - q-axis subtransient reactance, p.u.

L_q - q-axis synchronous inductance, p.u.

L'_d, L'_q - d-axis and q-axis synchronous inductance respectively, p.u.

$\tau = 2H/\omega_s$, where H is inertia constant, p.u. and ω_s is the synchronous generator rotor speed in rad/s. τ'_{do}, τ'_{qo} - d-axis and q-axis open circuit time constant

D - damping coefficient, p.u.

T_M - mechanical torque, p.u.

The equivalent circuit for the two axis machine model is given in Figure 2.1 [6].

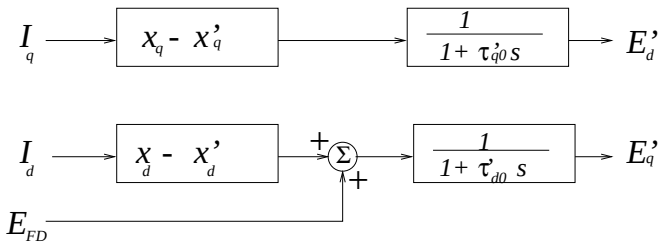

Figure 2.1: Two-Axis Model of the Synchronous Machine

2.2.2 Excitation System Modeling

The basic model of an exciter is provided by the state variable chosen as the exciter output voltage or generator field EMF, E_{FD} in the equation [131],

$$T_E \frac{dE_{FD}}{dt} = -(K_E + S_E(E_{FD}))E_{FD} + V_R \tag{2.10}$$

where the value of exciter constant related to self-excited field, K_E depends on the type of DC generator used, $S_E(E_{FD})$ is the saturation function, and V_R is the scaled voltage regulator output.

The steady state modeling given by [6] extends the above model to include both dynamics of E_{FD}, V_R, and some internal state variables of the exciter. A simplified linear model of a synchronous machine with excitation system is given as well.

Other excitation system models for large scale power system stability studies can be found in [73]. In general, the whole excitation control system includes:

- Power System Stabilizer
- Excitation system stabilizer
- (Automatic) Voltage Regulator
- Terminal voltage transducer and load compensator

The whole control system contributes to enhancement of generator and power system from the point of view of excitation control. Models of these components will be discussed in the following sections as needed.

2.2.3 PSS and AVR Models

Conventionally, the AVR is a first order lag controller and the PSS is a fixed structure controller with a gain in series with lead-lag networks. A PSS generates stabilizing signals to modulate the reference of the AVR [97]. For control study purposes, the PSS and AVR model transfer functions are given as: $K_{AVR}(s) = \frac{K_v}{T_v s+1}$ and $K_{PSS}(s) = K_s(\frac{T_1 s+1}{T_2 s+1})^n$.

A simple excitation system with a voltage regulator model represented by an amplifier and feedback rate dynamics is given by [72, 131] as,

$$\begin{aligned} T_F\frac{dR_f}{dt} &= -R_f + \frac{K_F}{T_F}E_{FD} \\ T_A\frac{dV_R}{dt} &= -V_R + K_A V_{in} \\ &= -V_R + K_A R_f - \frac{K_A K_F}{T_F}E_{FD} + K_A(V_{ref} - V_t) \\ V_R^{min} &\leq V_R \leq V_R^{max} \end{aligned}$$

where R_f is rate of feedback, V_{in} is the amplifier input voltage, T_A is the amplifier time constant, K_A is the amplifier gain, V_{ref} is the voltage regulator reference voltage (determined to satisfy initial conditions), T_F is the stabilizer time constant, and V_R^{min}, V_R^{max} is voltage regulator output voltage lower and upper limit respectively.

Several types of AVR-PSS system, and a new co-ordinated AVR-PSS type design method are given in [97].

The basic models for AVR and PSS can be found in the literature, [6, 14, 15, 73, 95, 123, 131]. Detailed nomenclature relating to excitation systems can be found in [73].

2.3 Load Modeling

Power system loads play a large role in power system dynamics and stability behavior. Many serious power system instability problem like voltage collapses are caused by load behavior [112]. Even in steady-state, load dynamic characteristics can have great impact on system behavior. For example, a disturbance such as starting an induction motor can introduce significant voltage drop locally and even cause protection equipment to operate to prevent system instability. In such operation, the induction motor dynamics should be added to the usual ones for the system, and should be considered for small signal stability analysis. There are many studies concerning the influence of motor dynamics on system stability [20, 33, 82, 118]. It is shown for instance that system damping is highly dependent on load parameters.

For study of the stability problem, good load modeling is a key issue; poorly modeled load dynamics will give misleading information for system analysis and operation,

but it is difficult in practice to get adequate data. There are many well established modeling methods and relatively new methods have been given in the literature [20, 22, 33, 64, 74, 82, 117, 118, 130, 131]. There are generally two approaches to describe the load models, i.e., input-output modeling and state modeling [64]. Depending on the recovery characteristics of the load after a voltage step, specific load models are the exponential load model [64, 68] or an adaptive recovery load model [149].

The concept of generic load modeling was introduced in [64] as a general purpose nonlinear dynamic structure which represents the aggregate effect of all loads connected to the bus. Traditionally, the load is modeled in a static model as functions of bus voltages and frequency. This static load model has been used for years for load flow calculations. To capture the dynamics needed for stability analysis, especially in small signal stability study, more detailed load models describing not only the static behavior but the transient behavior of load were put forward. These kind of models naturally are called dynamic load models.

There are two ways to obtain aggregation in load models. One is to survey the customer loads in a detailed load model, including the relevant parts of the network and carry out system reduction. Then, a simple load model can be chosen so that it has similar load characteristics to the detailed load model. Another approach is to choose a load model structure and identify its parameters from measurements.

2.3.1 Static Load Modeling

Static load models are expressed as algebraic functions of the bus voltage and frequency. The traditionally used power system static load model consists of an exponential form like $P = P_0(\frac{V}{V_0})^\alpha$ and $Q = Q_0(\frac{V}{V_0})^\beta$ for real and reactive load respectively. Depending on the values of α and β, the model represents constant power (α or $\beta = 0$), constant current (α or $\beta = 1$), and constant impedance (α or $\beta = 2$) respectively. The value usually taken for α is in the range of 0.5 to 1.8, and the range for β is usually between 1.5 and 6 [95]. Another widely used static load model is the polynomial model as given below:

$$P = P_0[p_1(\frac{V}{V_0})^2 + p_2\frac{V}{V_0} + p_3]$$

$$Q = Q_0[q_1(\frac{V}{V_0})^2 + q_2\frac{V}{V_0}|q_3]$$

where included in this model are constant impedance, constant current and constant power components [95].

However, besides bus voltages, system frequency variation is also considered in more general static load modeling. As a function of bus voltage and frequency, the model takes the general form:

$$P = F_p(P, V, \Delta f) \tag{2.11}$$

$$Q = F_q(Q, V, \Delta f) \tag{2.12}$$

where P and Q are power system real and reactive load powers, V and f are bus voltage and frequency respectively, and Δ denotes a small variation of associated variables.

The static load models listed above may produce computational problems at low voltage level. In some computer software analytical packages, the static load model at certain low voltages will be treated as constant impedance.

2.3.2 Dynamic Load Modeling

In power system stability analysis, it is necessary to pay attention to the response of load components. Load dynamic aspects should be considered for stability analysis of today's power systems in cases of voltage stability, inter-area oscillations, long-term stability analysis, and small signal stability analysis. A considerable portion of the load dynamics usually comes from derivatives of bus voltage, load powers and system frequency. Some dynamics also take into consideration the system frequency variations. The source of these dynamics come from induction motor start-up/speed modulations, extinction and restart of discharge lamps under certain conditions, operation of power system control devices like protective relays, tap change transformers, flexible AC transmission devices. A composite load model representation is shown in Figure 2.2.

Consider the power system load response after a voltage disturbance; after the system voltage returns to a stable post disturbance level, the magnitude of the particular load power will recover to a new state following different recovery characteristic curves. The general load response is given in Figure 2.3 [64]. from which

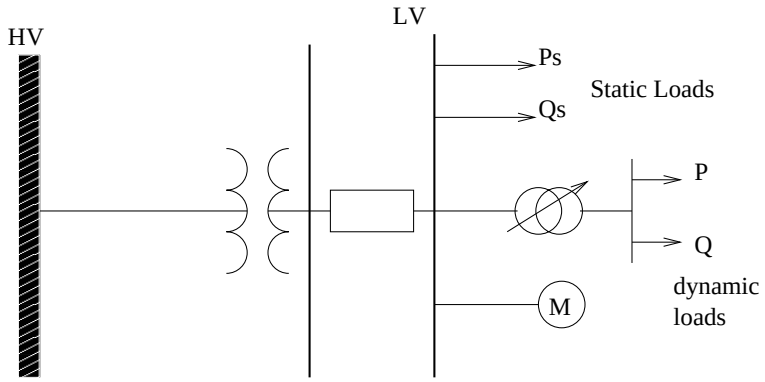

Figure 2.2: Example of Mixed Load

it can be seen that:

- Load drop immediately after the voltage step drop;
- After the sudden drop, if no voltage collapse, the load begins to recover to a post disturbance state;
- The trajectory of load recovery can be different depending on the load dynamic characteristics;
- Finally, the load will retain a stable level which is different from the predisturbance one.

To formulate the load model in a general form, the state model is given in [64], as having the general form

$$\dot{x} = f(x, V) \tag{2.13}$$

$$P_d = g_p(x, V) \tag{2.14}$$

$$Q_d = g_q(x, V) \tag{2.15}$$

where x is a vector of state variables. For example, x can be the slips of induction motor. f and g describe the dynamic and static aspects of the load model. This model can be used in voltage stability studies. The input output (I-O) version of this general load model can take the form as given in the equations below [64]:

$$\dot{P} + f_p(P_d, V) = g_p(P_d, V)\dot{V} \tag{2.16}$$

$$\dot{Q} + f_q(Q_d, V) = g_q(Q_d, V)\dot{V} \tag{2.17}$$

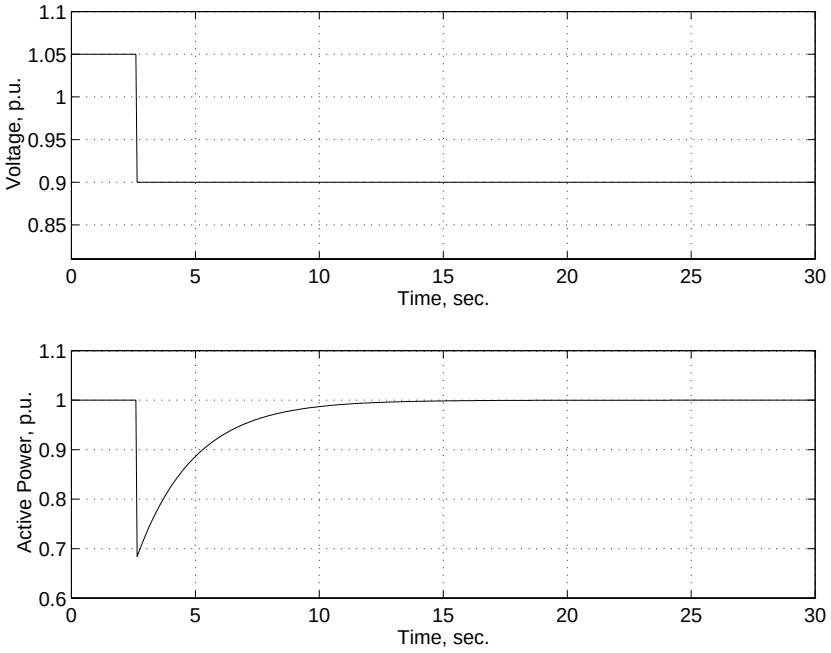

Figure 2.3: General Load Response

The general model steady state property is defined by $\dot{P} = 0$, $\dot{Q} = 0$, and $\dot{V} = 0$, i.e. $f_p(P_d, V) = 0$ or $f_q(Q_d, V) = 0$. The transient property is given by the function $g_q(Q_d, V)$. A higher order I-O version load model has been used to examine power system load oscillatory stability problems [127]. In order to formulate a load model suitable for control and stability studies, the I-O form can be converted to the state variable form. The state need not have direct physical meaning, and the model equations therefore represent an aggregate load of the system.

Based on the recovery properties of load models, specific models are considered. The exponential recovery load model -see Figure 2.4- takes the I-O form

$$T_p \dot{P}_d + P_d = P_s(V) + T_p P_t(V) \dot{V} \tag{2.18}$$

$$\tag{2.19}$$

where T_p is the recovery time constant defining the load response after a voltage step change, P_d is the power demand, and P_s, P_t define steady state and transient load behavior respectively. For this model, if we define the transient load characteristic

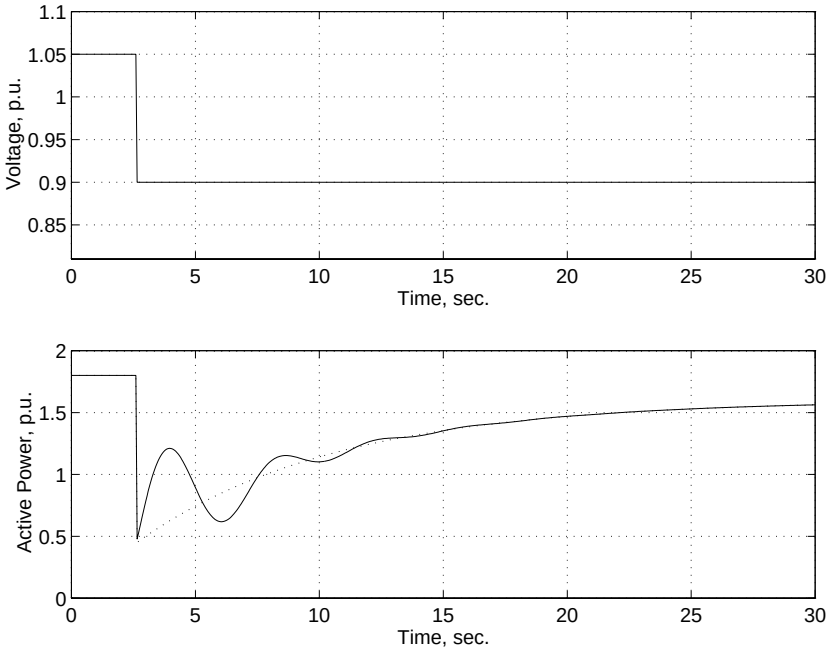

Figure 2.4: Exponential Recovery Load Model Recovery Characteristics

by $P_t(V) = \int_0^V p_t(t)dt + Const.$ and compose a state variable x_p as $x_p = P_d - P_t$, then the state form model can be derived as:

$$T_p \dot{x}_p = -x_p + P_s(V) - P_t(V) \tag{2.20}$$

where the formulation for P_s and P_t can take an exponential form such as: $P_s(V) = P_0(\frac{V}{V_0})^{\alpha_s}$ and $P_t(V) = P_0(\frac{V}{V_0})^{\alpha_t}$. V_0 is the nominal bus voltage and P_0 is the corresponding load power. Similar formulation applies to reactive load power modeling. The range of value for the constants α_s, α_t and T_p depends on different types of load to be studied. For induction motor dominated loads such as industrial, air conditioning systems, or a metal smelter, the time constant T_p is in the range of up to one second. For some control devices, such as tap changers T_p can be several minutes. For heating loads, T_p can be in the units of hours, while the voltage index constant α_s and α_t can be within 0 to 2 and 1 to 1.25 respectively [64, 74, 84, 117, 118]. For a control property viewpoint, the block diagram of the exponential recovery load can be easily derived as follows.

For small signal stability analysis, the model needs to be linearized around some

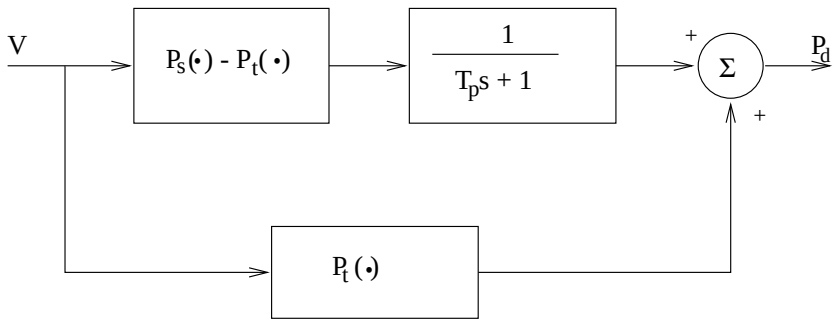

Figure 2.5: Exponential Recovery Load Model Block Diagram

operational points, so that afterwards, the load model can be included in the system linearized dynamic equations to help build the state matrix or Jacobian for eigenanalysis. The linearization results in the following equations for the exponential recovery load model:

$$\begin{aligned} T_p \Delta \dot{x}_p &= -\Delta x_p + \frac{P_0}{V_0}(\alpha_s - \alpha_t)\Delta V \\ \Delta x_p &= P_d - P_t(V) \end{aligned}$$

After simplifications of the above equations, the linearized model is:

$$\Delta P_d = \frac{P_0}{V_0}\alpha_s \frac{\frac{\alpha_t}{\alpha_s}T_p s + 1}{T_p s + 1}\Delta V$$

where Δ as usual represents a small variation of associated variables. It can be observed that the linearized load tends to different values at different frequencies, i.e.,

$$\lim_{s\to 0} \Delta P_d = \frac{P_0}{V_0}\alpha_s \qquad \lim_{s\to \infty} \Delta P_d = \frac{P_0}{V_0}\alpha_s$$

The influence of load model parameters on load dynamic behavior have been studied in detail in [117, 118].

A similar model, the adaptive load model has similar recovery characteristics to the exponential one. The adaptive load recovery curve after a voltage step change is given in Figure 2.6, and the model equations are listed below, [64, 118]

$$T_p \dot{x}_p = P_s(V) - P_d = P_s(V) - x_p P_t(V) \tag{2.21}$$

$$T_q \dot{x}_p = Q_s(V) - Q_d = Q_s(V) - x_p Q_t(V) \tag{2.22}$$

where P_d, Q_d are greater than zero. The state form model can be transformed into the I-O form as [68]:

$$T_p\dot{P}_d + P_t(V)(P_d - P_s(V)) = T_p P_d \frac{p_t(V)}{P_t(V)}\dot{V} \tag{2.23}$$

This adaptive load model does not make much difference in the load recovery response, although, it does make significant difference while considering its algebraic equation solvabilities. Such differences relate the fact that in the exponential recovery model, x_p is added to other loads, while in the adaptive recovery model, x_p is multiplied with transient load power [68].

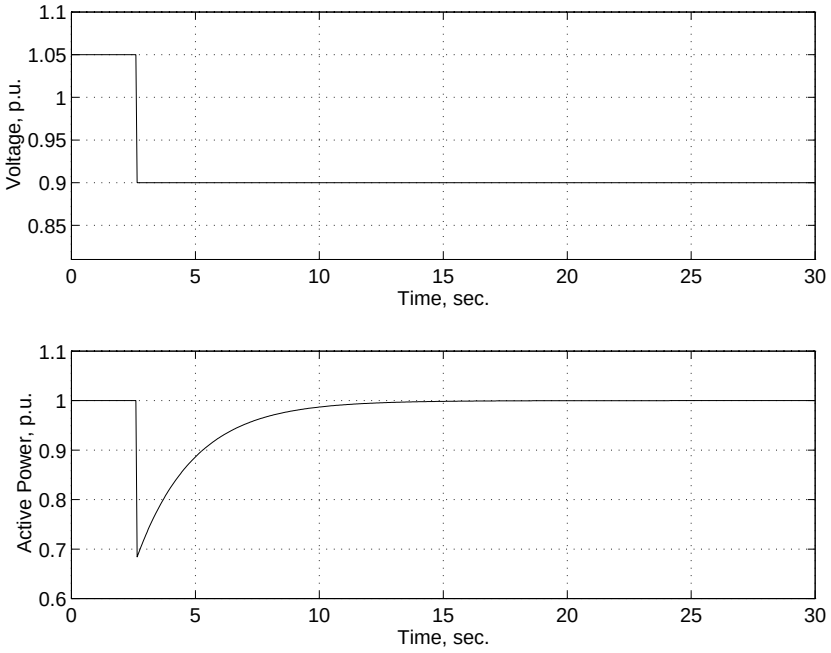

Figure 2.6: Adaptive Recovery Load Model Recovery Characteristics

To sum up, both of the recovery load models feature a similar recovery behavior. Besides the general characteristics mentioned above, we observe:

- The recovery trajectory of load power follows an approximately exponential law;
- The time constant, and other model constants affect the load power recovery behavior in an nonlinear way;

- The value of voltage step change also affects the recovery time in a relationship function defined by Equations (2.18,2.20,2.21,2.22,2.23).

The load models given above are summarized for comparison in the form of general load models, see Table 2.1.

For a real power system study, the load is very complicated; typically, there can be loads of different kinds. To study the mixed load influence on system stability properties, the load model of devices such as induction motors, tap changing transformers will be studied later.

Genetic Load Models

		Steady-State	Transient
1	Exponential Recovery	$P_d = P_s(V)$	$P_d = \frac{1}{T_p}x(0^-) + P_t(V)$
2	Adaptive Recovery	$P_d = P_s(V)$	$P_d = x(0^-)P_t(V)$
3	General State	$a(x,V) = 0$ $b_p(x,V) = P_d$	$P_d = b_p(x(0^-),V)$
4	General IO	$f_p(P_d,V) = 0$	$dP_d = g_p(P_d,V)dV$

Table 2.1: Comparison of Genetic Load Models (for Real Power)

2.4 Power System Modeling

Power system modeling requires modeling of all the system components including generators, transmission lines, transformers, loads, and other control devices/systems as discussed above. Since all stability analysis will be based on the system model, here the complete system model composed of differential and algebraic equations will be discussed.

A complete power system modeling approach involves forming the overall system equations in the form of differential algebraic equations (1.1) or (1.2) and are rewritten below:

$$\dot{x} = f(x,z,\lambda)$$

$$0 = g(x, z, \lambda)$$

where x is the vector of state variables, z is the vector of algebraic variables, and λ is the vector of system parameters.The differential equation set includes the dynamics of generators, excitation systems, load dynamics, and the algebraic equation set includes load flow equations and other algebraic relations of system components. However, for small signal stability analysis, linearization is needed to eliminate the algebraic part of the system equations. Linearization yields

$$\begin{aligned} \Delta\dot{x} &= \frac{\partial f}{\partial x}\Delta x + \frac{\partial f}{\partial z}\Delta z \\ 0 &= \frac{\partial g}{\partial x}\Delta x + \frac{\partial g}{\partial z}\Delta z \end{aligned}$$

Then the system Jacobian $J_s = \frac{\partial f}{\partial x} - \frac{\partial f}{\partial z}(\frac{\partial g}{\partial z})^{-1}\frac{\partial g}{\partial x}$ can be used for stability analysis via its eigenanalysis. For a power system, the matrix J_s can be of very large scale, because of contributions from the equations describing different network devices. For accurate small signal stability analysis, all relevant system dynamics should be included in the system model. The analysis of the system model requires efficient computation techniques and algorithms for different aspects of small signal stability problems.

In power system modeling studies, the parameter values are chosen as fixed values or within a certain range because the measurement of actual system parameters is very difficult. In particular, the load parameter values are difficult to obtain due to the large number of load components, the inaccessibility of certain customer loads, load compensation variation, and uncertainties of many load component characteristics.

2.5 Bifurcations and Power System Stability

This section begins consideration of stability boundaries and their characteristics in terms of bifurcations in the differential equation models. In order to sustain a power system in stable and reliable operation, the operating point must lie within a certain boundary or a limit space composed of power system parameters and control variables. The boundary can be very complicated. It is possible to study the surface via cut sets, for example, the cut set of selected power system load powers, the cut set of power system PSS gains. These cut sets will be named as power

system security boundaries. All the points on the security boundary fall into one or more of the categories of the stability characteristic points which include load flow feasibility boundaries, saddle node and Hopf bifurcations, and singularity induced bifurcations. The load flow feasibility boundaries are related to system load flow solvability, and all of the bifurcation characteristic points can be associated with system Jacobian eigenvalue attributes.

To explore these small signal stability boundary characteristic points, first the power system model will have to be composed, then the system Jacobian or state matrix should be calculated for stability eigenanalysis. Since a power system is a very large nonlinear system, the problem of finding all these characteristic points is not easy. Efficient numerical methods will be needed to perform these analyses.

Before going into the detail of the specific system operation and stability boundaries, the concept of a variable parameter space will be briefly presented. The space spanned by all power system parameters can be functionally divided into a set of system parameters which do not change during system operation and the set of operating parameters which can change during system operation. If a parameter changes during operation, the system state will change accordingly. Generally, particular change in the system state is associated with one or more particular parameter changes. There are relationships between system parameter changes and system equilibrium state variation, but the qualitative behavior of the system state space remains the same within each region in the parameter space. These boundaries may include load flow feasibility limits, and bifurcation boundaries. These boundaries divide the parameter space into several typical regions in which the structure of the state space remains identical. It includes the static properties and dynamic local properties as well as the dynamic global properties such as the stability boundary [142].

The notation of feasibility region in the parameter space is defined as the set of all operating points in the parameter space which can be reached by quasi static parametric variations as part of the system operation [142]. The system operation can be shifted freely while remaining stable under slow, continuous parameter changes. However, the size of the region of attraction normally decreases as the system operation point approaches the feasibility boundary [22].

2.6 Model Linearization and System Jacobian

To study a power system small signal stability problem, an appropriate linearized model for the machine and load dynamics is required. They include generator and excitation system differential equations, stator and network algebraic equations. These equations build up the set of differential-algebraic equations are rewritten here for clarity,

$$\begin{aligned} \dot{x} &= f(x, z, p) \\ 0 &= g(x, z, p) \end{aligned} \tag{2.24}$$

In the equation (2.24), x is the vector of state (differential) variables, z is the vector of algebraic variables, p is the vector of specified system parameters.

In small signal stability analysis, the set (2.24) is then linearized at an equilibrium point to get the system Jacobian and state matrix. The structure of the system Jacobian J_s is shown in Figure 2.7 [98], where J_{lf} stands for the load flow Jacobian,

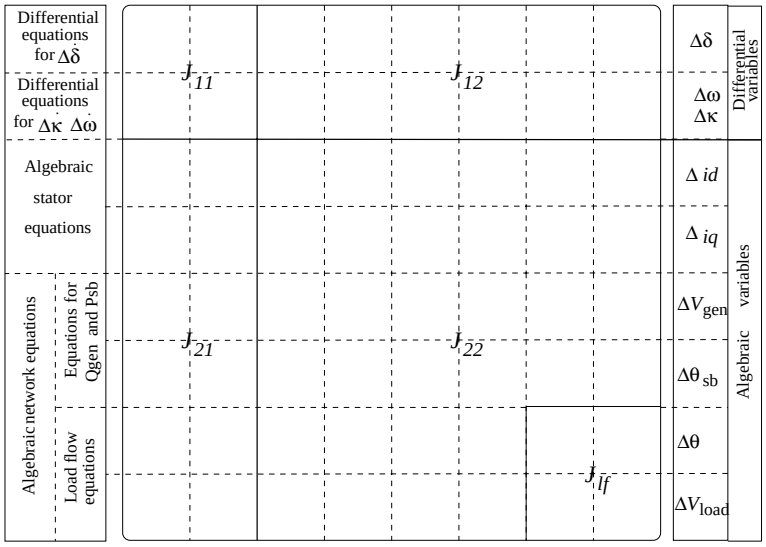

Figure 2.7: Structure of the System Jacobian.

$J_{11} = \partial f/\partial x$, $J_{12} = \partial f/\partial z$, $J_{21} = \partial g/\partial x$ and $J_{22} = \partial g/\partial z$ are different parts of J corresponding to differential and algebraic variables. In Figure 2.7, Q_{gen} stands for the reactive power at generator buses, P_{sb} is the active power at the swing bus, δ is the vector of machine rotor angles, ω is the vector of machine speeds, κ is the vector of the state variables except δ and ω (such as E'_q, E'_d, E_{FD}, V_R, and R_F; load

bus voltages V_{load} and angles θ should be considered as dynamic state variables in cases where load dynamics is considered [98]), i_d and i_q are vectors of d-axis and q-axis currents, and V_{gen} stands for generator bus voltages. The prefix Δ means a small increment in corresponding variables.

From the information provided by the structure of the state matrix or system Jacobian, bifurcation and other stability characteristic conditions can be studied.

2.7 Load Flow Feasibility Boundaries

The power system load flow feasibility region defines the solvability of the load flow equations in the parameter space which is bounded by the load flow feasibility boundary [52]. The power system must operate within its load flow feasibility boundary. For a system composed of 1 slack bus, n_g generator and voltage controlled buses, and n_{ld} load buses, the system load flow conditions are described in the equations below:

(1) Swing bus equation:

$$\vec{V}_1 = V_1 \angle \delta_1 \tag{2.25}$$

(2) Generator bus [P-V bus] load flow equations:

$$\begin{aligned} 0 = {} & \frac{V_i}{X'_{di}}(E'_{qi}\sin(\delta_i - \theta_i) - E'_{di}\cos(\delta_i - \theta_i)) \\ & -V_i \sum_{j=1}^{n_g} V_j(g_{ij}\cos\theta_{ij} + b_{ij}\sin\theta_{ij}) \end{aligned} \tag{2.26}$$

$$\begin{aligned} 0 = {} & \frac{V_i}{X'_{di}}(E'_{qi}\cos(\delta_i - \theta_i) + E'_{di}\sin(\delta_i - \theta_i) - V_i) \\ & -V_i \sum_{j=1}^{n_g} V_j(g_{ij}\sin\theta_{ij} - b_{ij}\cos\theta_{ij}) \end{aligned} \tag{2.27}$$

(3) Load bus [P-Q bus] load flow equations:

$$0 = P_{L_k} - V_k \sum_{j=1}^{n_{ld}} V_j(g_{kj}\cos\theta_{kj} + b_{kj}\sin\theta_{kj}) \tag{2.28}$$

$$0 = Q_{L_k} - V_k \sum_{j=1}^{n_{ld}} V_j(g_{kj}\sin\theta_{kj} - b_{kj}\cos\theta_{kj}) \tag{2.29}$$

where $\vec{V}_1$ is the swing bus voltage vector; generally it can be taken as $\vec{V}_1 = 1\angle 0$, and $S_{L_k} = P_{l_k} + jQ_{l_k}$ is the complex injected load at bus k, $(k = 1, 2, ..., n_{ld})$. Also note

that in the equations above, saliency effects, and rotor resistance of machine have been neglected, i.e. assume $X'_d = X'_q$ and $R_r = 0$.

For the classic 3-machine 9-bus power system [6] which contains 3 generators, and 9 buses where 3 are loaded. The system is given in Figure 2.8.

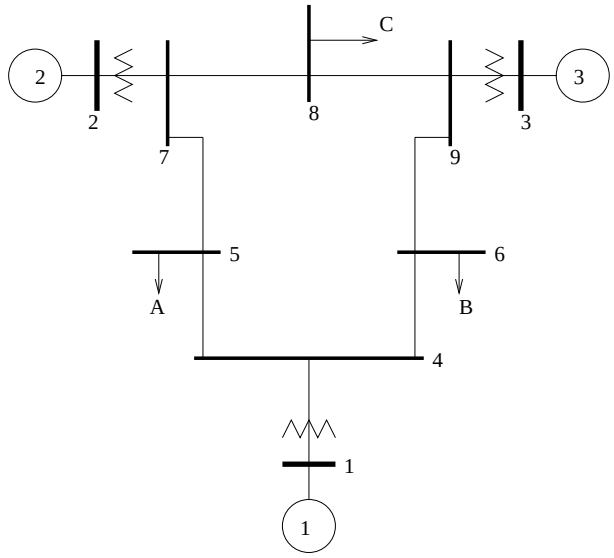

Figure 2.8: The 3-machine 9-bus system

If the active loads at buses 5, 6, and 8 are increased simultaneously, the load flow gives the following Figure 2.9. The load flow feasibility region is $D_{lf} = \{P_5, P_6, P_8 | P_5 \leq 3.007\ p.u., P_6 \leq 2.6508\ p.u., P_8 \leq 2.7618\ p.u.\}$. Within the range D_{lf}, the system has load flow solutions, which can be stable or unstable depending on the stability analysis. Generally, the upper $P - V$ curve branch is a stable branch, and the lower one is unstable. It seems that the straightforward method to obtain the load flow feasibility points is by consistently solving many load flow problems, and finding the nose point where the limit lies. However, more efficient methods of locating the load flow feasibility boundaries will be discussed in later chapters.

There are many studies concerning the load flow feasibility boundary, which is also known as the load flow singularity boundary because the load flow Jacobian is singular on it, i.e. $\det J(x,p)_{lf}|_{z \in D_{lf}} = 0$. The space of the boundary can be in nodal powers [67], synchronous machine parameters, bus voltages, control system

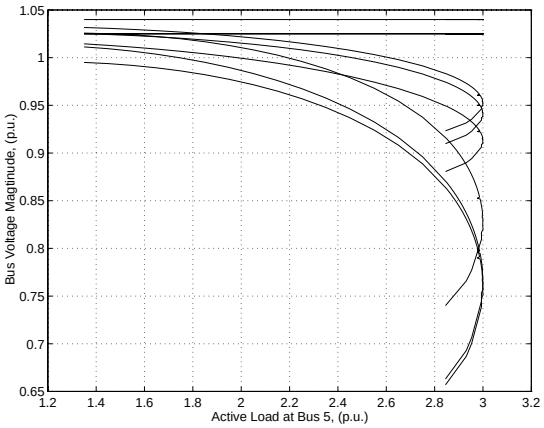

Figure 2.9: Load flow solution of the 3-machine, 9-bus system.

parameters, and combination of these parameters.

Small signal stability analysis is based on system equilibrium points. For a power system, the equilibrium point is a load flow solution point. In fact all stability questions will have to be based on a solution of load flow conditions. As usual, the $P-V$ or $Q-V$ curve reveals that the load flow feasibility limit corresponds to the nose point of these curves (for consistent power loads). Beyond the feasibility limit, there will be no power flow solutions, and it represents that no physical operation is possible.

Inside the load flow feasibility boundary, the system behavior can be further divided into several stability regions by different characteristic stability boundaries, which are described by bifurcation boundaries. The system retains a similar stability property within each region specified by a certain bifurcation boundary; crossing a bifurcation boundary, the system will experience significant property changes. It may lose stability, may change from a stable oscillatory operation state to an unstable oscillatory operation state, or vice versa, and in the case of a singularity induced bifurcation, the system behavior may become totally unpredictable.

2.8 Bifurcation Conditions and Power System Stability

In the remaining sections, we review the common local bifurcations occurring in power system models. For easy presentation of the bifurcation theory, let us take a nonlinear system described by the equation,

$$\dot{x} = f(x, \lambda) \tag{2.30}$$

where $x \subset R^n$ is a vector of the system state variables, and λ is a vector of system parameters which may be varying slowly and continuously. λ here is called the bifurcation variable because the slow continuous change of values of λ may result in bifurcation, which is qualitative change in system behavior. This change can happen suddenly, and after that the system may lose stability, or begin oscillation. Different bifurcations corresponding to different system behaviors. For power system stability analysis, saddle node bifurcations, Hopf bifurcations, singularity induced bifurcations, cyclic fold, period doubling, and blue sky bifurcations are of particular importance. The system behavior after these bifurcation have been studied in many literatures, for example in [32, 139, 145].

Local bifurcation analysis is based on the neighborhood of the system's equilibrium point, which is the solution of,

$$0 = f(x, \lambda) \tag{2.31}$$

for equation (2.30) when $\dot{x} = 0$. The equation (2.31) corresponds to the load flow equations [96]. A static bifurcation point, which is a bifurcation of system equilibrium points are associated with the dynamic bifurcation, i.e. a bifurcation of vector fields. A static bifurcation occurs when two or more equilibrium points coincide. A Hopf bifurcation occurs when a periodic solution emerges from a stable equilibrium; it can be a stable oscillation or unstable oscillation depending on the direction of eigenvalue transversality condition. Unlike the regular oscillations associated with dynamic bifurcations, chaos exhibits irregular oscillations. It is a result of a global bifurcation which is characterized by the system's non-local change in its phase portrait [49, 136].

When some of the system parameters vary slowly and continuously, the system slowly adjusts its operation equilibrium points to match the parameter change

within its stability boundaries composed by the load flow feasibility boundaries and bifurcation points. Then, as the parameter variation continues the system may undergo a sudden change in state and become unstable. Different bifurcations result in different system behavior and require different techniques to locate them. We will discuss the properties in the following section.

2.9 Saddle Node Bifurcations

One of the most important bifurcations is the saddle node bifurcation (SNB), which has found wide application in power system stability studies. A SNB occurs when the system Jacobian becomes singular,i.e. $det\frac{\partial f}{\partial x} = 0$. More specifically [46], let x^* and λ^* denote the system equilibria. x is to bifurcate from x^* at the parameter value λ^* if two distinct solutions emerge at x^* as λ varies toward λ^*. The stable equilibrium point disappears in a SNB. The definition and characterization of a saddle node bifurcation is given in the following result [61].

Theorem 1 *Assume that for $\lambda = \lambda^*$ system (2.30) satisfies the following hypothesis at an equilibrium point y^*,*

i $\frac{\partial f}{\partial x}(x^*, \lambda^*)$ *has $n-1$ eigenvalues with negative real part and a simple eigenvalue* 0 *with right eigenvector v and left eigenvector w.*

ii $w^T((\frac{\partial f}{\partial \lambda})(x^*, \lambda^*)) \neq 0$

iii $w^T((\frac{\partial^2 f}{\partial x^2}|_*)(v, v)) \neq 0$

Then there is a smooth curve of equilibria passing through (x^*, λ^*), tangent to $R^n \times \lambda^*$. Depending on the signs in **ii** *and* **iii**, *there are no equilibria near (x^*, λ^*) when $\lambda <$ or $> \lambda^*$, and two hyperbolic equilibria, one stable and one type-1, when $\lambda <$ or $> \lambda^*$.*

From the above theorem, the conclusion can be made that the system Jacobian has exactly one zero eigenvalue, and all other eigenvalues have negative real parts. This is the necessary conditions for locating SNBs. SNB can be depicted by the Figure (2.10). Theoretically, SNB can occur between a stable equilibrium point and a type 1 unstable equilibrium point as well as between unstable equilibrium points, even if the latter is of no real practical interest.

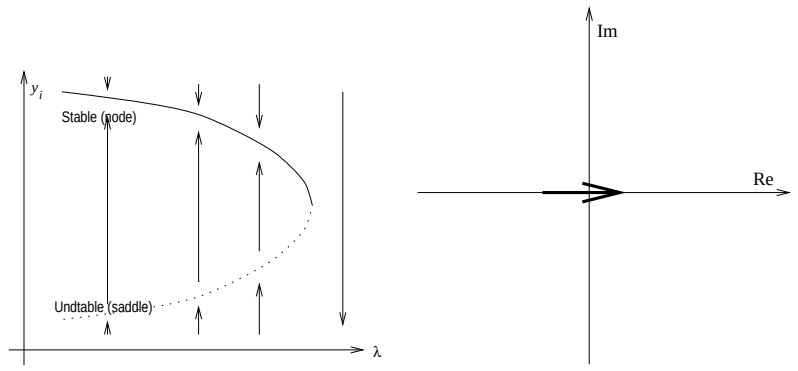

i. ii.

Figure 2.10: Saddle Node Bifurcation: i. Bifurcation Curve, ii. Eigenvalue Trajectory.

In power systems, saddle node bifurcations are associated with collapse type instabilities. For example, in the load flow P-V or Q-V curve, the system comes to its saddle node bifurcation point when it is being stressed to it's power transfer limit. The SNB point is also called the PoC point at which two distinct solutions emerge into one solution, and the load flow Jacobian becomes singular. There is no solution beyond the SNB point. The system will exhibit voltage collapse immediately after being perturbed beyond the point if the emergency control action fails.

It should be noted that saddle node bifurcations of the load flow function will not occur if the power system is operated well within its steady-state stability limits. The saddle node bifurcation can provide indices to estimate the distance from the current operating point to the bifurcation boundaries. The smallest eigenvalue, or critical eigenvalue of the linearized system, or the eigenvector can be used to build a distance in the parameter space to prevent instability [42, 43, 44, 49].

Regarding the characteristics of power systems, let us represent it by differential and algebraic equations (DAE's) which are rewritten here for clarity:

$$\dot{x} = f(x, z, \lambda) \tag{2.32}$$

$$0 = g(x, z, \lambda) \tag{2.33}$$

The eigenanalysis procedures require first that we solve the equations and so find the equilibrium points (x^*, z^*, λ^*), which satisfy:

$$\begin{aligned} 0 &= f(x, z, \lambda) \\ 0 &= g(x, z, \lambda) \end{aligned}$$

The set of equations above can be referred to as 'load flow' equations, although practical load flow calculation may use different models, based on different assumptions [96]. Then linearization of the equations at the equilibrium point gives,

$$\begin{aligned} \Delta\dot{x} &= \frac{\partial f}{\partial x}\Delta x + \frac{\partial f}{\partial z}\Delta z \\ 0 &= \frac{\partial g}{\partial x}\Delta x + \frac{\partial g}{\partial z}\Delta z \end{aligned}$$

Then form the reduced system Jacobian by $J_s = \frac{\partial f}{\partial x} - \frac{\partial f}{\partial z}(\frac{\partial g}{\partial z})^{-1}\frac{\partial g}{\partial x}|_*$. This Jacobian J_s is then analyzed based on its eigenproperties including left and/or right eigenvalues, and the corresponding eigenvectors.

As stated earlier, bifurcation occurs as a result of system parameter constant slow variation. The variation should be slow enough so that the system will stay in its equilibrium conditions without major property change until a bifurcation is met. Then the system suddenly undergoes qualitative change in its dynamic properties.

A saddle node bifurcation occurs when the system Jacobian is singular, i.e. $\det J_s|_* = 0$. If the Jacobian is by chance a load flow Jacobian, J_{lf} then the load flow saddle node bifurcation occurs, which coincides with the load flow feasibility boundary. However, not all saddle node bifurcations are load flow singularity points. Only under certain conditions, where many simplifications have been assumed, do these two kinds of characteristic points coincide [132, 143].

Before going into the mathematical aspects of saddle node bifurcation conditions, the system equations in (2.32–2.33) shall be replaced for simplification by $F(x, \lambda) = 0$, where F includes f and g, and the vector x in the function $F(x, \lambda)$ is merged with the vectors x and z in equations (2.32–2.33). Note that this simplification does not affect the bifurcation analysis to be performed [107].

Basically, there are two approaches to locating saddle node bifurcations: the direct or point of collapse method, and the continuation method. They will be studied later in the thesis. The mathematical description of the saddle node bifurcation can

be shown in the equations

$$F(x,\lambda) = 0 \tag{2.34}$$

$$\frac{\partial F(x,\lambda)}{\partial x} v = 0 \quad \text{or} \quad w^T \frac{\partial F(x,\lambda)}{\partial x} = 0 \tag{2.35}$$

$$||v|| = 1 \quad \text{or} \quad ||w|| = 1 \tag{2.36}$$

where $v, w \in R^N$ is the left and right eigenvector of the Jacobian, $\frac{\partial F(x,\lambda)}{\partial x}$. Solution of these equations is used in the direct approach, i.e. the solution of the equations gives the saddle node bifurcations directly. A nontrivial condition is ensured by equation (2.36) and the equilibrium constraints condition is given by equation (2.34). The solution of the problem can be obtained by applying the Newton-Raphson-Seydel method to the equations (2.34–2.36). Neighboring equilibrium points very close to the saddle node bifurcation point can be calculated by solving the equations,

$$F(x,\lambda) = 0 \tag{2.37}$$

$$(\frac{\partial F(x,\lambda)}{\partial x} - \varepsilon I)v = 0 \tag{2.38}$$

where I is the identity matrix of the same order as $\frac{\partial F(x,\lambda)}{\partial x}$, $\varepsilon \in [-\varepsilon_a, \varepsilon_b]$ and $\varepsilon_a, \varepsilon_b > 10^{-12}$. It is evident that $\varepsilon = 0$ corresponds to the bifurcation solution point itself [96].

When a saddle node bifurcation occurs, the system may experience a static type of voltage collapse or angle instability beyond the limit determined by the SN bifurcation.

Saddle node bifurcations have become a well accepted means to define indices for voltage instability. The most common way to build indices is in terms of some measures of the singularity of $\frac{\partial F}{\partial x}$. Also, the saddle node bifurcation points of the load flow Jacobian help locating the load flow feasibility boundary.

2.10 Hopf Bifurcation Conditions

Another important kind of bifurcation is the Hopf bifurcation (HFB). This bifurcation corresponds to emergence of a periodic solution from an equilibrium point of the equation (2.30); in this way, the HFB is responsible for power system oscillatory behavior. At a HFB point, the system Jacobian has a pair of imaginary eigenvalues

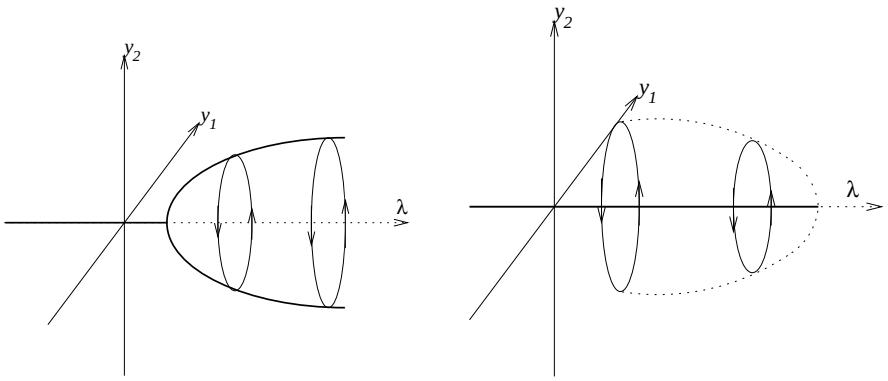

Figure 2.11: Hopf Bifurcations: (solid line - stable solution branches, dotted line - Unstable solution branches.)

1. [left] Stable limit cycle for supercritical Hopf bifurcation;
2. [right] Unstable limit cycle for subcritical Hopf bifurcation;

passing the imaginary axis, and no other eigenvalues with non negative real part. These two pure imaginary eigenvalues result in the system's oscillatory modes, depending on the direction of a transversality condition stated below [1, 3, 136],

Theorem 2 *For the equation (2.30), where $x \subset R^n$, the following conditions defines Hopf bifurcation at the equilibrium point given by y^* and λ^*,*

i. $f(x^*, \lambda^*) = 0$

ii. *Jacobian $\frac{\partial f(x,\lambda)}{\partial x}|_{(x^*,\lambda^*)}$ has a simple pair of purely imaginary eigenvalues $\mu = 0 \pm i\beta$ and all other eigenvalue with negative non-zero real parts.*

iii. $\frac{d(\Re\mu(\lambda))}{d\lambda}|_{\lambda^*} \neq 0$

Then there is a birth or death of limit cycles at the point (x^*, λ^*) depending on the sign of equation iii. The initial period of the generated limit cycle is $T_0 = \frac{2\pi}{\beta}$.

A HFB can be supercritical or subcritical. A supercritical Hopf bifurcation has negative sign for the derivative in **iii**. The periodic solution branch is initially stable for the supercritical case. On the other hand, a subcritical Hopf bifurcation is associated with an unstable periodic solution branch. The periodic solution branches of these two kinds of Hopf bifurcation are given in Figure (2.11).

Moreover, the Hopf bifurcation theorem shows the existence of small amplitude of oscillations for λ near λ^*. It is adapted from [62], and is given below as Theorem 3,

Theorem 3 The Hopf bifurcation theorem,

i. [Existence] *There is $\nu_H > 0$ and a C^{r-1} function $\lambda(\nu) = \lambda_0 + \lambda_2\nu^2 + O(\nu^3)$, such that for each $0 < \nu \leq \nu_H$, there is a nonconstant periodic solution $y_\nu(t)$ of equation (2.30) near the equilibrium $y^*(\lambda)$ for $\lambda = \lambda(\nu)$. The period of y_ν is a C^{r-1} function $T(\nu) = 2\pi\beta^{-1}[1 + T_2\nu^2] + O(\nu^3)$, and its amplitude grows as $O(\nu)$.*

ii. [Uniqueness] *If $\lambda_2 \neq 0$, there is a $\nu_1 \subset (0, \nu_H]$ such that for each $\nu \subset (0, \nu_1]$, the period orbit y_ν is the only periodic solution of equation 2.30 for $\lambda = \lambda(\nu)$ lying in a neighborhood of $y^*(\lambda(\nu))$.*

iii. [Stability] *Exactly one of the characteristic exponents of $y_\nu(t)$ approaches 0 as $\nu \to 0$, and it is given by a real C^{r-1} function $\mu(\nu) = \mu_2\nu^2 + O(\nu^3)$. the relationship $\mu_2 = -2\alpha'(\lambda_0)\lambda_2$ holds. Moreover, the periodic solution $y_\nu(t)$ is orbitally asymptotically stable with an asymptotic phase if $\mu(\nu) < 0$ but is unstable if $\mu(\nu) > 0$.*

If $\nu_2 \neq 0$, then the periodic solution $z_\nu(t)$ occurs for either $\nu > \nu_0$ or $\nu < \nu_0$. Accordingly, the Hopf bifurcation is said to be supercritical for $\nu > 0$ and subcritical for $\nu < 0$.

For power system analysis, Hopf bifurcations may be provided by many sources including excitation control, nonlinear damping, load changes, losses of the transmission line, frequency dependence of the electric torque. There are many examples of Hopf bifurcations reported in the literature [49, 1, 12, 47, 125, 145, 150]. Hopf bifurcations of nonlinear systems can be studied by the computer packages *AUTO* and *BIFOR2* [145]. Generally, a Hopf bifurcation may happen typically as a subcritical bifurcation where the operating point is stable, but its region of transient stability is reduced by the surrounding unstable periodic orbit. In some cases, a Hopf bifurcation exists with other bifurcations, and they can reduce the system operation security domain. Numerical methods computing Hopf bifurcation boundaries will be addressed later in the thesis.

A Hopf bifurcation is characterized by a pair of pure imaginary eigenvalues passing the imaginary axis in the complex plane while all other eigenvalues remain on the left side of the complex plane. Different Hopf bifurcations are associated with different oscillatory behaviors. It has long been observed that badly damped low frequency inter-area oscillations can take place in complicated power systems, and they can reduce power transfer capabilities [27]. Such cases appear in bulk power systems for large separated subsystems which are coupled by long transmission lines, as well as

for post contingency operating conditions [27, 137].

In accordance with the definition of the Hopf bifurcation, which feature a pure pair of imaginary eigenvalues $0 \pm j\omega$ of the system Jacobian $J_s = \frac{\partial F(x,\lambda)}{\partial x}|_{(x_0,\lambda_0)}$, the Hopf bifurcation condition gives [136]:

$$J_s v = j\omega v \tag{2.39}$$

where complex eigenvector $v = v' + jv$.

Separating the real and imaginary parts, which gives,

$$J_s v' = -\omega v'' \quad \Leftrightarrow \quad J_s v'' = \omega v' \tag{2.40}$$

After formulating the equation for vector operation, and normalization of the eigenvector v, the power system [described by DAE's] equilibrium point is considered Hopf bifurcation point when it satisfies the equations which follow. Note here, the system Jacobian J_s is the reduced form from the DAE approach, i.e., $J_s = \frac{\partial f}{\partial x} - \frac{\partial f}{\partial z}(\frac{\partial g}{\partial z})^{-1}\frac{\partial g}{\partial x}$

$$F(x,\lambda) = 0 \tag{2.41}$$
$$J_s^T(x,\lambda)v' + \omega v'' = 0 \tag{2.42}$$
$$J_s^T(x,\lambda)v'' - \omega v' = 0 \tag{2.43}$$
$$v'_k = 1 \tag{2.44}$$
$$v''_k = 0 \tag{2.45}$$

where $0+j\omega$ is the eigenvalue corresponding to the Hopf bifurcation, and $v = v'+jv''$ is the corresponding left eigenvector, superscript ^{T} indicates transpose of the matrix J_s, and the last two equations give the nontrivial condition provided by the $_k$-th element of eigenvector v.

Solving the above equations with the Newton-Raphson-Seydel method produces the Hopf bifurcation points in the parameter space. This approach of locating Hopf bifurcations is a direct method. The parameter continuation method will be used later in the thesis to explore the Hopf bifurcation boundary in the parameter space as part of the power system security boundary.

Depending on the stability of the periodic solutions arising from the bifurcation, supercritical and subcritical Hopf bifurcation can be identified. A stable oscillatory

orbit, or an unstable oscillation is the result of system operational behavior after these two kinds of Hopf bifurcations respectively. There are nonlinear control methods to prevent the system from voltage collapse after subcritical Hopf bifurcations. It requires precise switching of control actions after subcritical Hopf bifurcation occurs.

Hopf bifurcation studies have been paying more and more attention to their effects on system stability, because the system may lose its stability well before the point of collapse is reached. This can be initially an oscillation event and finally lead to system failure. What's more, subcritical Hopf bifurcations can reduce the system security operation limit, because of its property of introducing unstable system oscillatory behavior.

2.11 Singularity Induced Bifurcations

The singularity induced bifurcation (SIB) is another important bifurcation in power system small signal stability analysis. This kind of bifurcation is charactered by unbounded system Jacobian eigenvalues at the equilibrium point [142]. The eigenvalue motion is given in Figure (2.12). The theorem about singularity induced bifurcation

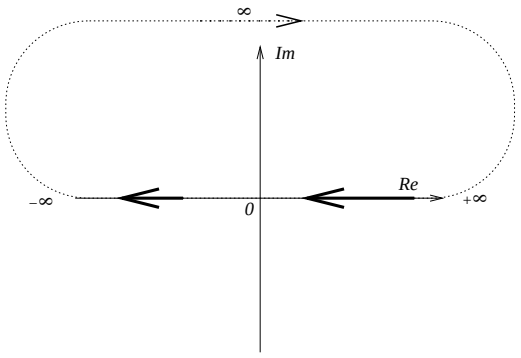

Figure 2.12: Singularity Induced Bifurcation Eigenvalue Trajectory

is given as Theorem 4, which is adopted from [142].

Theorem 4 Singularity Induced Bifurcation Theorem
For the system given in equations (2.32,2.33) with a 1-D parameter space, assume the following conditions are satisfied at $(0, 0, \lambda_0)$*:*

i. $f(0,0,\lambda_0) = 0$, $g(0,0,\lambda_0) = 0$, $\frac{\partial g}{\partial z}$ *has a simple zero eigenvalue and* $\text{trace}(\frac{\partial f}{\partial z}\text{adj}(\frac{\partial g}{\partial z})\frac{\partial g}{\partial x}) \neq 0$.

ii. *The system Jacobian* $\begin{pmatrix} \frac{\partial f}{\partial x} & \frac{\partial f}{\partial z} \\ \frac{\partial g}{\partial x} & \frac{\partial g}{\partial z} \end{pmatrix}$ *is nonsingular.*

iii. *The system's expended Jacobian* $\begin{pmatrix} \frac{\partial f}{\partial x} & \frac{\partial f}{\partial z} & \frac{\partial f}{\partial \lambda} \\ \frac{\partial g}{\partial x} & \frac{\partial g}{\partial z} & \frac{\partial g}{\partial \lambda} \\ \frac{\partial \Delta}{\partial x} & \frac{\partial \Delta}{\partial z} & \frac{\partial \Delta}{\partial \lambda} \end{pmatrix}$ *is nonsingular. Where* $\Delta = \det \frac{\partial g}{\partial z}$.

Then there exists a smooth curve of equilibria in $R^n + m + 1$ which passes through $(0,0,\lambda_0)$ and is transversal to the singular surface at $(0,0,\lambda_0)$. When λ is increased through λ_0, one eigenvalue of the system reduced Jacobian $\tilde{J}$ moves from C^- to C^+ or reverse along the real axis passing through inf. The other $(n-1)$ eigenvalues remain bounded.

The eigenvalue movement is shown in Figure 2.12.

A singularity induced bifurcation is the result of singularity of the algebraic part of the linearized power system DAE's model. At this bifurcation point, one of the system state matrix or Jacobian eigenvalues becomes infinity while others remain bounded. The system behavior can not be predicted close to this point, since the relationship between algebraic and differential parts of the system is broken. It is also impossible to simulate the system behavior around the vicinity of this point for a power system represented as DAE's [98, 142].

2.12 Power System Feasibility Regions

Besides above stated loadflow feasibility limits, and several types of bifurcations, power system stability and/or feasibility regions are often defined by the so called feasibility regions or steady-state stability limits.

As a typical large scale system, power system is composed of large number of devices and controls. Their limits have introduced the feasibility regions or steady-state stability limits. These limits are usually associated with the so called limit-induced bifurcations in the literature [42]. They occur in power systems when the system device reaches its limits and failed to provide further control or supply to the system,

then the system may undergo sudden loss of stability or voltage problem. One example of such kind of feasibility regions is the immediate loss of stability and subsequent voltage collapse due to loss of voltage control when reactive power limits are reached at generator models. The reactive power limits are revealed by armature current or field voltage limits. In real power systems, these feasibility regions often defines the system operational stability and/or feasibility regions.

2.13 Conclusion

Adequate power system modeling is necessary for system stability assessment. The major system equipment/devices may have an important impact on system stability behavior. They must be considered in power system stability studies with sufficiently detailed models. These devices include, generators and their excitation control system - including AVR and PSS, generator current limiters, transmission lines, loads, transformers and tap changers, SVCs and other FACTS devices as well as HVDC links. System stability analysis using static approaches which involves computation of eigenvalues and eigenvectors, such as model analysis of the reduced Jacobian matrix saves computation costs, and may provide sufficient insight into the mechanism of instabilities. On the other hand, based on the models provided, time domain simulations may be used as the decisive method to study fast transient dynamics.

The static bifurcations are common even in very simple power systems. They are results of solutions merging at the equilibrium points because of parameter or nodal power changes. Hopf bifurcations are associated with system oscillatory behavior. They result in emergence of stable or unstable limit cycles. It is important for power system analysis to study the Hopf bifurcations at equilibrium points. This kind of bifurcation is also very common in power system dynamics. Chaos which has been observed in simulations of small size power systems, deserves further study for practical power system analysis to prevent possible irregular system oscillations. Later in the thesis, saddle node and Hopf bifurcations will be studied in detail concerning their contribution to power system small signal stability properties, and computational techniques for their determination.

Chapter 3

Methods to Reveal Critical Stability Conditions

3.1 Introduction

Power system security operation requires that the system operates inside the security boundary determined by different criteria which include the load flow feasibility limit, saddle node and Hopf bifurcations, singularity induced bifurcations and critical damping conditions. However, since the power system is very complicated, it is essential to locate these security boundaries accurately for safe system operation. The complexity of the power systems, make the task of locating critical stability conditions very difficult and time consuming. However only those closest to the current normal power system operation point are of interest and the thesis will focus on obtaining these critical stability conditions. Before introducing approaches to obtain the critical stability conditions in a given loading direction, we review a method which is straight forward extension of those used in practice.

3.2 Step-by-Step Loading Approach

This step by step approach starts from the current system operating point and increases load in a direction defined by system loading conditions to solve the stability problem up to the load flow feasibility point. For a given power system modeled as $\dot{x} = f(x, p)$ and $0 = g(x, p)$, the approach generally comprises the following steps except for special additional stability condition calculations required:

1. Solve system load flow calculation based on current power system operating conditions.

2. Select system parameters, p, which are of interest to define the stability boundaries. These parameters are generally system nodal power(s) which give load variation direction. The selected nodal powers can be load active or reactive powers, machine generated active or reactive powers. These nodal powers selected are generally considered as close to the stability limits, and tend to cause system instability. Also the selected parameters can be control variables which can be adjusted to prevent instability. These selected parameters build up the space where stability boundaries lie in.

3. Vary the selected parameters in a certain direction in the space spanned by

them. i.e. $p = p_0 + \tau\Delta p$, where p is the vector of selected system parameters, τ defines the direction of parameter variation, Δp is a small variation of the parameter vector. Note the variation is small enough so that small signal stability analysis can be used, and p_0 is the current parameter value. Generally, $p^{n+1} = p^n + \Delta p$ gives a sequence of parameter changes.

4. Perform load flow calculation based on the new parameters after variation alone the selected direction. Check if the system load flow feasibility boundary is going to be met. If the system is close to point of collapse, special techniques will have to be used to find the exact Point of Collapse (PoC) point.

5. Perform the system state matrix or Jacobian calculation for the linearized system dynamic model based on the new parameters.

6. Calculated eigenvalues and eigenvectors of the state matrix or Jacobian, and check if the eigenvalues are prone to bifurcation or other instability problem.

7. Categorize and record all indices for instability or oscillatory behaviors.

8. Repeat steps **1.** –**7.** till load flow calculation does not converge, i.e. out side of the load flow feasibility boundary.

9. Repeat the procedures **1.** –**8.** for different loading directions until the interesting parameter(s) space(s) have been explored.

10. Analysis the recorded instability indices and instability points, locate the security boundary.

The method is rather straightforward, though very time consuming for computation. The operator needs to try all possible direction of parameter variation in order to get sufficient information about the stability characteristics. However, in some cases, the system operator need only perform the calculation along a well selected weak parameter variation direction based on experience and save much computation time.

3.3 Critical Distance Problem Formulation

Saddle node or Hopf bifurcations are useful concepts in analysis of power system security. The method here is to find the most dangerous directions for change of power

system parameters which drive the power system onto the bifurcation boundaries. The corresponding vectors in the space of parameters provide information about stability margins and measures of system security as well as providing optimal ways to improve the system security by variation of the adjustable available parameters so that the system can operate away from stability boundaries.

The direct step by step loading variation approach is too expensive with computation to adequately achieve this. To save computation costs, and find more reliable results will need more sophisticated methods. We now present a general formulation of the problem of finding closest points on the bifurcation boundaries.

Recall in Chapter 2, the power system structure preserving model is composed of DAE's, which are rewritten below for completeness,

$$dx_1/dt = f_1(x_1, x_2, p) \tag{3.1}$$

$$0 = f_2(x_1, x_2, p) \tag{3.2}$$

where $x_1 \in R^m$ is the dynamic state vector; x_2 is a vector composing of other system variables supplement to the full system state vector $x = (x_1^t, x_2^t)^t \in R^n, n \geq m$; p is a vector of controlled parameters; p can include any parameters of generators, control units, loads and networks which can be varied in planning, tuning and control, and whose influence on the dynamic stability is to be analyzed.

After linearization around a certain operation equilibrium point (x, p), the system state matrix or reduced Jacobian, J_s, can be obtained by,

$$J_s(x,p) = (f_1)'_{x_1} - (f_1)'_{x_2} \left[(f_2)'_{x_2}\right]^{-1} (f_2)'_{x_1} \tag{3.3}$$

which will be used for eigenanalysis. Also in order to simplify description, the system equilibrium will be denoted as $f(x, p) = 0$, where $x = \{x_1, x_2\}$.

Provided all the information about system dynamic and static equations are given as above, the points along the dynamic stability boundary for both aperiodic and oscillatory type, can be described by the equations below,

$$f(x,p) = 0 \tag{3.4}$$

$$J_s(x,p)\dot{r} - j\omega\dot{r} = 0 \tag{3.5}$$

where $f(x,p) = [f_1^t(x,p), f_2^t(x,p)]^t$, and $\dot{r} = r' + jr'' \neq 0$ is the right eigenvector of $J_s(x,p)$, corresponding to the eigenvalue $\lambda = 0 + j\omega$.

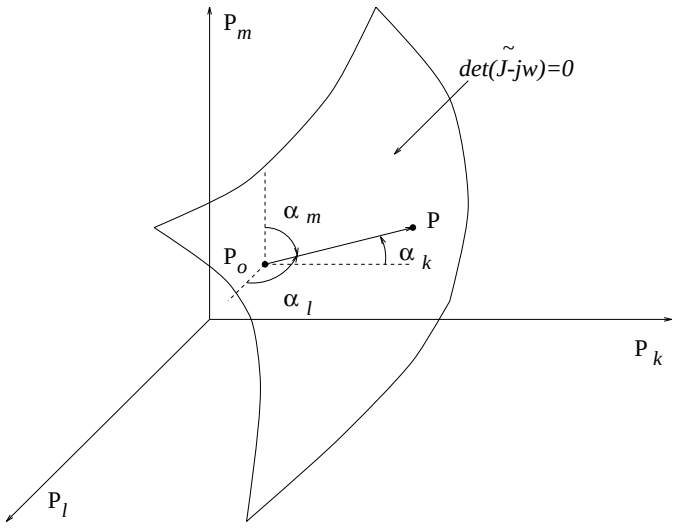

Figure 3.1: The Critical Distance in the Space of Controlled Parameters.

The aim of the method is to find a point at the stability boundary closest to the current operation point p_0 in the parameter space of p as shown in Figure (3.1). This point should satisfy the minimum distance condition:

$$f_{obj} = ||p - p_0|| \rightarrow \min_{x,p} \tag{3.6}$$

and the constraints listed in equations (3.4),(3.5) plus a nontrivial condition by setting the $i-th$ element of one of the eigenvectors to be:

$$\dot{r_i} = 1 + j0 \tag{3.7}$$

The solution presented here has strong points of contact with with earlier work, particularly in the Russian literature [85, 86, 88, 89] and work by Dobson [4, 42, 43, 47]. Some further refinements have been made here.

To solve the optimization problem given by equations (3.4) –(3.7) the Lagrange function method can be employed to transfer the constrained problem into an unconstrained one. The Lagrange function takes the form given below,

$$\begin{aligned} \mathcal{L} &= \frac{1}{2}\|p - p_0\|^2 + f^t(x,p)v + [J_s(x,p)r' + \omega r'']^t l' - \\ &\quad -[J_s(x,p)r'' - \omega r']^t l'' + (r_i' - 1)w_1 + r_i'' w_2, \end{aligned} \tag{3.8}$$

where $p \in R^k$, $v \in R^n$, $l', l'' \in R^m$, and $w_1, w_2 \in R^1$ are Lagrange multipliers.

The solution set $\{x, p, v, r', r'', l', l'', \omega, w_1, w_2\}$ must satisfy the conditions below in order to be extrema of the Lagrange function (3.8),

$$\frac{\partial \mathcal{L}}{\partial p} = p - p_0 + \left[\frac{\partial f}{\partial p}\right]^t v + [\frac{\partial s}{\partial p}]^t = 0 \tag{3.9}$$

$$\text{where} \quad \mathrm{s(x,p)} := r''^t J_s{}^t(x,p) l' - r'''^t J_s{}^t(x,p) l''$$

$$\frac{\partial \mathcal{L}}{\partial x} = J^t(x,p)v + [\frac{\partial s}{\partial x}]^t = 0 \tag{3.10}$$

$$\frac{\partial \mathcal{L}}{\partial \omega} = r'''^t l' + r'^t l'' = 0 \tag{3.11}$$

$$\frac{\partial \mathcal{L}}{\partial r'} = J_s{}^t(x,p) l' + \omega l'' + w_1 e_i = 0 \tag{3.12}$$

$$\frac{\partial \mathcal{L}}{\partial r''} = J_s{}^t(x,p) l'' - \omega l' - w_2 e_i = 0 \tag{3.13}$$

$$\frac{\partial \mathcal{L}}{\partial v} = f(x,p) = 0 \tag{3.14}$$

$$\frac{\partial \mathcal{L}}{\partial l'} = J_s(x,p) r' + \omega r'' = 0 \tag{3.15}$$

$$\frac{\partial \mathcal{L}}{\partial l''} = J_s(x,p) r'' - \omega r' = 0 \tag{3.16}$$

$$\frac{\partial \mathcal{L}}{\partial w_1} = r_i' - 1 = 0 \tag{3.17}$$

$$\frac{\partial \mathcal{L}}{\partial w_2} = r_i'' = 0 \tag{3.18}$$

where $J(x,p) = (\frac{\partial f}{\partial x})$ is the Jacobian matrix of (3.4); $e_i = (0, \cdot\cdot, 1, \cdot\cdot, 0)^t$ is the i-th unit vector. The system (3.9) –(3.18) has $k + 2n + 4m + 3$ equations and the corresponding number of unknown variables $\{x, p, v, r', r'', l', l'', \omega, w_1, w_2\}$. The system is similar that used to find the locally closest Hopf bifurcation system given in [42, Section 5]. There are some differences between [42] and the proposed set of equations. The proposed system normally has lower dimension than the system in [42], where all variables are considered as the dynamic ones ($m = n$); however, due to this the corresponding set has $k+6n+2$ equations and unknown variables. But the number of dynamic state variables m is normally less than n. The next distinction is that in [42] the saddle node bifurcations are eliminated from consideration; here they can be obtained from (3.9) –(3.18) simply by putting $\omega = 0$. Note that this method as well as other direct methods meet computational difficulties from calculation of the Jacobian matrix of either J or J_s. Although approximations to these Jacobians can be used, the equations may experience worse convergence problem while being solved. Normally, continuation methods are sufficient to approximate the Hopf

bifurcation points [23].

The equations (3.9) –(3.18) need to be studied carefully to obtain better understanding. First of all, the equations (3.15) and (3.16) are derived from equation (3.5) by separating its real and imaginary parts. These two equations reveal that for $\dot{r} = r' + jr \neq 0$, the state matrix $J_s(x,p)$ has an eigenvalue with zero real part, i.e. $\lambda_i = 0 + j\omega$, and the matrix $[J_s(x,p) - j\omega I]$ has a zero eigenvalue. Note that the matrix I is a identity matrix of the same dimension as $J_s(x,p)$.

Theorem 1 *The values of w_1 and w_2 in equations (3.12) and (3.13) are zero at the solution points of equations (3.9) –(3.18), which means that $\dot{l} = l' + jl''$ is the left eigenvector of $J_s(x,p)$ corresponding to the eigenvalue of $\lambda_i = 0 + j\omega$.*

Proof:

Suppose $\omega \neq 0$, then from (3.15) –(3.18), $r' \neq 0$, and $r'' \neq 0$. multiplying r'^t by equation (3.13),

$$r'^t {J_s}^t l'' - \omega r'^t l' - w_2 r'^t e_i = 0. \tag{3.19}$$

From (3.15) $r'^t {J_s}^t = \omega r''^t$, and from (3.17) $r'^t e_i = 0$, one can conclude

$$\omega(r''^t l'' - r'^t l') = 0. \tag{3.20}$$

On the other hand, from (3.11),

$$r''^t {J_s}^t l' + \omega r''^t l'' + w_1 r''^t e_i = 0. \tag{3.21}$$

As from (3.14) $r''^t {J_s}^t = -\omega r'' t$, and from (3.16) $r''^t e_i = 1$, one can get

$$\omega(r''^t l'' - r'^t l') - w_1 = 0. \tag{3.22}$$

By comparison of (3.20) and (3.22), the conclusion of $w_1 = 0$ can be drawn.

If multiply r'^t by (3.11),

$$r'^t {J_s}^t l' + \omega r'^t l'' + w_1 r'^t e_i = 0. \tag{3.23}$$

By substitution,

$$\omega(r''^t l' + r'^t l'') = 0. \tag{3.24}$$

From (3.12),

$$r'^t J_s{}^t l'' - \omega r'^t l' - w_2 r'^t e_i = 0, \quad (3.25)$$

$$-\omega(r'^t l' + r''^t l'') - w_2 = 0. \quad (3.26)$$

By comparison of (3.24) and (3.26), one can conclude that $w_2 = 0$. In case $\omega = 0$, there exist $r' \neq 0$, $r'' = 0$, and the fact that $w_1, w_2 = 0$ directly follows from equalities (3.22) and (3.26). □

Regarding equations (3.9) –(3.17), it can be concluded that as long as (3.10), (3.17), (3.14) hold, and $J_s(x,p)$ has no equal eigenvalues, the equation (3.9) can be expressed as

$$p - p_0 + 2(r'l' - r''l'')[\frac{\partial \Re(\lambda_i)}{\partial p}]^t = 0. \quad (3.27)$$

This equation helps explain the meaning of (3.9) –(3.17). Equations (3.9) and (3.10), represented as (3.27) with the help of (3.17), provide that the distance vector $(p-p_0)$ has an opposite direction compared to the real part of the sensitivity vector $[\frac{\partial \Re(\lambda_i)}{\partial p}]$. The dynamic stability domain is restricted by the surface where $\Re(\lambda_i) = 0$. The sensitivity vector $[\frac{\partial \Re(\lambda_i)}{\partial p}]^t$ is a normal vector with respect to the boundary. Thus:

Theorem 2 *The critical distance vector corresponds to one of the normal vectors of the stability domain boundary.*

Proof:

Suppose that (x,p) satisfies (3.14). The Implicit Function Theorem gives

$$J(x,p)(\frac{dx}{dp}) + (\frac{\partial f}{\partial p}) = 0. \quad (3.28)$$

By transposing of (3.28) and multiplying by $v \neq 0$, $v \in R^n$,

$$[\frac{dx}{dp}]^t J^t(x,p)v + [\frac{\partial f}{\partial p}]^t v = 0. \quad (3.29)$$

Let v satisfy (3.10). Then apply (3.10) and (3.29) in (3.9),

$$p - p_0 + [\frac{dx}{dp}]^t [\frac{\partial s}{\partial x}]^t + [\frac{\partial s}{\partial p}]^t = 0, \text{ or} \quad (3.30)$$

$$p - p_0 + 2\left\{\frac{\partial}{\partial p}\left[r'^t J_s{}^t(x,p)l' - r''^t J_s{}^t(x,p)l''\right]\right\}^t = 0 \quad (3.31)$$

Consider the second term in (3.31). It is known that the sensitivity of eigenvalues with respect to p is

$$\frac{\partial \lambda_i}{\partial p} = (\dot{r}^t \dot{l})^{-1} \dot{r}^t [\frac{\partial J_s}{\partial p}]^t \dot{l} \tag{3.32}$$

if all eigenvalues are different. From (3.32),

$$(r'^t l' - r''^t l'') \frac{\partial \Re(\lambda_i)}{\partial p} = r'^t [\frac{\partial J_s}{\partial p}]^t l' - r''^t [\frac{\partial J_s}{\partial p}]^t l'' \tag{3.33}$$

if (3.17) is true. In (3.31) all variables can be considered as independent ones, and (3.31) becomes (3.27). □

Equation (3.14) is the load flow equation which determines the system equilibrium conditions. Equations (3.17) and (3.18) are non-trivial conditions to prevent solution convergence to trivial solutions at $p = p_0$, and $v, \dot{r}, \dot{l}, w_1, w_2 = 0$.

The problem formulated in equations (3.9) –(3.18) is of large dimension, i.e. $k + 2n + 4m + 3$ as stated before, and thus carries with it difficulties for solution. This large dimension requires more computational costs, which may result in unfavorable effects on some of its practical applications. There are ways to reduce the dimension of the problem:

- Reduce the system dimension by mathematical transformation.

  As described in verification of conclusions concerning equations (3.9) –(3.11), it is possible to eliminate the vector v and equation (3.10). Then the system dimension can be reduced to $k + n + 4m + 3$. Also, in case $\omega \neq 0$, the vectors r'' and l'' can be expressed by equations (3.13) and (3.16) and substituted into all other equations, thus reduces the system dimension further to be $k + n + 2m + 3$.

- Equivalence conditions can help reduce the system.

  By an equivalence approach to the load flow condition in (3.14), the value of n can be decreased. In addition, equivalence of the dynamic portion can help reducing the value of m.

- Sparse matrix techniques can be applied to deal with the Jacobian matrix.

  The equations (3.9) –(3.18) contain many zero entries. The technique can speed up computations to solve the problem.

The solutions to the problem (3.9) –(3.18) corresponding to points on the bifurcation surface are characterized by $\Re(\lambda_i) = 0$. This surface can have a very complicated structure, and may cause a series of problems while locating it. For a given point p_0 there are a set of vectors normal to the surface, and all of them are solutions to (3.9) –(3.18). They represent local and global optima of the distance function $||p-p_0||^2$. To locate the closest one, proper choice of the initial value of the unknown variables is a necessity. Further, the surface bounds domains with certain numbers of non-zero real part eigenvalues, together with those with zero real part eigenvalues. Solution of the system (3.9) –(3.18) can produce all of them, so special numerical methods will be needed to get the right answer, i.e. find only the distance vectors to the part of the surface which contains the domain with zero real part eigenvalues. This numerical method requires checking of the determinant of matrix, i.e.. if $det(M(\omega_*, p)) = 0$. It will be discussed later in this chapter.

Newton-Raphson like methods are required to solve the problem (3.9) –(3.18), which involves computation of the Jacobian matrices. In cases when the algebraic part of the system equations f_2 given in (3.2) are dependent on the parameter p, the elimination of the state matrix (3.3) can cause a very complicated dependence relationship between J_s and p. Consequently, some parts of the Jacobian matrix of (3.9) –(3.18) have to be computed numerically. The multiple recalculation of (3.3) will take up lots of computation. Techniques employing higher order numerical methods dealing with the problem can be efficient by reducing the recalculations of the Jacobian matrix. Two possibilities to help increase computation efficiency are to use (1) simplified analytical representations of the state matrix for the equations (3.9) –(3.18), or (2) the numerical calculation of the state matrix by differences of the system states.

3.3.1 The Critical Distance Problem in The Space of Generator Control Gains

A particular task for locating the closest distances to the stability boundary is studied to illustrate the methods of solution to the critical distance problem and difficulties which may arise. The task is to define the most dangerous change of generator control gains which put the system close to or on the Hopf or saddle node bifurcation boundaries. The solution presented here introduces a convenient determinant minimization formulation for finding a point on the stability boundary.

The critical distance vector in this case shows how close the current tuning of control gains is to the stability boundaries. Projections of the critical distance vector $(p-p_0)$ along p_i, $p=(p_1,\cdots,p_k)^t$, indicate influences of tunings on stability properties. They give an alternative view of the parameter sensitivity concept. The traditional understanding of sensitivity is $(\frac{\partial \Re(\lambda_i)}{\partial p})$ taken at $p=p_0$. It might give misleading information as it is not clear which eigenvalue will cross the imaginary axis first, and the sensitivity can change both its value and even its sign under large changes of p. The critical distances based definition of sensitivity does not cause these problems, and it gives another way of achieving locally optimal changes of p.

We firstly derive the critical distance equations to a reduced form. The following assumptions are made for the analysis:

- The gains p do not affect the load flow conditions, i.e. $f_2(x,p)$ is not dependent upon p.
- Gains linearly appear in the dynamic state matrix, so that the state matrix can be expressed as,
$$J_s(p)=\sum_{i=1}^{k} J_i p_i + J_0 \tag{3.34}$$
- The operating point p_0 lies inside the stability domain, $Re\lambda_i < 0,\ i=1,\cdots,m$.

From the first two assumptions, the Lagrange function (3.8) becomes

$$\begin{aligned}\mathcal{L} &= 0.5\|p-p_0\|^2 + [J_s(p)r' + \omega r'']^t l' - \\ &\quad [J_s(p)r'' - \omega r']^t l'' + (r_i'-1)w_1 + r_i'' w_2,\end{aligned} \tag{3.35}$$

and the optimality conditions are reduced to

$$\frac{\partial \mathcal{L}}{\partial p} = p - p_0 + [\frac{\partial s}{\partial p}]^t = 0 \quad (3.36)$$

$$\frac{\partial \mathcal{L}}{\partial \omega} = r'''^t l' + r'^t l'' = 0 \quad (3.37)$$

$$\frac{\partial \mathcal{L}}{\partial r'} = J_s{}^t(p) l' + \omega l'' + w_1 e_i = 0 \quad (3.38)$$

$$\frac{\partial \mathcal{L}}{\partial r''} = J_s{}^t(p) l'' - \omega l' - w_2 e_i = 0 \quad (3.39)$$

$$\frac{\partial \mathcal{L}}{\partial l'} = J_s(p) r' + \omega r'' = 0 \quad (3.40)$$

$$\frac{\partial \mathcal{L}}{\partial l''} = J_s(p) r'' - \omega r' = 0 \quad (3.41)$$

$$\frac{\partial \mathcal{L}}{\partial w_1} = r_i' - 1 = 0 \quad (3.42)$$

$$\frac{\partial \mathcal{L}}{\partial w_2} = r_i'' = 0 \quad (3.43)$$

where $s(p) = r'^t J_s{}^t(p) l' - r'''^t J_s{}^t(p) l''$. The system (3.36) –(3.43) has $k + 4m + 3$ equations and the same number of unknown variables. Equations (3.36) –(3.41) are quadratic equations. The system given in equations (3.36) –(3.43) can be represented in a more compact form as

$$\underline{g}(z) = 0, \; z = (p^t, \omega^t, r'^t, r'''^t, l'^t, l'''^t, w_1^t, w_2^t)^t \quad (3.44)$$

To solve (3.44), several stages are now proposed:

Stage A. Locate a Point of the Stability Boundary with $\omega \to \omega_*$

We aim to find the point on the stability boundary associated with the critical distance to the boundary where an oscillatory mode becomes unstable, and the frequency of the mode ω is close to a given pre-set value of ω_*. The value ω_* can be chosen based on physical considerations. For example, if the inter-area oscillations are to be studied, then ω_* should be taken from 0.1 to 1 Hz, which is the normal range of inter-area oscillatory characteristic frequency.

To overcome the solution difficulties caused by the complexity of the bifurcation surface, a good initial estimation of z in (3.44) is required. The desired point satisfies [47, 136]

$$d(\omega_*, p) := detM(\omega_*, p) = 0 \quad (3.45)$$

$$\text{where } M(\omega,p) \quad = \quad \begin{pmatrix} \omega I & J_s(p) \\ J_s(p) & -\omega I \end{pmatrix} \tag{3.46}$$

The fundamental point of this first step technique relies on the variation of p along the gradient of $d(\omega,p)$ to get p close to singularity of $M(\omega_*,p)$ as shown in equation (3.45). It is realized by an iterative process given in the formula

$$p^{(i+1)} = p^{(i)} + \rho_{(i)} \nabla_p d(\omega_*, p^{(i)}) \tag{3.47}$$

where $\rho_{(i)}$ is the step length at the i-th iteration, and $\nabla_p d(\omega_*, p^{(i)})$ is the gradient of $d(\omega_*,p))$ computed at $p = p^{(i)}$. The step $\rho_{(i)}$ can be chosen, for example, as

$$\rho_{(i)} = -\xi_{(i)} \frac{d(\omega_*, p^{(i)})}{||d(\omega_*, p_0)||} \tag{3.48}$$

where ξ_i is the step factor. It should be very small initially, and then increased if subsequent changes of $d(\cdot)$ are not big enough or decreased if the determinant increases or changes its sign. The ratio $\frac{d(\omega_*,p^i)}{||d(\omega_*,p_0)||}$ provides continuous decrease of the step ρ_i to prevent passing of the solution point (3.45). Numerical experiments show that sufficiently good guesses of (3.45) are obtained when $d(\omega_*, p^{(i)})$ becomes several orders less than $d(\omega_*, p_0)$. A way of computing of $\nabla_p d(\omega_*, p^i)$ in (3.47) is given below.

Stage B. Computation of $\nabla_p d(\omega_*, p^{(i)})$ in (3.47)

Based on equations (3.34) and (3.46), the matrix $M(\omega,p)$ can be represented as

$$M(\omega,p) = \sum_{i=1}^{k} M_i p_i + M_\omega \omega + M_0, \text{ where} \tag{3.49}$$

$$M_i = \begin{pmatrix} 0 & J_i \\ J_i & 0 \end{pmatrix}, i = 0, \cdot\cdot k, \text{ and } M_\omega = \begin{pmatrix} I & 0 \\ 0 & -I \end{pmatrix} \tag{3.50}$$

are constant $(2m \times 2m)$ matrices. As from the Schur Lemma, for $\omega = \omega_*$, and $p = p_0 + \Delta p,\ \Delta p \to 0$,

$$\frac{d(\omega_*,p)}{d(\omega_*,p_0)} \to 1 - \sum_{i=1}^{k} \Delta p_{0i} \sum_{j=1}^{m} e_j^t M^{-1}(\omega_*,p_0)\mu_{ij}, \tag{3.51}$$

where e_j is the j-th unit vector, μ_{ij} is the $j-th$ column of the matrix M_i. Further, it is clear that

$$\sum_{j=1}^{m} e_j^t M^{-1}(\omega_*,p_0)\mu_{ij} \quad = \quad Tr\{M^{-1}(\omega_*,p_0)M_i\} \text{ and} \tag{3.52}$$

$$d^{-1}(\omega_*,p_0)\nabla_p d(\omega_*,p) \quad = \quad -Tr\{M^{-1}(\omega_*,p_0)M_i\} \tag{3.53}$$

The last formula can be applied at each iteration of (3.47). As M_i contains few nonzero elements, (3.53) requires several solutions of the linear system $LUy = \mu_{ij}$, where L and U are lower and upper sparse triangular matrices, $LU = M(\omega_*, p_0)$, for all nonzero columns μ_{ij}. The determinant $d(\omega_*, p_0)$ is calculated as a product of diagonal elements of U.

Stage C. Validity Check of the Stability Boundary Points

Having a point on the surface characterized by $\Re(\lambda_i) = 0$, it is necessary to check whether it belongs to the stability domain boundary or not. As stated before, this point may correspond to the surface restricting unstable domains with distinct but nonzero numbers of the right hand plane eigenvalues. To check the situation of the point, a similar method as in Section (3.3.1) is used.

Suppose there exists an initial guess of p_* which is close to a point p of the boundary where $detM(\omega_*, p) = 0$. Define Δp as $p_* - p_0$, and consider the line $p_0 + \gamma\Delta p$. Starting from $\gamma = 0$, and $\omega = \omega_*$, the task to search for γ and ω which satisfy the conditions below,

$$d(\omega, \gamma) = \det M(\omega, \gamma) = 0 \tag{3.54}$$

The iterative formulae similar to (3.47) are used, i.e.

$$\gamma^{(i+1)} = \gamma^{(i)} + \rho_{(i)}(\frac{\partial d}{\partial \gamma}) \tag{3.55}$$

$$\omega^{(i+1)} = \omega^{(i)} + \rho_{(i)}(\frac{\partial d}{\partial \omega}) \tag{3.56}$$

where $\rho_{(i)}$ is the step size. Note that the process (3.54) and (3.55) can theoretically converge to any intersection point of the line $p_0 + \gamma\Delta p$ and the bifurcation surface as well as to the local nonzero extrema of $d(\omega, \gamma)$. Those cases were not detected in all our practical computations, where we always got a point of the stability domain boundary. Robustness of the process can be improved by using different steps for γ and ω as in (3.54), (3.55). The partial derivatives in (3.54), (3.55) can be obtained in the way similar to the calculating of $\nabla_p d(\omega_*, p^{(i)})$ in (3.47),

$$d^{-1}(\omega, \gamma)(\frac{\partial d}{\partial \omega}) = Tr\{M^{-1}(\omega, \gamma)M_\omega\} \tag{3.57}$$

$$d^{-1}(\omega, \gamma)(\frac{\partial d}{\partial \gamma}) = Tr\{M^{-1}(\omega, \gamma)M_\gamma\} \tag{3.58}$$

where $M_\gamma = \sum_{i=1}^{k} M_i$.

Stage D. Refinement for Initial Values of p, ω, $\dot{r}$, $\dot{l}$, w_1, and w_2

The former procedures should have already provided rather good estimates of p and ω. However, the initial values of $\dot{r}$, $\dot{l}$, w_1, and w_2 are also necessary for solution of equations (3.36) –(3.43) as well. Basically, they can be taken from the solutions to the original system for either saddle node or Hopf bifurcation conditions. The estimation of $\dot{r} = r' + jr''$ can be obtained as the solution of the linear system (3.40) – (3.43). Further improvement can be achieved by solution of the set of equations below,

$$J_s(p_0 + \gamma\Delta p)r' + \omega r'' = 0 \tag{3.59}$$

$$J_s(p_0 + \gamma\Delta p)r'' - \omega r' = 0 \tag{3.60}$$

$$r_i' - 1 = 0 \tag{3.61}$$

$$r_i'' = 0 \tag{3.62}$$

Direct solution of (3.59) –(3.62) without the steps **A** concerning $\omega \to \omega_*$ and **C** giving a validity check of the solutions typically leads to substantially more computation. For the considered problem, the correct choice of Δp is very difficult, and numerical methods might converge badly or not converge at all. Similarly, the initial value of the left eigenvector $l = l' + jl''$ can also be obtained. While, as can be recalled from the former sections, the remaining variables, w_1 and w_2 are zeros as explained in the proof of Theorem 1.

Stage E. Solution of The Critical Distance System (3.36) –(3.43)

To solve the system (3.36) –(3.43), the high order numerical method addressed in detail in Appendix (B.1) can be effectively used. The high order numerical method is used from the initial point obtained in earlier steps and provide further motion along the solution domain Σ. This method may be considered as either a generalization of the Newton-Raphson method including nonlinear terms of the Taylor series, or a parameter continuation technique providing more reliable solution properties.

It has the following advantages [104]:

1. Minimal number of iterations and re-computations of the Jacobian matrix.

2. Reliable solution of nonlinear algebraic problems up to points of singularity.

3. Convergence to a singular point of the problem if it occurs on the way of the iterative process.

4. Straight motion of the iterative process in the space of mismatches.

5. Retention of zero components of mismatch functions.

The feature (1) minimizes computations related to numerical evaluation of the Jacobian matrices of (3.9) –(3.18). The properties (2) and (3) ensure reliable performance of the step E. , and give an opportunity to localize singular points of (3.9) –(3.18) or (3.36) –(3.43). Having a singular point, it is possible to skip it by additional changing of ω in the direction of its variation on iterations, and repeating of the procedure starting from the step 3.3.1. The properties (4) and (5) provide motion of the iterative process along the bifurcation boundary and load flow constraints once (3.12)-(3.16) or (3.38) –(3.41) satisfy to the initial guesses [108].

Once the critical distance point is obtained, it is necessary to execute the step of validity checking to make sure that this point belongs to the stability boundary. If validity checking gives a closer point, this normally means that the previous point belongs to the surface restricted domains with unstable eigenvalues, and the search is to be continued by repeating the steps of validity checking, initial value refinement, and numerical solving of the system.

3.3.2 Numerical Testing of Determinant Minimization Techniques

The developed technique for generator gains was tested on the 10 generator, 39 bus New England Test System [16] shown in Figure 3.2. The used mathematical models contain 78 algebraic and 89 differential equations (Case 1), and 79 algebraic and 93 differential equations (Case 2). In the Case 1, the critical distances were found in the space of AVR voltage gains K_A of generators 1,2,..9. As each of the parameters K_A has its own range of variation, a normalization of K_A is required. After the normalization, the problem is represented in the space of rated values of K_A corresponding to current positions of regulator knobs. The maximal values of K_A should be taken as a base. As the information about ranges of K_A is omitted in [16], we take the bases of K_A as twice the initial value of each parameter. It

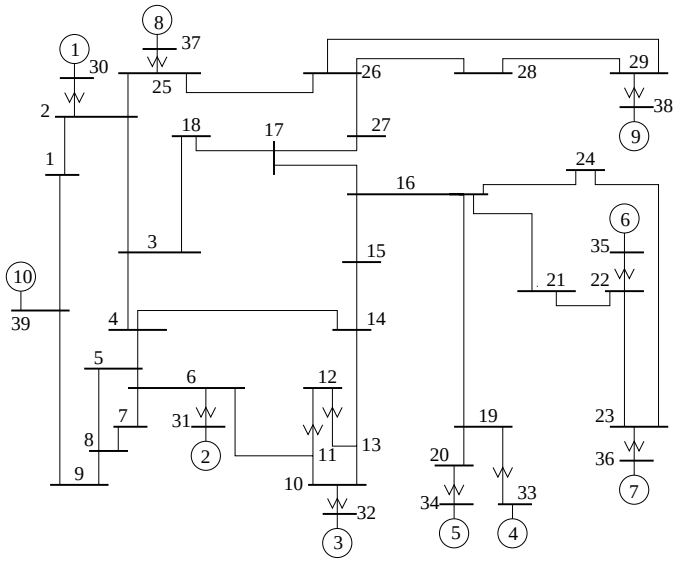

Figure 3.2: The Structure of New England 39-Bus Test System

is obvious that $K_{Amin} = 0$. By using the proposed technique, we have got several critical distance vectors in the 9-th dimensional space of K_A. Four of them are given in Table (3.1). The solutions 1 and 2 have a simple interpretation. They correspond to aperiodic instabilities caused by negative signs of K_A and forming of positive feedbacks. The solutions 1 and 2 illustrate a possibility to get points of the aperiodic stability boundary from the system (3.36) –(3.43). However, they indicate the necessity to take into consideration the controlled parameter constraints as well.

The solutions 3 and 4 are more interesting from the physical point of view, and they are not so obvious. They indicate generators which are responsible for excitation of unstable modes with frequencies close to the given initial guesses. They refer to generators 9, 5, 7 and 4 (solution 3), and the generator 9 (solution 4). In the last case, the gains of generators 1,..,8 have relatively small influence on stability at frequencies being close to 0.9 Hz.

To give a more pictorial illustration of the proposed technique, we consider the *Case 2* where the critical distances are defined on the plane of PSS gains. For that purpose we add a PSS and change the AVR model at generator 9 -see Figure (3.3). The parameters are given at base 100 MVA. We use the additional normalization in such a way, that 1 p.u. of power (K_p) and frequency (K_w) gains correspond to maximal values of parameters (0.1 p.u. and 30 p.u. at 100 MVA base respectively). The bifurcation boundary for the frequency range 0.5...1.8 Hz is plotted on the

Gene-rators	Basic values of K_A	Initial values of gains	Solutions			
			1	2	3	4
1	10	0.5	0.5	0.5	0.996	0.503
2	12.4	0.5	0.5	0.5	0.743	0.502
3	10	0.5	0.5	0.5	0.796	0.502
4	10	0.5	0.5	0.5	1.135	0.495
5	80	0.5	0.5	0.5	1.630	0.636
6	10	0.5	0.5	0.5	1.019	0.501
7	80	0.5	0.5	-0.077	1.345	0.505
8	10	0.5	0.5	0.5	0.668	0.503
9	80	0.5	-0.018	0.5	1.849	2.295
Guess of frequency, Hz			0.06	0.1	0.6	0.9
Frequency of solution, Hz			0	0	0.580	0.898
Distance			0.518	0.577	2.21	1.80

Table 3.1: The shortest distance solution in space of AVR gains

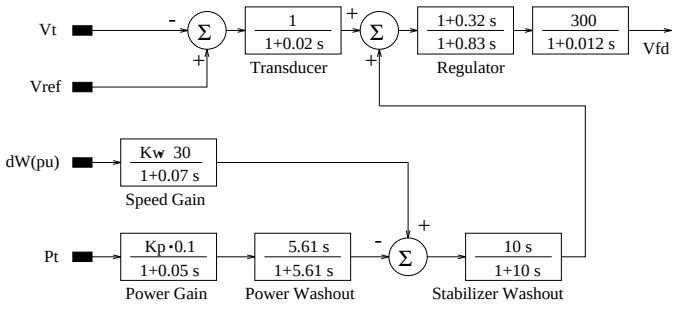

Figure 3.3: The Structure of AVR and PSS of the 9-th Generator

plane of K_w, K_p (3.4). The curve was obtained by using the POISK[1] program [59]. The operating point A corresponds to $K_w = 0.32$, and $K_p = 0.92$. There are 3 solutions of the critical distance problem: B, C, and D. The vectors AB, AC, AD are perpendicular to the stability boundary. The method gives all those solutions depending on the initial guesses of frequency. For instance, we get the solution B ($\omega = 0.52Hz, K_w = -0.177, K_p = 0.934$) for the initial guesses of frequency from $0.5Hz$ to $1.0Hz$. The vector AE is a normal to the bifurcation boundary as well, but the point E is not a solution, as it belongs to the curve separating domains with

[1]POISK is the Russian word for 'Search'; The program had been developed in St. Petersburg and made available by Drs. Maslennikov and Ustinov while visiting Sydney University

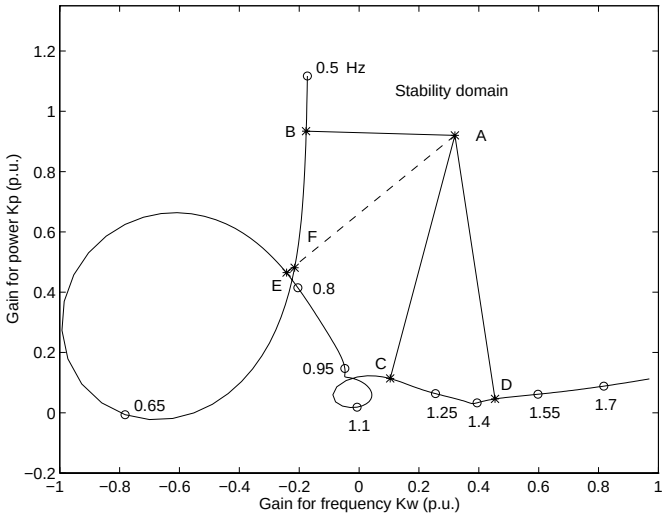

Figure 3.4: Critical Directions in the Plane of PSS Gains

unstable eigenvalues. This point is obtained at step E. for the initial frequencies ω_* from 0.67 to 1.0 Hz. The point F is computed on steps 3.3.1 and 3.3.1. After that step E. is repeated starting from the point F, and the solution B is obtained. The solution B is not practicable as it corresponds to the negative frequency gain K_w. The actual solutions C and D indicate that decreasing of power gain K_p is dangerous for stability. Changes of K_w have an influence on damping of oscillations, but they can not cause instability.

3.4 Initial Value Approximation Techniques

To solve the problem of locating the bifurcation boundaries, initial guessed variable values are necessary for the optimization procedure. Traditionally, as described in Section 3.2, load flow computation is performed along some specified system parameter variation direction, and system state matrix eigenvalue calculation is performed at the same time to observe the eigenvalue behavior. Computation costs are dependent on choice of parameter variation direction, which is normally based on experience or on a trial and error basis. In this section, we show how the bifurcation point in a particular direction can be estimated approximately.

3.4.1 Sensitivity-based Technique

Now we show that the bifurcation point can be located approximately with an eigenvalue sensitivity based technique. This point and the system parameter values associated with it, can be used as the initial guess values for the optimization problem to locate the closest distance point to instability. Again, the ideas are developed from some in the Russian literature [60, 116]. The essential steps are:

- The system to be studied is modeled as,

$$f(x, p_0 + \tau\Delta p) = 0 \tag{3.63}$$

$$F(x, p, J, \dot{r}, l, w) = 0 \tag{3.64}$$

$$\dot{r}_i - 1 = 0 \tag{3.65}$$

  where $F(J, \dot{r}, l, w) = 0$ stands for all the optimization equations concerning system state variables, parameters, state matrix, eigenvalues, and eigenvectors as described in (3.9 –3.18).

- Suppose at some initial load flow equilibrium point, the system variables are $X = X_0$ and the bifurcation parameters $\tau = \tau_0$ are known. At this point, compute the eigenvalues, $\lambda_i = \alpha_i + j\omega_i$ and corresponding left and right eigenvectors, L_i and R_i.

- Select the most important eigenvalues (say, corresponding to inter-area oscillations or aperiodic modes of interest) among the λ_i.

- For each λ_i chosen (or just for the most sensitive one) execute the following procedure. Compute the damping sensitivity as in [50]:

$$\frac{\partial \alpha_j}{\partial \tau_i} = \Re\left\{\frac{L_j^t \frac{\partial J_s}{\partial \tau_i} R_j}{L_j^t R_j}\right\} \tag{3.66}$$

By linear approximation of the function $\alpha_i(\tau)$, an increment of τ which gives zero real part of the selected eigenvalue λ_i can be assessed as following:

$$\Delta\tau = t(-\alpha_i)\frac{\partial \alpha_i}{\partial \tau}, \tag{3.67}$$

where t is the step parameter. Then compute a new value of τ as $\tau_1 = \tau_0 + \Delta\tau$, recalculate the operating point to get a new vector X_0, and repeat this step until the value of α_i becomes small enough. A graphical illustration of the technique is given in Figure 3.5.

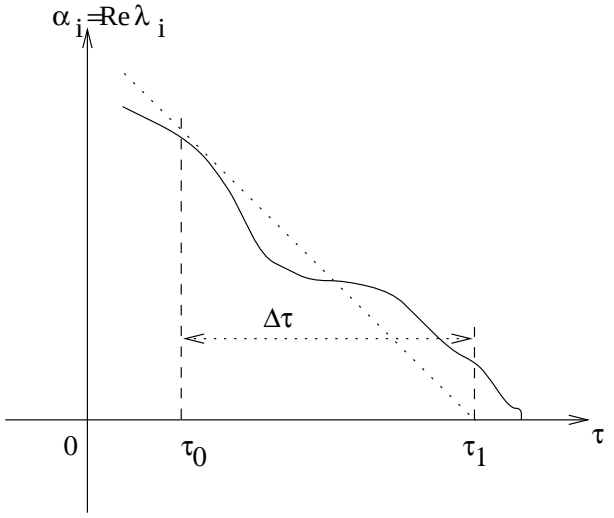

Figure 3.5: Estimation of the initial bifurcation point

In the procedure, it is necessary to follow the chosen eigenvalue which is likely to become purely imaginary or zero. At each iteration, a decision must be made about the correspondence of newly obtained eigenvalues to the ones at previous step. Incorrect tracking may pose obvious difficulties. In the tracking step, either linear forecasts of eigenvalue imaginary parts or analysis of eigenvectors can be used. Numerical studies reported below show a good and fast convergence of this technique.

This approach is used as an ancillary technique to get initial points on the small signal stability boundary. However for more complicated systems, where there are many eigenvalues to be tried one by one, other techniques will have to be tried to locate the initial points of interest. Among these techniques, Genetic Algorithms(GA) is promising for locating the globally closest distance point to instability as well as local points which can be chosen as approximation solutions; numerical methods can then be employed to find the exact solution points. The use of GA in small disturbance stability problems is considered in Chapter 5.

3.4.2 Testing of The Initial Value Approximation Technique

The method has been applied to a model power system composed of one generator, one infinite bus and a load bus feeding a motor load and connected with a shunt capacitor [33]. The system is shown in Figure 3.6.

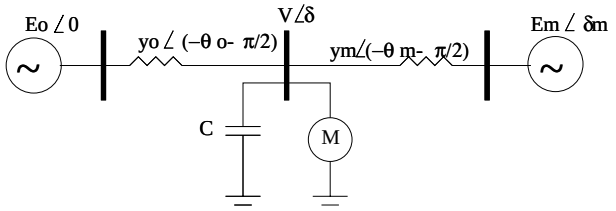

Figure 3.6: The Single Machine Infinite Bus with Induction Motor Load Power System

The model consists of four differential equations (3.68) –(3.71), which cover both generator and load dynamics. The mathematical model of the system is the following:

$$\dot{\delta_m} = \omega \tag{3.68}$$

$$\begin{aligned} M\dot{\omega} &= -d_m\omega + P_m + \\ &\quad + E_m y_m V sin(\delta - \delta_m - \theta_m) + \\ &\quad + E_m^2 y_m sin\theta_m \end{aligned} \tag{3.69}$$

$$\begin{aligned} K_{qw}\dot{\delta} &= -K_{qv2}^2 V^2 - K_q v V + \\ &\quad + E_0' y_0' V cos(\delta + \theta_0') + \\ &\quad + E_m y_m V cos(\delta - \delta_m + \theta_m) - \\ &\quad - (y_0' cos\theta_0 + y_m cos\theta_m)V^2 - \\ &\quad - Q_0 - Q_1 \end{aligned} \tag{3.70}$$

$$\begin{aligned} k_4\dot{V} &= K_{pw}K_{qv}^2 V^2 + (K_{pw}K_{qv} - K_{qw}K_{pv})V + \\ &\quad + \sqrt{K_{qw}^2 + K_{pw}^2}[-E_0' y_0' V cos(\delta + \theta_0 - h) - \\ &\quad - E_m y_m V cos(\delta - \delta_m + \theta_m - h) + \\ &\quad + (y_0' cos(\theta_0 - h) + y_m cos(\theta_m - h))V^2] - \end{aligned}$$

$$-K_{qw}(P_0 + P_1) + K_{pw}(Q_0 + Q_1) \tag{3.71}$$

where $k_4 = TK_{qw}K_{pv}$ and $h = tan^{-1}(K_{qw}/K_{pw})$. Parameters of the system are the following [33]: $K_{pw} = 0.4$, $K_{pv} = 0.3$, $K_{qw} = -0.03$, $K_{qv} = -2.8$, $K_{qv2} = 2.1$, $T = 8.5$, $P_0 = 0.6$, $Q_0 = 1.3$; P_1 and Q_1 are taken zero at the initial operating point.

Network and generator values are: $y_0 = 20.0$, $q_0 = -5.0$, $E_0 = 1.0$, $C = 12.0$, $y_0' = 8.0$, $\theta_0' = -12.0$, $E_0' = 2.5$, $y_m = 5.0$, $\theta_m = -5.0$, $E_m = 1.0$, $P_m = 1.0$, $M = 0.3$, $\delta_m = 0.05$.

All parameters are given in per unit except for angles, which are in degrees. The active and reactive loads are featured by the following equations:

$$P_d = P_0 + P_1 + K_{pw}\delta + K_{pv}(V + T\dot{V}) \tag{3.72}$$

$$Q_d = Q_0 + Q_1 + K_{qw}\delta + K_{qv}V + K_{qv2}V^2 \tag{3.73}$$

The system (3.68) –(3.71) depends on four state variables δ, δ_m, ω, V. Their values at the initial load flow point are the following: $\delta = 2.75$, $\delta_m = 11.37$, $\omega = 0$, and $V = 1.79$. Note that the initial point is not a physical solution; the voltage V is too high as Q_1 is zero.

Starting from the normal operation point, the first bifurcation point approximation is thus obtained by forcing the real part system Jacobian eigenvalue to zero. So either Saddle or Hopf bifurcations corresponding to aperiodic or oscillatory stability characteristic points can be approximated by applying this technique. The graph shown below in Figure 3.7 gives the eigenvalue real part trajectory leading to bifurcations. It can be seen very clearly that the technique works very efficiently, after 4 or 5 iterations, the approximated point is very close to the real solution, which can be either saddle node or Hopf bifurcations. By following this procedure, the work of deciding the initial value for the later optimization procedure can be greatly reduced.

3.5 Direct vs Indirect Methods

Our goal is to present a comprehensive framework for computing small signal stability characteristics. Before this it is useful to review some key ideas obtained in

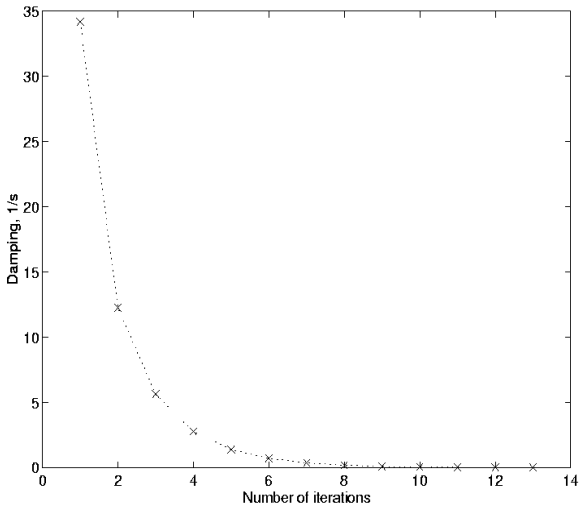

Figure 3.7: The Trajectory of Eigenvalue Real Part Leading to a Bifurcation Point.

prior work.

Dobson et al. has developed methods for locating the closest bifurcations by using iterative and direct methods in the multidimensional parameter space [42, 44]. Similar approaches also had been reported by Makarov et. al in [66, 108, 110]. These methods are based on a matrix singularity property, which is worth examining in greater depth.

3.5.1 Matrix Singularity Property

For a physical system modeled by nonlinear differential and algebraic equations of the form of equation (3.4), which after eliminating the algebraic equations can be written as

$$\dot{x} = f(x, p) \quad \text{where } x \in R^n, \text{ and } \quad p \in R^m, \ m \geq 2$$

where the state variable vector x represents the dynamic static variables.

The problem of locating the closest bifurcation points on the parameter space depends on the normal vectors at the bifurcation hyper surfaces.They can be evaluated from the eigenvalues and eigenvectors of the system Jacobian [44, 108].

For saddle node bifurcations, the transversality conditions ensure the eigenvalue

moves from left hand plane into the right hand plane as defined in [42, 136],

$$l_* f_p|_* \neq 0 \tag{3.74}$$

$$l_* f_{xx}(r_*, r_*)|_* \neq 0 \tag{3.75}$$

where l_* and r_* are the right and left eigenvectors of the system Jacobian $f_x|_*$ corresponding to the zero eigenvalue, and the subscript $_*$ denotes that all values are taken at (x_*, p_*). We take $\sum_T^{SN}$ as the set of $p_* \in \sum^{SN}$ for which the system has a saddle node bifurcation at (x_*, p_*) with $f_x|_*$ having a unique simple zero eigenvalue and satisfying the transversality conditions given above. Under the condition of $p_* \in \sum_T^{SN}$, it had been proven in [37] that there exists an open set $V_{SB} \ni p_*$ so that $\sum_T^{SB} \cap V_{SB} = \sum^{SB} \cap V_{SB}$, and $\sum_T^{SB} \cap V_{SB}$ is a smooth hypersurface. The bifurcation equilibrium near x_* are given by the smooth function $\varphi : \sum_T^{SB} \cap V_{SB} \to R^n$ and $\varphi(p_*) = x_*$. Therefore, $\sum^{SB}$ has a normal vector $N(p_*)$ at $p_* \in \sum_T^{SB}$ and with a smooth Gauss map $N : \sum_T^{SB} \to S^{m-1}$, where S^{m-1} is the $m-1$ sphere of unit vectors in R^m. The normal vector for p is

$$N(p_*) = \xi l_* f_p|_* \tag{3.76}$$

where $p_* \in \sum_T^{SN}$ and ξ is a scaling factor whose norm is designated to make $|N(P_*)| = 1$, and sign is chosen so that x will be driven to disappear by changing p along the direction set by $N(p_*)$.

In case of Hopf bifurcations, assign subset $\sum_T^{HB}$ of parameter $p_* \in \sum^{HB}$ where the system has Hopf bifurcation at (x_*, p_*) while the system Jacobian $f_x|_*$ has a pair of eigenvalues $0 \pm j\omega_*$, and $\omega_* \neq 0$. The transversality conditions for $p_* \in \sum_T^{HB}$ are,

$$c \neq 0 \tag{3.77}$$

$$\frac{d\Re[\varphi(p)]}{dp} \neq 0 \tag{3.78}$$

where c is a coefficient of cubic terms in the flow reduced to the center manifold and is a complicated function of triple derivatives of f [61]; and here the system variable x is supposed to be related to the parameter p so that $\varphi(p_*) = x_*$, and $\varphi(p) = x$ and $f(\varphi(p), p) = 0$. It can be reasoned that $\varphi_p = -f_x^{-1} f_p$, provided f_x is non-singular. Also the normalized right and left eigenvectors of f_x are also implicit functions of p, i.e. $l = l(p)$ and $r = r(p)$. It had been given by [37] that there exist an open set $V_{HB} \ni p_*$, so that the common set $\sum_T^{HB} \cap V_{HB} = \sum^{HB} \cap V_{HB}$ is a

smooth hyper surface given by $\Re[x(p)] = 0$. Therefore, the hyper surface $\sum^{HB}$ has a normal vector $N(p_*)$ at $p_* \in \sum_T^{HB}$ with a smooth Gauss map $N : \sum_T^{HB} \to S^{m-1}$,

$$N(p_*) = \zeta \Re[l(-f_{xx} f_x^{-1} f_p + f_{xp})r]|_* \tag{3.79}$$

where ζ is a real scaling factor whose norm is chosen to make unity norm of $N(p_*)$ and whose sign is chosen to ensure that changing of p in the direction of $N(p_*)$ leads to instability of the system equilibrium [42].

The conditions for a closest bifurcation at $p_* \in \sum_T$ depends on the normal vector and the curvature of $\sum_T$ at p_*, where $\sum_T = \sum_T^{SB} \cup \sum_T^{HB}$, and the normal vector $N(p_*)$ gives the map $N : \sum_T \to S^{m-1}$. Let $d(p'_*) = |p'_* - p_0|$ represent the distance vector of p'_* based on the original value of p at p_0. Then a closest bifurcation point to p_0 is a local minimum of d, where $p_* - p_0$ is parallel to $N(p_*)$. The following conditions ensures a point p_* is strictly a local minimum, i.e. the closest bifurcation point [42],

$$d = |p_* - p_0| < \frac{1}{\rho^{max}} \quad \text{if} \quad \rho^{max} > 0 \tag{3.80}$$

where ρ^{max} is the maximum principle curvature of the hyper surface $\sum_T$ at p_*. The equation reveals that the radius $|p_* - p_0|$ of the sphere centered on p_0 must smaller then the minimum radius of curvature $\frac{1}{\rho^{max}}$ of $\sum_T$ at p_*. It has been known [42] that the condition (3.80) is always satisfied if p_0 is close enough to the surface $\sum_T$ or if $\rho^{max} < 0$.

There are established continuation, direct, and iterative methods to compute the closest bifurcation along a ray defined in the parameter space starting from current equilibrium point p_0 [136]. Starting from some ray based at p_0, these methods compute the normal vector $N(p_*)$ with equations (3.76) and (3.79). Then a new ray is formed along the direction defined by $N(p_*)$ and the procedure is iterated until the ray becoming a fixed one, and thus the corresponding parameter value of p_* is obtained as a locally closest bifurcation point.

3.5.2 Iterative Method

Dobson [47] presented an iterative method to locate closest saddle node or Hopf bifurcations in the parameter space by globally minimizing the distance from the current equilibrium p_0 to a series of tangent hyperplane approximations to either

$\sum^{SB}$ or $\sum^{HB}$. The method finds a step direction vector n_r normal to both the bifurcation hypersurface and its tangent hyperplane. The direction n_{r+1} at each new iteration points to a point at the tangent hyperplane closest to p_0

$$p_* = p_0 + t_* n \in \sum \tag{3.81}$$

$$n_{r+1} = N(p_*(n_r)) \tag{3.82}$$

It was also given that the iteration procedure for the fixed solution of n_* and corresponding p_* is exponentially stable if

$$\frac{1}{\rho^{min}} < |p_* - p_0| < \frac{1}{\rho^{max}} \tag{3.83}$$

where ρ^{max} and ρ^{min} are maximum and minimum principle curvatures of the bifurcation hyper surface at p_*. For a not too concave hyper surface $\sum$ at p_0, if this approach converges exponentially to a solution p_*, then p_* indicates a locally closest bifurcation point regarding to the original equilibrium p_0. The second order curvature conditions need to be checked, otherwise, the iterative method may not converge at this point.

3.5.3 Direct Method

Other approaches proposed in [4, 42] are the direct methods, which are aimed to locate the locally closest saddle node and/or Hopf bifurcations. This method is based on solving the set of equations designated to minimize the eigenvalue real part of the system Jacobian.

The equations for directly finding Saddle Node bifurcations are:

$$F^{SN}(x,p,l,\rho) = \begin{cases} f(x,p) & = 0 \\ l f_x & = 0 \\ l f_p (l f_p)^T - 1 & = 0 \\ \rho(p - p_0)^T - l f_p & = 0 \end{cases} \tag{3.84}$$

where l is the left eigenvector, which is scaled to satisfy $l f_p (l f_p)^T = 1$. For a locally closest bifurcation of $\sum_T^{SB}$ at p_*, $p_* - p_0$ is parallel to the normal vector $l_* f_p|_*$, i.e. $l_* f_p|_* - \rho_*(p_* - p_0) = 0$ for some nonzero real ρ_*. Then Newton-type optimization method can be applied to solve the problem given by Equation 3.84. The dimension of the problem is $2n + m + 1$.

Similar methods can be used to locate the closest Hopf bifurcations in the parameter space. The closest Hopf bifurcation location equations are given here for completion [42],

$$F^{HB}(x, p, \omega, r', r'', l', l'', u, \rho) = 0 \tag{3.85}$$

where

$$F^{HB} = \begin{cases} f(x,p) & = 0 \\ f_x| * r' - \omega r'' & = 0 \\ f_x| * r'' + \omega r' & = 0 \\ q^T r' & = 0 \\ r'^T r' - 1 & = 0 \\ (l' f_x|_* - \omega l'')\pi & = 0 \\ (l'' f_x|_* + \omega l')\pi & = 0 \\ l' r' + l'' r'' - 1 & = 0 \\ l' r'' - l'' r' & = 0 \\ f_x|_* u - f_p|_* & = 0 \\ \rho(p - p_0)^T - l'(f_{XX} u + f_{xp})|_* r' - l''(f_{xx} u + f_{xp})|_* r'' & = 0 \end{cases} \tag{3.86}$$

where as in case of Saddle node bifurcations, the last equation in (3.86) represents the parallel conditions for the vector $p_* - p_0$. π is a map C^n onto C^{n-1}. The dimension of the set of equations is $6n + m + 2$, which makes it very difficult to solve if the problem itself has very large number of variables, n.

3.6 A General Method to Reveal All Characteristic Points

In this section, we extend the ideas of locating one or two types of specific characteristic points, e.g. saddle node bifurcation and / or Hopf bifurcation, to a more general procedure, i.e. to locate all of the characteristic points in one approach. Recall from Chapter 1 that there are more characteristic points related to power system stability than saddle node and Hopf bifurcations. These points include,

- load flow feasibility boundaries,
- minimum and maximum damping conditions,

- saddle node and Hopf bifurcations,
- singularity induced bifurcations,
- limit induced bifurcations.

So far the eigenvalue sensitivity approach or matrix minimization approach can only locate one kind of bifurcation conditions for each formulation. The general method here is designed to locate all the small stability characteristic points (with the exception of limit induced bifurcations, which need special optimization techniques such as Genetic Algorithms in order to be located.) alone a ray specified by power system parameters in one optimization approach, provided there are such characteristic points. The problem addressed here, where the system is described by differential and algebraic equations (2.24), is that these different small signal stability conditions correspond to different physical phenomena and mathematical descriptions [96]. Saddle node bifurcations happen where the state matrix $J_s = J_{11} - J_{12}J_{22}^{-1}J_{21}$ becomes singular and, for example, a static (aperiodic) type of voltage collapse or angle instability may be observed as a result. Hopf bifurcations occur when the system state matrix J_s has a pair of conjugate eigenvalues passing the imaginary axis while the other eigenvalues have negative real parts, and unstable oscillatory behavior may be seen. Singularity induced bifurcations are caused by singularity of the algebraic submatrix J_{22}, and they result in fast collapse type of instability [142]. The load flow feasibility boundary corresponds to a surface where the load flow Jacobian matrix J_{lf} is singular, and it restricts a region in the space of power system parameters where load flow solutions exist. Under certain modeling simplifications, this boundary coincides with the saddle node bifurcation conditions [143, 132], but in general case it should be taken into account separately.

To locate the saddle node and Hopf bifurcations along a given ray in the space of p, the following equations can be employed,

$$f(x, p_0 + \tau\Delta p) = 0 \tag{3.87}$$

$$J_s^t(x, p_0 + \tau\Delta p)l' + \omega l'' = 0 \tag{3.88}$$

$$J_s^t(x, p_0 + \tau\Delta p)l'' - \omega l' = 0 \tag{3.89}$$

$$l_i' - 1 = 0 \tag{3.90}$$

$$l_i'' = 0 \tag{3.91}$$

where ω is the imaginary part of a system eigenvalue; l' and l'' are real and imaginary parts of the corresponding left eigenvector l; $l'_i + jl''_i$ is the $i-th$ element of the left eigenvector l; $p_0 + \tau\Delta p$ specifies a ray in the space of p; J_s stands for the state matrix obtained from the linearized model provided that the algebraic submatrix J_{22} is nonsingular.

In the above set, (3.87) is the load flow equation and conditions (3.88)-(3.91) provide an eigenvalue with zero real part and the corresponding left eigenvector.

Solutions of the system (3.87)-(3.91) correspond to either saddle node ($\omega = 0$) or Hopf ($\omega \neq 0$) bifurcations. Nevertheless the extreme load flow feasibility conditions (if they do not coincide with the saddle node bifurcations) can not be located by means of this system. Actually, if the load flow feasibility boundary is met on the ray $p_0 + \tau\Delta p$ but there is no an eigenvalue with zero real part, the system (3.87)-(3.91) becomes inconsistent and has no a solution.

Therefore, if the system (3.87)-(3.91) is used, it is necessary to analyze the load flow feasibility conditions additionally. The corresponding procedures are well known - see [42, 67, 108] for instance. The general idea behind these procedures is illustrated by the following system:

$$f(x, p_0 + \tau\Delta p) = 0 \tag{3.92}$$

$$J^t_{lf}(x, p_0 + \tau\Delta p)l = 0 \tag{3.93}$$

$$l_i - 1 = 0 \tag{3.94}$$

where l is the left eigenvector corresponding to a zero eigenvalue of the load flow Jacobian matrix J_{lf}. The system (3.92)-(3.94) gives the load flow feasibility boundary points along the ray $p_0 + \tau\Delta p$ by a similar way as the system (3.87)-(3.91) generates saddle node and Hopf bifurcation points.

By subsequent solution of both the problems (3.87)-(3.91) and (3.92)-(3.94), the general issue may be resolved, but a challenging task is to find a single procedure which can generate all small-signal characteristic points.

3.6.1 The General Method

To locate the min/max damping points, the saddle node and Hopf bifurcations as well as the load flow feasibility boundary points within one procedure, the following

constraint optimization problem is proposed:

$$\alpha^2 \Rightarrow max/min \tag{3.95}$$

subject to

$$\begin{aligned} f(x, p_0 + \tau\Delta p) &= 0 && (3.96)\\ J_s^t(x, p_0 + \tau\Delta p)l' - \alpha l' + \omega l'' &= 0 && (3.97)\\ J_s^t(x, p_0 + \tau\Delta p)l'' - \alpha l'' - \omega l' &= 0 && (3.98)\\ l_i' - 1 &= 0 && (3.99)\\ l_i'' &= 0 && (3.100) \end{aligned}$$

where J_s is the state matrix, α and ω are real and imaginary part of an eigenvalue of interest λ respectively, $l = l' + jl''$ is the corresponding left eigenvector.

To solve this optimization problem, several methods can be used. For example, to consider the load flow constraint, this constrained optimization problem can be represented with Lagrange function form as

$$\begin{aligned} \Phi &= \alpha^2 + f^t(x, p_0 + \tau\Delta p)\eta \Rightarrow min_{x,\tau,\eta}\\ &= \alpha^2 + \Phi' \Rightarrow min_{x,\tau,\eta} \end{aligned} \tag{3.101}$$

The optimization problem can be depicted by Figure 3.8. Then in each direction defined by input Δp, considering the state variables shown in Figure 3.8, the load flow constraint is computed first, while the state variables, which are to be optimized, provide the input value to set up the state matrix. The eigenvalue computation is then based on this matrix. In the algorithm, the real part of the critical eigenvalue(s) will be used to form the objective function Φ. The value of the objective function f, as the output, will then provide information used to proceed the optimization procedure and the state variables will be adjusted accordingly. When the optimization process converges, all characteristic points along the direction defined by Δy can be located. To locate all these points in the whole plane, a loop is needed to rotate the direction and repeat the optimization procedure along the new direction. By subsequent rotations, we can locate all characteristic points in the whole plane/space of interest. Generally, this plane/space is a cutset of the space spanned by all parameters of interest.

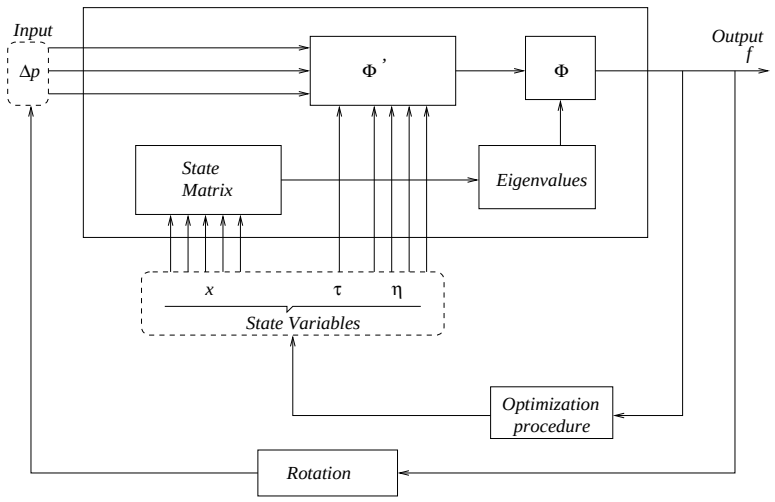

Figure 3.8: System Model Diagram for Small Signal Stability General Method Optimization

The problem may have a number of solutions, and all of them presents different aspects of the small-signal stability problem as shown in Figure 3.9.

The minimum and maximum damping points correspond to zero derivative $\frac{d\alpha}{d\tau} = 0$. The constraint set (3.96) –(3.100) gives all unknown variables at these points. The minimum and maximum damping, determined for all oscillatory modes of interest, provides essential information about damping variations caused by a directed change of power system parameters.

The Saddle Node or Hopf bifurcations correspond to $\alpha = 0$. They indicate the small-signal stability limits along the specified loading trajectory $p_0 + \tau\Delta p$. Besides revealing the type of instability (aperiodic for $\omega = 0$ or oscillatory for $\omega \neq 0$), the constraint set (3.96) –(3.100) gives the frequency of the critical oscillatory mode. The left eigenvector $l = l' + jl''$ (together with the right eigenvector $r = r' + jr''$ which can be easily computed in turn) determine such essential factors as sensitivity of α with respect to p, the mode shape, participation factors, observability and excitability of the critical oscillatory mode [60, 66, 95].

The load flow feasibility boundary points reflect the maximal power transfer capabilities of the power system. Those conditions play a decisive role when the system is stable everywhere on the ray $p_0 + \tau\Delta p$ up to the load flow feasibility boundary. The optimization procedure stops at these points as the constraint (3.96) can not be satisfied anymore. Consider the trajectory of $x(\tau)$, $\tau \to \infty$ satisfying (3.96). At

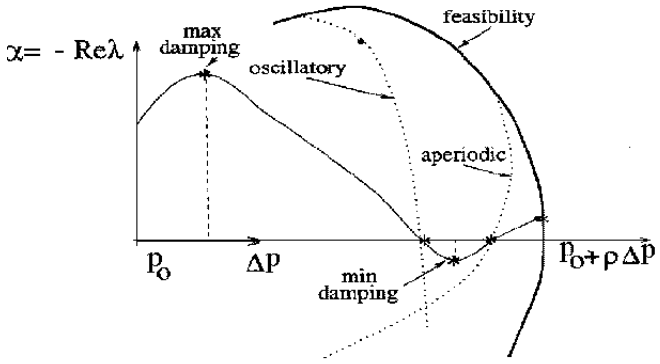

Figure 3.9: Different Solutions of The Problem (3.95)-(3.100) - Eigenvalue Trajectory Showing the Characteristic Points of Power System Small Signal Stability Conditions as Intersecting with Different Stability Boundaries:
Maximum / Minimum Damping Points (local),
Saddle Node ($\omega = 0$) or Hopf ($\omega \neq 0$) bifurcation,
Load Flow Feasibility Limit Point.

the load flow feasibility point, parameter τ can not be increased anymore beyond its limit value τ_*. Nevertheless, the trajectory $x(\tau)$ can be smoothly continued by further decreasing τ - see [109], for example. Suppose that the function $\alpha[x(\tau)]$ is monotone and continuous in the vicinity of τ_*, say; along the trajectory $x(\tau)$, suppose the increment $d\alpha$ is positive. As the increment $d\tau$ changes its sign at the point τ_* - see Figure 3.10 - this means that the derivative $\frac{d\alpha}{d\tau}$ changes its sign at τ_*. Thus enough optimality conditions (the constant sign of the second derivative of the objective function with respect to τ) are met at the point τ_* [55].

The problem (3.95)-(3.100) takes into account only one eigenvalue each time. The procedure must be repeated for all eigenvalues of interest. The choice of eigenvalues depends upon the concrete task to be solved. The eigenvalue sensitivity, observability , excitability and controllability factors [66, 95], can help to determine the eigenvalues of interest, and trace them during the optimization. For example, the inter area oscillatory modes can be identified and then analyzed using (3.95) –(3.100) for eigenvalues with frequency range from 0.1 –1 Hz [110].

The result of the optimization depends on the initial guesses for all variables in (3.95) –(3.100). To get all characteristic points for a selected eigenvalue, different

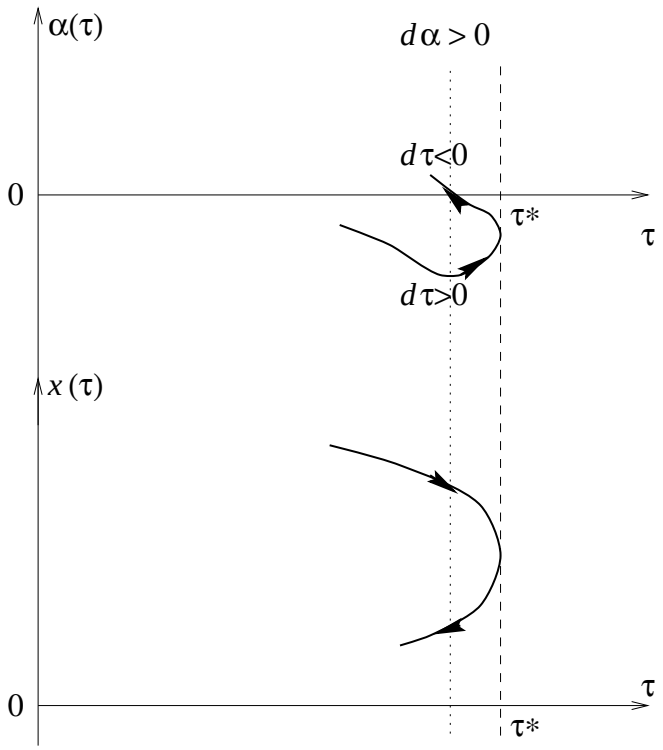

Figure 3.10: Locating the Load Flow Feasibility Limit
α - selected eigenvalue real part,
τ - scaling factor for system parameter variation,
$x(\tau)$ - vector of system state variables, which is depending on τ

initial points may be computed for different values of τ. At each point, the load flow conditions, state matrix eigenvalues and eigenvectors can be obtained, and then a particular eigenvalue selected to start the optimization procedure. More effective approaches for finding all characteristic points require additional development. At the moment, an initial guess technique based on eigenvalue sensitivity and Genetic Algorithms have been utilized.

3.6.2 Numerical Results for the General Method

The purpose here is to demonstrate whether the proposed method is able to locate all these characteristic points depending on the initial guesses of τ, x, α, ω, l' and l''. The results will be then validated by comparing some of them with the results obtained in the literature, and by dynamic simulations conducted close to these

characteristic points.

The single machine infinite bus power system model [33] presented in Figure 3.6, and the classical 3-machine 9-bus power system [6] shown in Figure 2.8 will be studied here.

Similar models were studied in [6, 121, 122, 129, 130].

The standard Gauss -Newton procedure from *Matlab* was used here for optimization [58].

Example 1. The Single Machine Infinite Bus System Model

The power system model has been given in Section 3.4.2; it is composed of four differential equations describing the system dynamics (3.68)-(3.71). The system load dynamics is given in equations (3.72)-(3.73). The state consists of four state variables δ, δ_m, ω, V. Their values at the initial load flow point are the following: $\delta = 2.75$, $\delta_m = 11.37$, $\omega = 0$, and $V = 1.79$. Note again, that the initial point is not a physical solution as the voltage V is too high as Q_1 is zero. Detailed study of the system can be found in [33, 45].

The results of numerical simulations are presented in in Figures 3.11 -3.18.

The dependence of the real part $\alpha = Re\lambda$ of critical eigenvalue λ upon Q_1 is shown in Figure 3.11. It is seen that there are both subcritical (point I) and supercritical (point II) Hopf bifurcations along the chosen loading direction. Figure 3.12 presents the root locus for the critical eigenvalue conjugate. The subcritical (point I) and supercritical (point II) Hopf bifurcation points are displayed. Both these characteristic points were successfully located by the proposed method, (3.95 -3.100).

Figure 3.13. shows the load flow feasibility and bifurcation boundaries on the plane of the load parameters P_1 and Q_1. The boundaries were obtained by the proposed optimization method when the loading direction was changed by subsequent rotation of Δy in the plane P_1 and Q_1. It was checked that exactly the same curves were computed by separate solution of the problems (3.87) –(3.91) and (3.92) – (3.94). To verify the results, transient simulations were performed at several points in the plane P_1 - Q_1. Point A with $P_1 = 0$ and $Q_1 = 10.88$ was placed within the load flow feasibility region close to subcritical bifurcation boundary. Then a

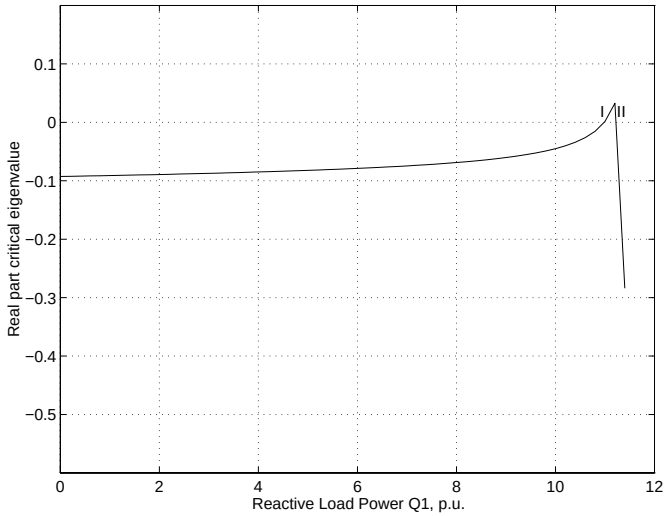

Figure 3.11: $\alpha = Re\lambda$ Computed for $P_1 = 0$ and $Q_1 = variable$

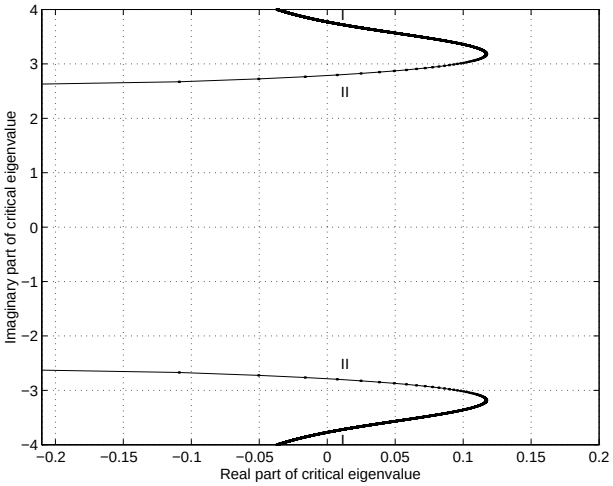

Figure 3.12: Subcritical (I) and Supercritical (II) Hopf Bifurcations

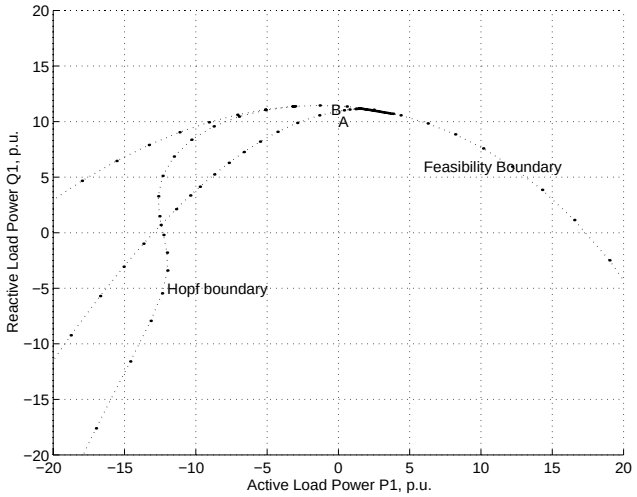

Figure 3.13: The Feasibility and Hopf Bifurcation Boundaries

small disturbance was applied. The corresponding phase portrait is shown in Figure 3.14. In complete correspondence with the theoretical expectations, the system has experienced sustained oscillations.

Those oscillations can be viewed in Figure 3.15 where the load bus voltage against time is presented.

Point B with $P_1 = 0$ and $Q_1 = 11.4$ was placed within the load flow feasibility region close to the supercritical bifurcation boundary. (Note that, in the vicinity of points A and B, the Hopf bifurcation boundary as shown in Figure 3.13 actually consists of internal subcritical and external supercritical boundaries located in close proximity). All eigenvalues at point B have small negative real parts. The phase portrait for a small disturbance applied at point B is given in Figure 3.16. The system undergoes decreasing oscillations. The corresponding voltage behavior is shown in Figure 3.17.

The next point was taken close to the point B but outside the load flow feasibility boundary. The system experiences voltage collapse as illustrated by Figure 3.18.

By solving the optimization problem, the system small signal stability boundaries were obtained.

The minimum and maximum damping conditions on the plane P_1 - Q_1 were studied as well. Table 3.2 presents the curves of minimum and maximum damping for

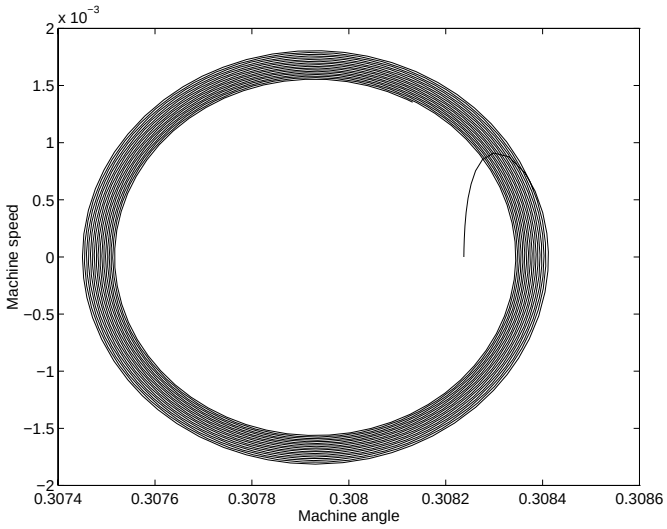

Figure 3.14: Phase Portrait at Point A Near Subcritical Bifurcation

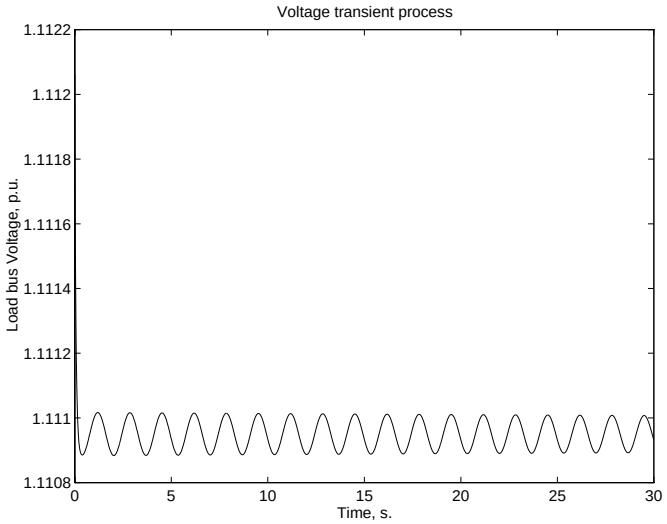

Figure 3.15: Transient Process Near Subcritical Bifurcation (Point A)

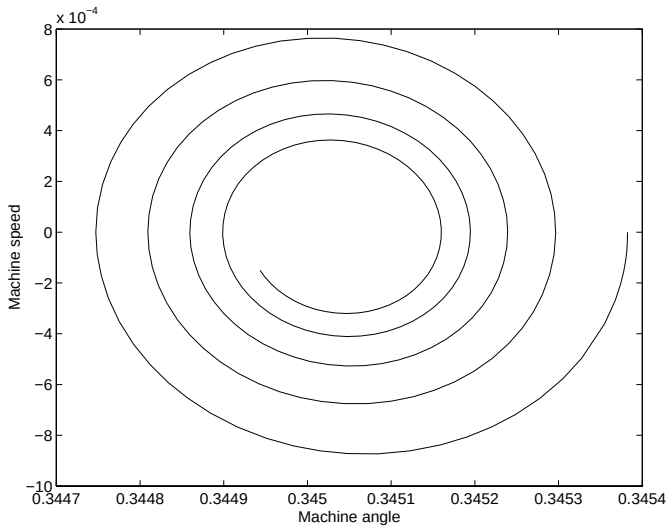

Figure 3.16: Phase Portrait at Point B Near Supercritical Bifurcation

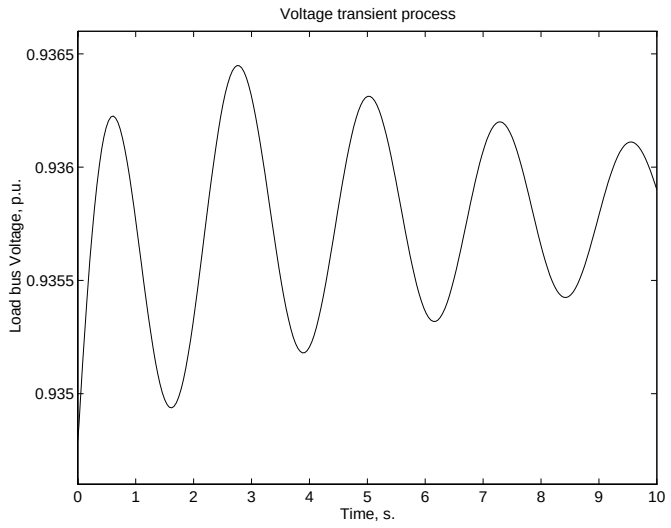

Figure 3.17: Load Bus Voltage Transients Near Supercritical Bifurcation

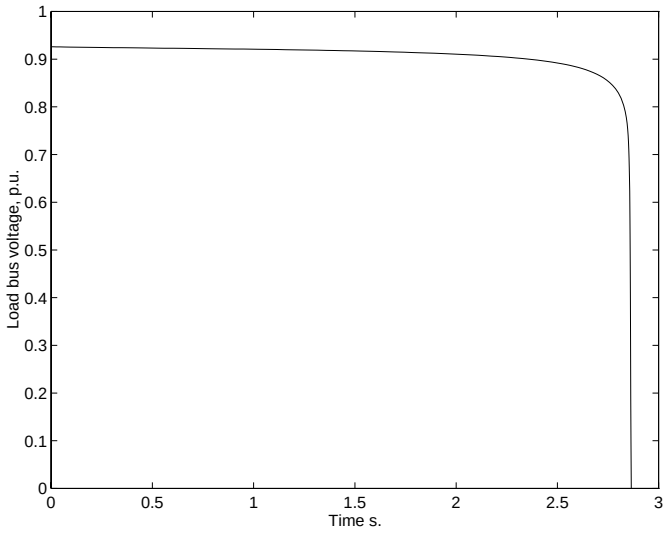

Figure 3.18: The system load bus voltage transients near feasibility boundary

different eigenvalues.

Example 2. The Three-Machine Nine-Bus Power System Model

As given in Figure 2.8, the model power system is composed of three machines and nine buses. Buses 1, 2, and 3 are connected to generators; bus 1, which is connected with generator 1, is taken as infinite bus, and buses 5, 6, and 8 are load buses feeding active and reactive loads, which are modeled as static loads. Machine 1 is modeled by classical model, and machines 2 and 3 are modeled by the two-axis model. The equations modeling these machine dynamics are as follows,

$$\begin{aligned}
\tau_{j1}\dot{\omega_1} &= T_{m1} - E_1 I_{q1} - D_1\omega_1 && (3.102)\\
\dot{\delta}_1 &= \omega_1 && (3.103)\\
\tau'_{qoi}\dot{E}'_{di} &= -E'_{di} - (x_{qi} - x'_i)I_{qi} && (3.104)\\
\tau'_{doi}\dot{E}'_{qi} &= E_{FDi} - E'_{qi} + (x_{di} - x'_i)I_{di} && (3.105)\\
\tau_{ji}\dot{\omega_i} &= T_{mi} - D_i\omega_i - I_{di0}E'_{di} \\
&\quad -I_{qi0}E'_{qi} - E'_{di0}I_{di} - E'_{qi0}I_{qi} && (3.106)\\
\dot{\delta}_i &= \omega_i && (3.107)\\
i &= 2, 3
\end{aligned}$$

In order to obtain a set of independent system equations, the last two equations

min-damping		max-damping	
P_1	Q_1	P_1	Q_1
-2.5709	-7.9124	-4.5537	-0.9679
-0.8391	-3.1315	-4.6069	-1.2344
0.0111	0.2113	-4.7900	-2.1326
0.0000	0.3836	-4.9317	-2.8473
-0.0165	0.3152	-5.0219	-3.2612
-0.107	1.0240	-5.1184	-3.7187
-0.1131	0.7142	-5.2218	-4.2286
-0.1640	0.7717	-5.3329	-4.8017

Table 3.2: Minimum and Maximum Damping Data for the Single-Machine Infinite Bus System

above are combined into one as,

$$\dot{\delta_{1i}} = \omega_1 - \omega_i \text{ where } \quad i = 2, 3. \tag{3.108}$$

These equations are linearized around equilibrium points to obtain the state matrix thus stability analysis can be performed on them. To obtain the state matrix, however, the following equations are necessary for linking state variables and the system parameters,

$$I_r + jI_s = I\angle(\beta - \phi) = \frac{(P - jQ)}{V} \tag{3.109}$$

$$\tan(\delta - \beta) = \frac{x_q I_r}{V - x_q I_x} \tag{3.110}$$

$$E'_q = V_q - I_d x'_d \tag{3.111}$$

$$E'_d \approx V_d + I_q x'_d \tag{3.112}$$

$$I\angle[-(\delta - \beta + \phi)] = I_q + jI_d \tag{3.113}$$

$$V\angle(-\delta) = V_q + jV_d \tag{3.114}$$

where I_d, I_q are d-axis, q-axis currents, $V\angle\beta$ is generator terminal voltage and its angle, ϕ is the power factor angle lag of voltage [6].

Unlike the results in [129] and [121], the excitation system dynamics have been neglected, so the state variables here are the following: δ, ω, E'_q, and E'_d. Algebraic

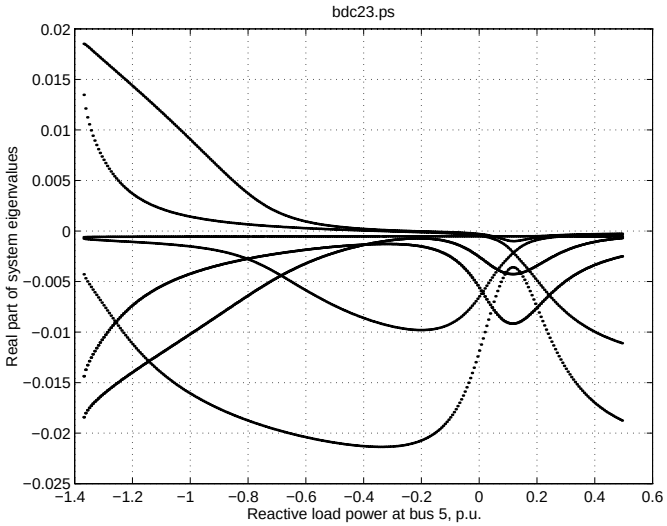

Figure 3.19: System Eigenvalue Real Parts Behavior along Reactive Power Variation

variables were I_d, I_q, θ, and V; bifurcation parameters were P_{ld} and Q_{ld}. The notations, parameter values and description of the system (3.102) –(3.107), (3.109) – (3.114) can be found in [6].

Unlike the single machine infinite bus example, which includes an induction motor load, this three-machine nine-bus model considers constant load models only. In the general case of small signal stability analysis, the load dynamics should be definitely taken into consideration. Nevertheless some stability aspects can be studied with the constant load model [35].

In the preliminary examination, the loads P_{ld} and Q_{ld} at buses 5, 6 and 8 were increased in proportion with the load size. The increase of load was followed by the corresponding increase of generation in proportion with the generator size. The total increment in load was equal to the total increment in generation. The loading was repeated till the point where load flow did not converge. At each step, eigenvalues of the state matrix were computed to reveal the bifurcation points and minimum and maximum damping conditions.

The system eigenvalue behavior along the chosen loading direction is shown in Figure 3.19,

There are several points of interest which can be clearly seen in Figure 3.19. They include the maximum damping, minimum damping, bifurcation points and points

Bus	1st minimum damping point		2nd minimum damping point		Bifurcation point	
	P_{ld}	Q_{ld}	P_{ld}	Q_{ld}	P_{ld}	Q_{ld}
1	0	0	0	0	0	0
2	0	0	0	0	0	0
3	0	0	0	0	0	0
4	0.0000	-0.0000	0.0000	-0.0000	0.0000	-0.0000
5	-0.8125	-0.3250	-0.5000	-0.2000	-0.5781	-0.2313
6	-0.5850	-0.1950	-0.3600	-0.1200	-0.4163	-0.1388
7	0.0000	-0.0000	0.0000	-0.0000	0.0000	-0.0000
8	-0.6500	-0.2275	-0.4000	-0.1400	-0.4625	-0.1619
9	0.0000	0.0000	0.0000	0.0000	0.0000	-0.0000

Table 3.3: Load Powers at Some Small Signal Stability Characteristic Points

close to the load flow feasibility boundary. Some of the obtained characteristic points are summarized in Table 3.3.

In the examination of the proposed method based on the optimization problem (3.95) –(3.100), the method has been applied to locate these points of interest. The results showed that the constrained optimization procedure converged toward all the points of interests depending on the initial guess of variables. The initial guesses were chosen using the rough estimates of the characteristic points obtained in preliminary examination.

3.7 Conclusion

This chapter discussed methods which can be used to reveal critical stability characteristic points in the parameter space. These characteristic points include: load flow feasibility boundary points, minimum and maximal damping, saddle node and Hopf bifurcations. Many existing techniques can only compute one or two kinds of these points at one time, however, the proposed comprehensive general method is capable of locating all these characteristic points within one procedure. The method has been tested and validated by numerical simulations, comparison with

the previous results obtained for the test systems, and by transient simulations conducted at the characteristic points. Further developing work is required to develop techniques for obtaining the initial guesses of variables, fast and reliable solution of the constrained optimization problem, and handling of large power systems.

Chapter 4

Methods to Visualize Power System Security Boundaries

4.1 Introduction

So far we have studied techniques to locate the closest distance to the security boundary and methods to find all the critical points in a given direction defined by a ray of system parameters. It is possible to locate the security boundary or hypersurface in the space of power system parameters by varying the direction of the ray. Once the boundary or hypersurface is found, control actions to enhance the system security and power transfer capacity can be decided. For these ideas to be implemented in real-time security control, it is important to develop acceptable approximations of the boundary or hypersurface for large power systems.

In Chapter 3, we introduced methods to locate the critical stability characteristic points in the space of power system parameters. These critical points can provide important information on system operation and control for security. In general, the critical points must be seen as surfaces in parameter space. The natural planes defined by physical parameters only give a limited view of the boundaries. It would be useful if the hyperplane containing all these characteristic points could be fully manoeuvred to more fully view the boundaries. Further, this would improve the optimal planning and control direction away from contingency. Their representation and visualization in the parameter space requires special techniques which will be discussed in this chapter.

The structure of the chapter is as follows. Firstly, we introduce the basic idea of indirect methods using an objective evaluation function. Then, parameter continuation to locate critical points is described along with a reformulation of the critical distance problem treated in Chapter 3. The formulation is specifically related to the space of nodal powers. Whereas Chapter 3 used a direct method and higher order solution techniques, here we will concentrate on indirect methods. Also we aim to exploit more the structural properties of the power flow equations expressed in quadratic form. A review of various methods, with emphasis on less known contributions in the Russian literature is made. This motivates the need for techniques to efficiently compute load flow feasibility and stability boundaries. The remainder of the chapter presents a new so called Δ-plane method for computing load flow feasibility boundaries in a chosen cut plane defined by three different operating points. Finally, a continuation method for tracing the power system small signal stability boundaries is presented.

4.2 Indirect Approach to Compute Stability Boundary

In indirect methods, the solution approximation is updated from the data obtained from a continuation procedure, evaluated by the objective test function of the problem to be solved. For example, consider a system represented by the equation:
$f(x, \lambda, \mu) = 0$
where x is vector of state variables and λ is the slowly varying system parameter where $\lambda \in [\lambda_1, \lambda_2]$, and μ is an objective evaluation function used to evaluate the solution accuracy. For example, μ can be the real part of the state matrix critical eigenvalue(s) in case saddle node or Hopf bifurcations are to be studied. Suppose indirect methods are to be used to locate the solution value of λ of the system in the neighborhood of $[\lambda_1, \lambda_2]$. As shown in Figure 4.1, starting from initial guessed

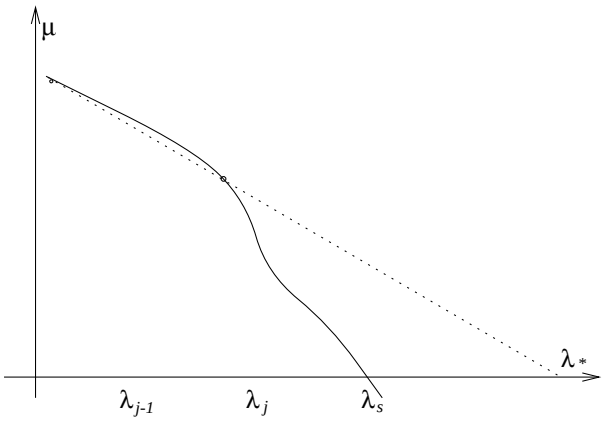

Figure 4.1: Indirect Solution Approach

solution point (x_0, λ_0, μ_0), the continuation procedure at step j gives approximation of the solution as

$$(x_j, \lambda_j, \mu_j) \quad j = 1, 2, ... \tag{4.1}$$

Knowing that the solution exists in $[\lambda_1, \lambda_2] = [\lambda_{j-1}, \lambda_j]$ then an approximation, λ_* of the final solution λ_s can be calculated by the straight line interpolating function,

$$\lambda_* = \lambda_{j-1} + \mu_{j-1} \frac{\lambda_j - \lambda_{j-1}}{\mu_{j-1} - \mu_j} \tag{4.2}$$

This approximation is close enough to the solution if the distance of $|\lambda_j - \lambda_{j-1}|$ are small enough. There are many other interpolation formula which can be used here for approximation [136].

Followed by the approximation of parameter λ_*, the approximation of system variable x can be obtained similarly,

$$x_* = x_{j-1} + \mu_{j-1}\frac{x_j - x_{j-1}}{\mu_{j-1} - \mu_j} \tag{4.3}$$

where x_* is the approximation to the solution x_s. Generally without any singularity problems, with small enough distance of $|\lambda_j - \lambda_{j-1}|$, the approximation for x_* will be close enough to the actual solution. The indirect method can be used in many occasions of stability problems, e.g. to trace the stability boundaries, to locate critical solutions. As one of the very important classes of indirect methods, we proceed to explore the continuation methods.

4.3 Parameter Continuation Techniques to Locate the Critical Solution Points

In locating critical solution points, such as saddle or Hopf bifurcations, load flow point of collapse points, traditional Newton-Raphson like optimization methods do not always converge close to such points because of singularity properties associated with them. In order to overcome such problems caused by singularity, which can be load flow Jacobian singularity or state matrix singularity, the parameter continuation techniques can be employed.

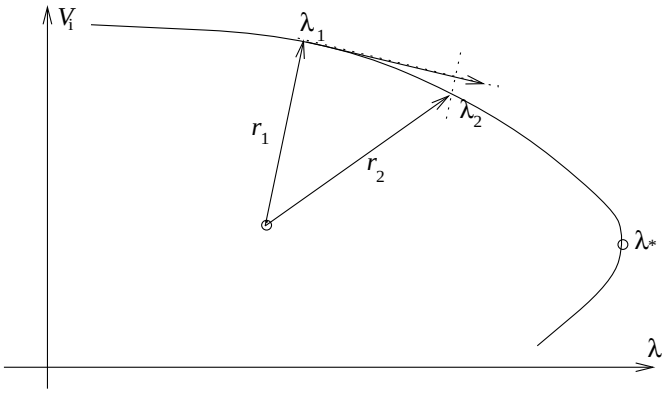

Figure 4.2: The System Stability Limits Revealed in Power Flow Q-V Curve

One of the most important tasks of locating the power system critical stability points is the load flow feasibility point, or the Point of Collapse (PoC) characterized as

a saddle node bifurcation point. Continuation methods to locate such points have been proposed in [4, 24, 108, 136]. For a power system given by equation (3.63), the continuation methods differ from direct methods in the way that these methods solve (3.63). The direct methods require solution of the set of equations (3.63) - (3.65) to locate the bifurcation point. For continuation methods, the equations are subjected to a variable parameter. Rather then repeatedly solving the equations, the previous solution is updated by a predictor-corrector procedure.

The continuation method involves operations:

- Predictor
- Corrector
- Parameterization
- step size control

To find the PoC point of power flow problem, the parameter continuation method starts from a known load flow solution point, and then starts the predictor corrector technique to find the subsequent solutions. The continuation step size can be adjusted so that large step size is selected where the current solution point is far from the PoC, and smaller step size is selected where the solution is close to the PoC. Parameterization is necessary to over come the load flow Jacobian singularity problem around the PoC. It is suggested in [26] to use the continuation method in tracing the power flow curves and the point of collapse. Cañizares and Alvarado in [26] proposed the following scheme for a continuation method applied to the system modeled by $\dot{x} = f(x, \lambda)$, where x is the state variable, λ is the parameter to be continuously changed.

- The predictor steps in state space and parameter space are defined based on the derivative of state variables with respect to the parameter via $\Delta\lambda = \frac{k}{|dx/d\lambda|}$ and $\Delta x = \Delta\lambda \frac{dx}{d\lambda}$, where k is a user determined constant.
- The corrector is determined by solving the intersection between the perpendicular plane to the tangent vector and the branch curve.

- For parameterization, the parameter to be continuously changed is the one with maximum sensitivity to variation, i.e. $\lambda = max\{|\frac{\Delta x_i}{x_i}|, |\frac{\Delta\lambda}{\lambda}|\}$, where $i = 1, 2, ..., n$.

This method can trace the power flow curves around the PoC point, and allow solution of the lower (normally unstable) branches of P-V or Q-V curves.

To find the closest saddle node bifurcation points in the parameter space, another form of continuation approach is proposed in [108]. The proposed technique requires a two stage searching to find the closest (locally) saddle node bifurcation point to the current power system operation point. The first step is to find a point on the singularity surface which is composed of saddle node bifurcation points; the second step is to move from this initially found point to the critical closest point on the bifurcation surface. The second step depends on the proposed continuation method which is robust in tracing the solution trajectory.

4.3.1 Revised Critical Distance Problem formulation

In this section, we revise the critical distance problem with the aim of a more specific formulation with nodal powers as parameters.

A power system load flow problem can be modeled abstractly by the set of n non-linear algebraic equations,

$$F(x, p) = 0 \tag{4.4}$$

where x is now the vector of state variables (dynamic and algebraic), p is the vector of system parameters. The equation can often be further simplified into this form:

$$p^0 + f(x) = 0 \tag{4.5}$$

where $p^0 \in R^n$ is the vector of specified independent power system parameters such as active and/or reactive powers of loads and generators or fixed voltages, $x \in R^n$ is the vector of state variables, consisting of nodal voltages. The vector function $f(x)$ defines the sum of power flows or currents into each bus from the rest of the network. If nodal voltages x are expressed in rectangular coordinates then $f(x)$ is a quadratic function of x [69].

The critical distance problem, as discussed in Section 3.3, aims to minimize the distance function,

$$d(p) = \|\mu[p - p^0]\| \tag{4.6}$$

where we introduce μ as a diagonal matrix of weight coefficients, with diagonal elements,

$$\mu_i = 1/p_i^b \tag{4.7}$$

where p_i^b is a 'normalizing' factor for the i-th parameter. The distance (4.6) can be used as an aperiodic stability index. By comparing the distance $d(p)$ with a preset value of the stability index I_s which ensures safe operation, it is possible to decide to which extent the current operating state is close to aperiodically unstable limits.

The parameter p^b in (4.7) should be a constant value, and not dependent on the operating point p^0. Otherwise, the nonlinear dependence of $d(p)$ on p^0 may result in solution difficulties when $p^b = p^0$.

The idea of locating the closest aperiodic stability point in the parameter space is achieved by variation of some parameters. However, in the optimization problem given by,

$$\min_{p \in \Sigma_p} d(p) = \min_{p \in \Sigma_p} \|\mu[p - p^0]\| \tag{4.8}$$

not all parameters are free to vary. Some parameters must stay unchanged. For example, the power injected at buses without load or generation must remain constant and therefore can not vary freely. These kinds of parameters can be effectively held constant by assigning them very large values of weight coefficients μ in (4.6). However, consequently, this will lead to an ill-conditioned problem, and numerical difficulties will arise. To overcome this difficulty, a modified power flow formulation will now be given and should be employed.

The modified load flow equations achieve the task by dividing the parameters into two groups p_1 and p_2 which are free varying parameters and fix value parameters respectively. Then all m parameters p_2 with fixed values are put into a group of equations, and the remaining $n - m$ parameters p_1, which can vary freely, are put into another set of equations. Then the system (4.5) can be rewritten as,

$$p_1 + f_1(x) = 0 \tag{4.9}$$

$$p_2^0 + f_2(x) = 0 \tag{4.10}$$

Based on the equations (4.9) and (4.10), the square of the distance $d(p)$ defined at (4.6) can be written as,

$$\begin{aligned} d(p)^2 &= \|p - p^0\|^2 && (4.11)\\ &= \|p_1 - p_1^0\|^2 && (4.12)\\ &= \|p_1^0 + f_1(x)\|^2 && (4.13) \end{aligned}$$

Note that μ is taken as the identity matrix I for simplification. The case when $\mu \neq I$ requires trivial transformations of all these equations.

Consider the constraint optimization problem,

$$\underset{x}{\text{extrema}} \ \|p_1^0 + f_1(x)\|^2 \qquad (4.14)$$

$$st.$$

$$p_2^0 + f_2(x) = 0 \qquad (4.15)$$

From (4.11) –(4.13), it can be seen that the cost function (4.14) defines the square of the distance between the points p_1 and p_1^0, with both points belonging to the constraint hyperplane defined by $p_2 = p_2^0 = const.$

To solve the optimization problem, the Lagrange function can be defined as,

$$l(x, \lambda) = \|p_1^0 + f_1(x)\|^2 + 2[p_2^0 + f_2(x)]^t \lambda \qquad (4.16)$$

then the constrained optimization problem (4.14) and (4.15) can be formulated as an unconstrained problem of locating the extrema of $l(x, \lambda)$ in the space spanned by x and λ. Solutions of the Lagrange function satisfy the nonlinear system,

$$\begin{aligned} J_1^t(x)[p_1^0 + f_1(x)] + J_2^t(x)\lambda &= 0 && (4.17)\\ p_2^0 + f_2(x) &= 0 && (4.18) \end{aligned}$$

where $J_1 = \frac{\partial f_1}{\partial x}$ and $J_2 = \frac{\partial f_2}{\partial x}$. This system of equations can be written in more general form as $\phi(x, \lambda) = 0$. The system (4.17) and (4.18) can be rewritten by using the substitution $s = p_1^0 + f_1(x)$ in(4.17) as,

$$\begin{aligned} -s + p_1^0 + f_1(x) &= 0\\ p_2^0 + f_2(x) &= 0 && (4.19)\\ J_1^t(x)s + J_2^t(x)\lambda &= 0 \end{aligned}$$

It is clear that the system (4.19) has the same solutions as the original system (4.17) and (4.18), so

$$\phi(x, \lambda) = 0 \Leftrightarrow \underline{\phi}(x, s, \lambda) = 0 \tag{4.20}$$

where $\underline{\phi}(x, s, \lambda) = 0$ represents the system (4.19). The last equation in (4.19) can be rewritten as,

$$J^t(x)s_\lambda = 0 \tag{4.21}$$

where $J^t = [J_1^t \ J_2^t]$ and $s_\lambda = [s^t \ \lambda^t]^t$.

If $s_\lambda \neq 0$, to fulfill the equation (4.21), the Jacobian matrix $J(x)$ must be singular, hence the vector s_λ is a left eigenvector of $J(x)$ corresponding to a zero eigenvalue. Therefore, based on the original optimization problem (4.14) and (4.15), and the condition (4.21) for $s_\lambda \neq 0$, the conclusion can be drawn that the critical points, i.e., points on Σ that are composed of minimal distance (locally) points from the operating point y^0, satisfy the system (4.19). Later analysis of the continuation method will be based on these equations.

4.3.2 Locating the closest saddle node bifurcations with continuation method

Not all solutions to the equations (4.19) which describe the critical points, are closest saddle node bifurcation points. Solutions with nonzero left eigenvector defined in (4.21), i.e. $s_\lambda \neq 0$, are nontrivial solutions belonging to the singular surface where $\det J = 0$. Whereas those solutions where $s_\lambda = 0$ are actually the normal power flow solutions which are global minima of the distance function with $d(p) = 0$. These solutions are trivial and should be eliminated. As a result, the algorithm for finding critical points must consist of two parts:

1. an approach which is capable of obtaining a good estimate of the unknown state variables $\{x, s, \lambda\}$ in the vicinity of the critical point;

2. a numerical technique that will converge reliably from that initial estimation to a desired critical point which is locally closest to the operating point p^0.

Such an algorithm is described as follows.

Stage 1: Initial Estimation Technique

The first step of this closest point approach must obtain an initial estimation of the state variables $\{x, s, \lambda\}$ close to the critical distance point. In order to find this initial point, a direction of parameter variation will have to be provided so that the states can be calculated from the operating point toward the desired critical point. This direction is based on human expertise by using existing knowledge of power system operation and control activities. Generally, most power system operators and planners. have enough idea of the direction in parameter space from the operating point to the most probably closest aperiodic instability point(s). Later discussion will show that, by using Genetic Algorithms, the need for this knowledge can be ignored. The self adaptive heuristic algorithm is powerful enough to locate the best available estimation for the problem. This parameter variation direction, e.g. loads variation direction, is denoted as Δp_1 in the space of parameters can be varied. Recall that the remaining parameters $p_2 = p_2^0$ are those parameters that are not to be varied throughout the procedure.

The initial estimate of the critical point is a point on the solution boundary Σ where $p + f(x) = 0$ and $\det J_{(x,p)} = 0$ in the direction Δp_1 from the operating point. That point is given by

$$\beta \Delta p_1 + p_1^0 + f_1(x) = 0 \tag{4.22}$$

$$p_2^0 + f_2(x) = 0 \tag{4.23}$$

$$J^t(x) s_\lambda = 0 \tag{4.24}$$

$$s_\lambda^t s_\lambda = 1 \tag{4.25}$$

where β is the loading parameter in the specified direction Δp_1, and $\|\Delta p_1\| = 1$. An alternative formulation of (4.24) and (4.25) uses the right eigenvector to achieve the singularity condition, rather than the left eigenvector s_λ. Both the direct method and continuation method can be used to solve the problem. Many methods had been proposed for solving this problem in the literature [4, 5, 26, 40, 67, 136].

Stage 2: Continuation Toward The Critical Point Along the Singular Margin

After performing the first stage, the initial estimated solution point on Σ in the vicinity of the desired critical point is available. This point is denoted as $x^*, \beta^*, s^*_\lambda = [s^{*t}\ \lambda^{*t}]^t$ for later analysis. The aim of this stage is to move from this initial point to the critical point on the singular margin Σ, which is defined in equations (4.22) – (4.25), and this can be achieved by the equations below,

$$\alpha(\beta^* \Delta p_1 + s^*) - s + p_1^0 + f_1(x) = 0 \quad (4.26)$$

$$p_2^0 + f_2(x) = 0 \quad (4.27)$$

$$J^t(x) s_\lambda = 0 \quad (4.28)$$

Note that when $\alpha = 1$, the initial point $\{x^*, \beta^*, s^*_\lambda\}$ is a solution of (4.26) –(4.28). The problem is the same as that of (4.19) if $\alpha = 0$, which means that the solution is the critical point if $\alpha = 0$. Therefore, the process of moving from the initial point to the critical point is done while α is varied from 1 to 0. The constraint condition in equation (4.28) makes sure that all solutions along the path lie on the singular margin Σ. Constraint condition (4.27) indicates that the parameters $p_2 = p_2^0$ are not varied during the process. Scaling s_λ so that $\|s\| = \beta^*$ at the initial point $\alpha = 1$ will help solve the problem. Note that this scaled s_λ will still satisfy (4.28).

A special numerical solution technique listed in the appendices B.1, put forward in [108] is suitable for solving the problem. That technique has the following features:

- For an appropriate choice of the maximum deviation ϵ_g defined in equation (B.12) (see Appendix B.1), and the corresponding step sizes α_i, the technique will follow the linear path through parameter space given by $\alpha(\beta^* \Delta p_1 + s^*)$.

- The method can always find a solution point if no singular points exist along the search direction defined by the line $\alpha(\beta p_1 + s^*)$. Otherwise, the method will iterate towards and become very close to the singularity point. Though, in some cases, the solution point could be stepped over without being detected by the method. In some cases, it involves several trial and error processes to find a solution point. Further improvement of the method is required to overcome this problem.

- This method costs as much computation time as a normal Newton-Raphson method does, or at least in the same order. The time consumed at each iteration is proportional to the reduction of the number of iterations [108].

There is an alternative approach to move the solution point from the initially obtained point by Stage 1 to the critical point along the singularity margin. It is based on the equations below,

$$\beta^* \Delta p_1 (1-p) - ps + p_1^0 + f_1(x) = 0 \quad (4.29)$$

$$p_2^0 + f_2(x) = 0 \quad (4.30)$$

$$J^t(x) s_\lambda = 0 \quad (4.31)$$

When $p = 0$, the initial point $x^*, \beta^*, s_\lambda^*$ satisfies (4.29) –(4.31). But $p = 1$ corresponds to the critical point problem. So in this case, by varying p from 0 to 1, the solution of (4.29)-(4.31) is distorted from the Stage 1 point to the desired critical point. Because of (4.30) and (4.31), this path again traverses the intersection of the $p_2 = p_2^0$ hyperplane and Σ. As with the previous case, it is helpful to scale s_λ such that $\|s\| = \beta^*$ at the initial point $p = 0$. Many numerical techniques exist for solving this continuation problem [67, 54, 136].

Stage 3: Local Optimal Direction of Distance Minimization

Starting from an operating point, the algorithm finds an initial solution point on the intersection of Σ and the $p_2 = p_2^0$ hyperplane in Stage 1; then from the initial point motion is toward the solution point aiming to minimize the distance from operating point along the singular surface by Stage 2 of the algorithm. The final aim is thus to locally reduce the distance set by $\|p_1 - p_1^0\|$ while satisfying $p_2 = p_2^0$.

At the vicinity of a point on the power flow solution space boundary Σ_p, the surface Σ_p can be approximated (locally) by its tangent hyperplane $\mathcal{P}$. The optimal motion direction can be derived from the intersections of Σ_p and $\mathcal{P}$ with the $p_2 = p_2^0$ hyperplane. These intersections are referred to as Σ_{p_1} and $\mathcal{P}_s$ intersection respectively. A graphical illustration of the intersections are given in Figure 4.3. where point `A` on Σ_{p_1} intersection satisfies $p_1 = -f_1(x)$, and the hyperplane $\mathcal{P}_s$ is tangent to Σ_{p_1} at point `A`. Point `B` is the point closest to the operating point p_1^0 on the $\mathcal{P}_s$. It can be seen that the vector from p_1^0 to `B` is orthogonal to the hyperplane $\mathcal{P}_s$. Therefore, if

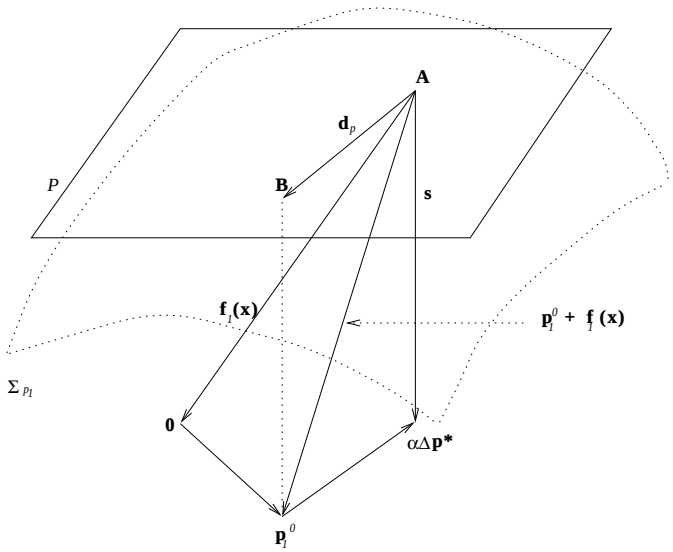

Figure 4.3: Locally optimal direction of distance minimization.

Σ_{p_1} is approximated by the plane $\mathcal{P}_s$, the motion from A to B will give the minimal distance $\|p_1 - p_1^0\|$. That is, the locally optimal direction is given along the vector $d_{\mathcal{P}} \in \mathcal{P}_s$.

The conclusion drawn above can be used in analyzing the first solution motion in Stage 2 of the algorithm. Since s is orthogonal to $\mathcal{P}_s$, its projection onto $\mathcal{P}_s$ is a point. Therefore, (4.26) is a connection between the projections onto $\mathcal{P}_s$ of $\alpha(\beta^*\Delta p_1 + s^*) = \alpha\Delta p^*$ and $p_1^0 + f_1(x)$, by the relations given below,

$$(\alpha\Delta p^*)_{\mathcal{P}} + (p_1^0 + f_1(x))_{\mathcal{P}} = 0 \tag{4.32}$$

So,

$$-(\alpha\Delta p^*)_{\mathcal{P}} = (p_1^0 + f_1(x))_{\mathcal{P}} = d_{\mathcal{P}} \tag{4.33}$$

α is varied from 1 to 0 during the solution process. It can be seen from equation (4.33) that the component of motion in the $\mathcal{P}_s$ plane is in the locally optimal direction. Though, there may be a component of motion normal to $\mathcal{P}_s$. As results of variation of α from 1 o 0, the vectors $(\alpha\Delta p^*)_{\mathcal{P}}$ and $(\alpha\Delta p^*)_{\mathcal{P}}$ will also approach zero. Consequently this means that the continuation algorithm will only approach a minimal value of distance $\|p_1^0 + f_1(x)\| = \|p_1 - p_1^0\|$ and will never converge to maxima.

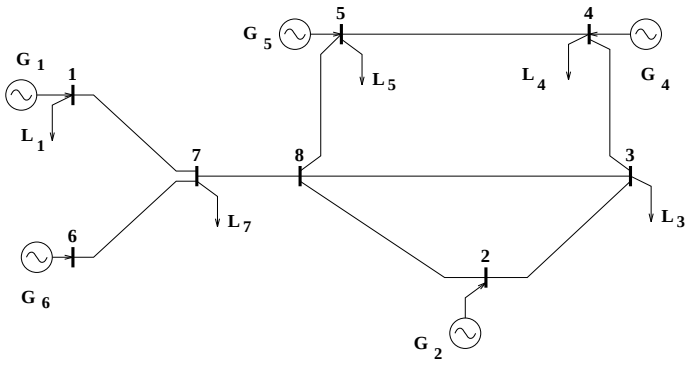

Figure 4.4: Eight Bus Power System.

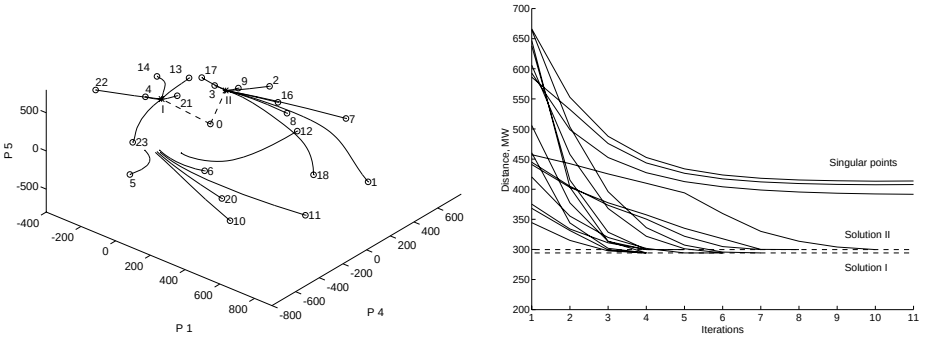

A B

Figure 4.5: A - Trajectories of The Stage Two Continuation Process in The space of Free Varying Power System Parameters. B - Distance changes during the stage two iterative process.

4.3.3 Numerical Testing of the Continuation Method

In [108] two model power systems, including a three bus system, and an eight bus system were studied about the solution characteristics as well as validating the proposed continuation technique by using the numerical methods listed in the Appendix B.1. The eight bus system (given in Figure 4.4) and the continuation motions and distance changes of Stage 2 of the algorithm is quoted here (in Figure 4.5) for completion.

This continuation algorithm converges to desired critical distance points under normal conditions. However, the algorithm may experience solution difficulty because

of the singularity of critical distance equation Jacobian on a very bad estimate of direction. In such cases, the left eigenvector of the Jacobian can be used to find out the nature of the singularity [108].

4.4 State of Art for Computing Security Boundaries in the Parameter Space

In order to keep the power system in a secure operating state, efforts must be made to ensure the system is operating state is inside the feasibility and stability domains which are restricted by the hypersurface Σ satisfying the conditions below,

$$\begin{aligned} \det[J(x)] &= 0 \\ \det[J_s(x) \pm j\omega I] &= 0 \end{aligned}$$

where $J(x)$ is either the load flow Jacobian (J_{lf}) or dynamic state matrix (J_s), x is a vector of load flow independent parameters (nodal voltages) or state variables, I is the identity matrix, and $\omega \neq 0$ is the imaginary part of an eigenvalue with zero real part. When power system parameters are varied slowly, either conditions listed above can be achieved, and this means that the system is on the edge of its transfer capability ($J(x) \equiv J_{lf}$) or small signal stability ($J(x) \equiv J_s$). Either saddle node or Hopf bifurcations (instabilities) may occur in the system. In some special cases the transcritical and pitchfork bifurcations may happen as well [22].

Power system control and planning should provide safe stability and loadability margins. Knowledge of the stability boundary geometrical configuration gives guidance for development of control strategies and proper decision making. Hence it follows that study of the bifurcation surfaces Σ is an important task. However, as the conditions listed above correspond to a very complicated surface in the space of power system parameters, it is very hard to observe the topology of the stability surface composed of different stability boundaries.

The study of nonlinear power system behavior associated with multiple equilibrium points (load flow solutions) and their relationship with bifurcations has attracted considerable attention recently - see [63] for a recent collection of review papers. Among these, the paper [96] contains an extended review of modern local bifurcation

theory, its application to power system analysis and control, and some relevant computational aspects. An important reference is [42] which is devoted to mathematical and computational issues of bifurcation analysis, namely, to finding the closest saddle node, Hopf, transcritical and pitchfork bifurcation in parameter space. Many of the ideas can be used to study the bifurcation boundary geometry.

In the works [52, 81, 69, 141, 87], the singularity condition $detJ(x,p) = 0$ is substituted by the following equivalent equations

$$J_{lf}^t(x,p)w = 0 \;\Leftrightarrow\; J_{lf}(x,p)v = 0 \tag{4.34}$$

where v and w are the right and left eigenvectors of $J_{lf}(x,p)$ corresponding to the zero eigenvalue. The vectors v and w have remarkable properties [42] which are very useful in stability analysis. The right eigenvector v indicates the direction of the initial dynamics of the unstable behavior (voltage collapse, for example), and the extent to which a variable collapses is given by the relative magnitude of the corresponding components of v. The left eigenvector w may be interpreted as the normal vector to Σ^{lf}, or more precisely, to the tangent hyperplane spanned by the columns of $J_{lf}(x,p)$.

The picture given in Figure 4.6 is commonly used to illustrate voltage stability limits at one bus$_i$, suppose the load flow limit point for reactive power variation case is point A, current operation point is point C, and there are two marginal points, B_1 and B_2 regarding the security margin and limit.

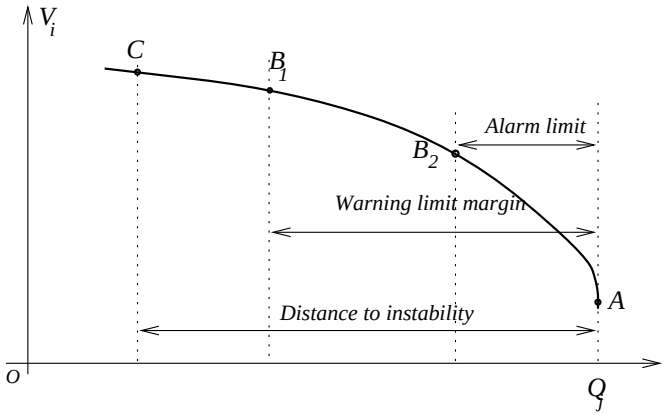

Figure 4.6: The System Stability Limits Revealed in Power Flow Q-V Curve

Techniques for locating one of these boundary points have been discussed in Chapter 3 and 4. However, different techniques are required to more completely explore

the security boundaries in the parameter space. The following sections discuss known techniques used to explore these security boundaries presenting the current state of art for solution techniques. Then a new Δ-plane method and a parameter continuation technique are proposed.

4.4.1 Supporting Hyperplane Method

In the works [51, 52, 81] based on quadratic representation of the load flow problem $F(x,p) = p + g(x) = 0$, the feasibility region $\mathcal{R}_p = \{p | F(x,p) = 0, x \in \mathbf{R}^n\}$ is a cone whose vertex is at the origin of $\mathbf{R}_p^n$. The supporting (tangent) hyperplanes T_p imply the condition $w^t p = 0$, where w is the normal vector to T_p, and, if the cone is convex, all feasible independent parameters p satisfy the inequality $w^t p \geq 0$ (see Figure 4.7). In [51, 52, 81] it was conjectured that the feasibility region is convex.

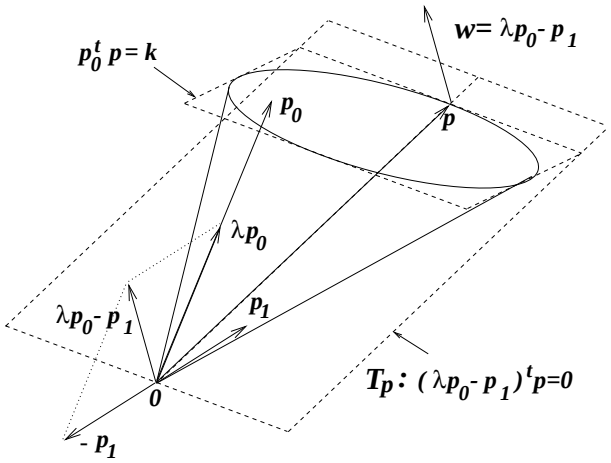

Figure 4.7: A supporting hyperplane in $\mathbf{R}_p^n$ [51]-[81]

Examples [69] show that this is not true in general. Though, under what situation it is true remains to be proven by further research. For vectors p within the feasibility region, the following optimization problem gives the tangent planes:

$$\max_p \; p_1^t p \quad (\text{ or } \min_p \; p_1^t p) \tag{4.35}$$

$$p_0^t p = k \tag{4.36}$$

where p_0 is a vector corresponding to a positive definite $J(p_0)$ (where $J(p_0)$ is a linear matrix function of p_0 [51, 52, 81]), and p_1 is a vector not parallel to p_0, and k is a nonzero constant. The constraint (4.36) defines a plane which intersects the

cone (Figure 4.7). The problem (4.35)-(4.36) can be expressed as follows [51, 52, 81]:

$$\max_x \; x^t J(p_1) x \quad \left(\text{ or } \min_x \; x^t J(p_1) x \right) \tag{4.37}$$

$$x^t J(p_0) x = k \tag{4.38}$$

By means of differentiation of the Lagrange function $L(x, \lambda) = x^t J(p_1) x + \lambda[k - x^t J(p_0) x]$ with respect to x, the following generalized eigenvalue problem can be stated:

$$[J(p_1) - \lambda J(p_0)] x = 0 \tag{4.39}$$

To get the supporting planes T_p, the minimal ($\lambda = \lambda_{min}$) and maximal ($\lambda = \lambda_{max}$) eigenvalues of the problem (4.39) are used. The set of tangent hyperplanes for different p_0 and p_1 gives an approximation of the feasibility region boundary Σ^{lf}. Difficulties may arise for nonconvex feasibility regions.

Further developments are given in [87, 88, 89] and [43]. The authors present methods for finding the load flow feasibility and saddle node bifurcation points by solving a system which can be generalized as follows:

$$F(x, p_0 + l\Delta p) = 0 \tag{4.40}$$

$$J^t(x, p_0 + l\Delta p) w = 0 \tag{4.41}$$

$$w^t c - 1 = 0 \tag{4.42}$$

where equations (4.40) and (4.42) are the load flow and $w \neq 0$ conditions respectively, p_0 is the vector of independent parameters at a given operating point, Δp is a direction of variation of p, l is a scalar unknown parameter, and c is a nonzero vector. In [42] and [43], this system is used to obtain the locally closest bifurcation point, but it can give sequences of the saddle node bifurcation points as well. By successive rotations of Δp in a plane, it gives the intersection of Σ^{lf} ($J \equiv J_{lf}$) or Σ^{sn} ($J \equiv J_s$) by this plane. In the last case, the system (4.40)-(4.42) can be inconsistent if there is no saddle node bifurcation point $detJ_s = 0$ along the straight line $p_0 + l\Delta p$ within the load flow feasibility domain, i.e. the system is aperiodically stable, and its operating conditions are restricted by the network transfer capability only.

There are some other questions regarding the technique for generating bifurcation boundaries:

(i) What is a reliable way to get an initial estimate of x, l, w on Σ?

(ii) How reliable is the procedure in view of the geometric peculiarities and nonsmoothness of Σ?

(iii) Whether is it possible to obtain all the parts of Σ?

(iv) How many points are to be found for an accurate assessment of Σ?

4.4.2 High Order Numerical Method

Regarding question (i) at the end of the above section, the initial estimate of the critical point can be taken as the point on the solution boundary$\sum$ in the direction Δp from the operating point [108]. A high order numerical method is used to get the initial point and provide further motion along Σ^{lf} [108]. This method may be considered as either a generalization of the Newton-Raphson method including nonlinear terms of the Taylor series, or a parameter continuation technique providing more reliable solution properties. The idea of the method is the following. A nonlinear system $\phi(z) = 0$, which is the power flow problem or set (4.40)-(4.42), can be expressed as

$$\Phi(z, \gamma) = (\gamma - 1)\phi_0 + \phi(z) = 0, \tag{4.43}$$

where the equation $\Phi(z, \gamma) = 0$ implicitly defines the function $z = z(\gamma)$, ϕ_0 is a given nonzero vector, and γ is a scalar parameter. If $\gamma = 0$, a solution of (4.43) corresponds to the point where $\phi(z) = \phi_0$. At $\gamma = 1$, z becomes a solution of the original problem $\phi(z) = 0$. The dependence $z(\gamma)$ can be expressed as the Taylor series

$$z(\gamma) = z_0 + \sum_{k=1}^{\infty} \frac{\gamma^k}{k!} \frac{d^k z}{d\gamma^k} = z_0 + \sum_{k=1}^{\infty} \frac{\gamma^k}{k!} \Delta z_k, \tag{4.44}$$

Formula (4.44), where the upper infinite sum limit is replaced by a given finite number K, is used at each iteration of the method. The correction vectors Δz_k are defined recurrently through the values of the mismatch function $\phi(\cdot)$ computed at certain points, and γ is chosen within the range $(0, 1]$ to get reliable convergence of (4.44) and good accuracy of the method [108]. The method provides many desirable features: reliable solution of nonlinear algebraic problems up to points of singularity; convergence to a singular point if it occurs on the way of the iterative process; almost straight line motion of the iterative process in the space of mismatches; and retention of zero mismatches of (4.43).

4.4.3 Permanent Loading Technique

To get an initial point on Σ^{lf}, the permanent loading technique can be used [91, 108]. In this application, z and $\phi(z)$ are dependent variables x and load flow mismatch functions $F(x,p)$ as in equations (4.45) –(4.47) respectively. For a specified direction $\Delta p = \Delta p_1$ in (4.40), and parameter $l = l_*$ which gives a point outside the feasibility region, the method follows this direction unless a singular point $detJ_{lf} = 0$ has been met - see Figure 4.8, Step 1. The system (4.40)-(4.42) is used after that to refine

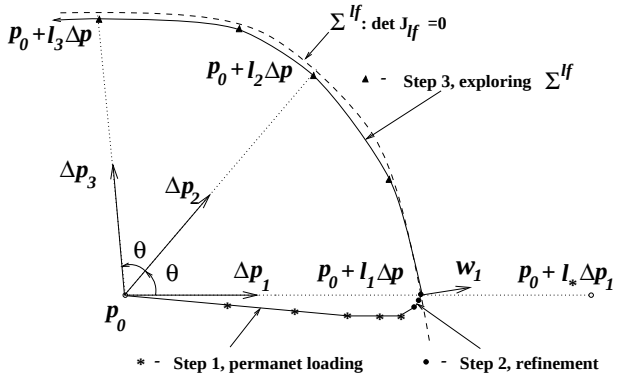

Figure 4.8: Application of the technique [108] to explore Σ^{lf}

the initial estimate of x and get proper initial values of $w = w_1$ and $l = l_1$ - see Figure 4.8, Step 2. To get an initial guess of w_1 for Step 2, the fact that $x(\gamma) \to v_1$ when $p \to \Sigma^{lf}$ can be effectively used [108]. For further exploring the intersection of Σ^{lf} by a plane going through the points p_0 and $p_0 + l_*\Delta p$, the vector Δp is rotated in the plane through the angle increment θ - see Figure 4.8, Step 3. Again, the high order method is applied at the second stage. As mismatches of (4.41) and (4.42) are initially zeros, they are preserved close to zeros afterward, and due to this the high order method follows the feasibility domain boundary. Note that the series (4.44) taken as a function of γ provides an analytical approximation of Σ^{lf}. Equations:

$$F(x,p) = 0 \tag{4.45}$$

$$J^t(x,p)w = 0 \tag{4.46}$$

$$||w|| = 1 \tag{4.47}$$

where y is now a vector of any two independent parameters, and the predictor-corrector method [124] are used in [67] to explore the power flow solution space boundary. The system (4.45)-(4.47) is presented as $\phi(z) = 0,\ z = [x^t, w^t, p^t]$. The unit predictor vector $\Delta p,\ ||\Delta p|| = 1$, that is tangent to the curve (4.45), is given

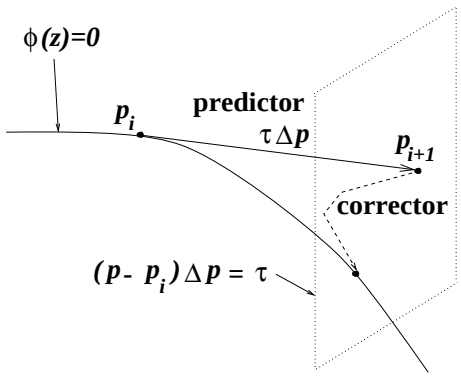

Figure 4.9: The predictor-corrector procedure [124, 67]

by $[\partial\phi/\partial z]\Delta p = 0$ - see Figure 4.9. Predictions of the next point p_{i+1} are found as $p_{i+1} = p_i + \tau\Delta p_i$, where τ is the step length. Corrections of a step are computed by simultaneous solution of equations describing hyperplanes perpendicular to p, that is $(p - p_i)^t\Delta p = 0$, and $\phi(z) = 0$. The initial point on Σ is found by application of the same predictor-corrector technique to solution of the problem $f(x, p) = 0$. The predictor-corrector technique is considered as a very reliable parameter continuation method [124]. Nevertheless the above questions (ii)-(iv) remain relevant.

4.4.4 Predictor Corrector Method

For the Hopf bifurcation boundary Σ^h, the state matrix J_s has to satisfy the following conditions [42, 110]:

$$\begin{array}{l} J_s^t(x,p)w' + \omega w'' = 0 \\ J_s^t(x,p)w'' - \omega w' = 0 \end{array} \Leftrightarrow \begin{array}{l} J_s(x,p)v' + \omega v'' = 0 \\ J_s(x,p)v'' - \omega v' = 0 \end{array} \tag{4.48}$$

In (4.48), $w = w' + jw''$ and $v = v' + jv''$ are the left and right eigenvectors corresponding to eigenvalue $\lambda = 0 + j\omega$. By using (4.48) instead of (4.34), the following set can be proposed to get a Hopf bifurcation point in the direction of Δy

$$F(x, p_0 + l\Delta p) = 0 \tag{4.49}$$

$$J_s^t(x, p_0 + l\Delta p)w' + \omega w'' = 0 \tag{4.50}$$

$$J_s^t(x, p_0 + l\Delta p)w'' - \omega w' = 0 \tag{4.51}$$

$$w_i' - 1 = 0 \tag{4.52}$$

$$w_i'' = 0 \tag{4.53}$$

From the dimensions for the original DAE system model, the set (4.49)-(4.53) consists of $n + 2m + 2$ equations and depends upon the same number of unknown variables x, w', w'', l, and ω, where n and m are the number of load flow and dynamic state variables respectively. Both the Hopf ($\omega \neq 0$) and saddle node ($\omega = 0$) bifurcation boundaries can be plotted by means of successive rotation of Δp. Many difficulties arise regarding the solution of (4.49)-(4.53): absence of bifurcation points on the line $y_0 + l\Delta p$ - see previous comments to the system (4.40)-(4.42) - large dimension, complicated topology of the bifurcation surface, and other computational problems [110].

An alternative way for computing the Hopf bifurcations on the ray $p_0 + l\Delta p$ can be proposed. It consists in the use of eigenvalue sensitivity factors to get the zero real part for a certain oscillatory mode. The procedure implies the following steps:

1. Set $p^1 = p_0$ and $i = 1$.
2. Take x^i as a solution of the load flow problem $F(x^i, p^i) = 0$. Find the vectors x_s^i and x_a^i from x^i.
3. Compute the state matrix $J_s(x_s^i, p^i)$ using (3.92).
4. Find the eigenvalue of interest $\lambda^i = \alpha^i + j\omega^i$ for the matrix $J_s(x_s^i, p^i)$, and corresponding eigenvectors v^i and w^i. If α^i is small enough, stop the procedure.
5. Evaluate the derivative dJ_s/dl at the current point (x_s^i, p^i) numerically.
6. Compute the sensitivity factor
$$\frac{d\alpha^i}{dl} = Re\left\{\left[(w^i)^t \frac{dJ_s}{dl} v^i\right]\left[(w^i)^t v^i\right]^{-1}\right\}$$
7. Find the increment of l as $\Delta l^i = -\alpha^i [d\alpha^i/dl]^{-1}$ and $p^{i+1} = p^i + \Delta l^i \Delta p$.
8. Go to step 2 with $i = i + 1$.

The procedure can be used to get the initial guesses for Σ^h including the eigenvectors and ω. It allows choice of a particular oscillatory mode (for example, an inter-area mode) to get its bifurcation point. Difficulties may be caused by the nonlinear dependence $\alpha(l)$, and by tracing the selected mode between steps.

For the special cases when p does not affect the load flow conditions, p linearly appears in $J_s(p)$, and the operating point p_0 lies inside the stability domain ($Re\lambda_i \leq 0, i = 1, ;m$), we saw equation 4.49 can be eliminated from the system, and x is fixed vector x_*. A special determinant minimization method can be used to solve the problem.

4.5 New Δ-Plane Method

This method is efficient for locating the power flow feasibility boundaries in the space of power system parameters. Besides its application in power system problems, it is also efficient for any quadratic algebraic problem. When applied to power system studies, it is a robust method for finding the power system power flow feasibility boundaries on the Δ-plane defined by any three vectors of dependent variables (e.g. nodal voltages). The method exploits some quadratic and linear properties of the load flow equations and state matrices written in rectangular coordinates. One of the advantages of the method is that it does not require iterative solution of nonlinear equations except for calculating the eigenvalues. Besides locating the boundaries in the parameter space, the method is also useful for topological studies of power system multiple solution structures and stability domains.

4.5.1 Properties of Quadratic Systems

The proposed Δ-plane method is based on the quadratic load flow system properties. The solution and singularity property of the quadratic problem is essential in application of the method.

Consider a power flow problem which requires solution of nonlinear equations of the form given below,

$$F(x, p) = p + f(x) = 0 \tag{4.54}$$

where $p \in R_p^n$ is the vector of specified independent parameters such as active and reactive powers of loads and generators or fixed generator terminal voltages, and $x \in R_x^n$ is the state variable vector, consisting of nodal voltages. The vector function $f(x)$ reflects the sum of power flows into each bus from the rest of the network or generator bus voltages. If nodal voltages x are expressed in rectangular coordinates

then $F(x)$ is a quadratic function of x, and the Jacobian matrix $J(x) = \partial F/\partial x$ is a linear function of x.

The important properties associated with the quadratic systems are given below; more detailed study can be found in [105], [106] and [109].

Property 1. For any two points $x_1 \neq x_2$ and $detJ(x_1) \neq 0$, the number and location of singularities of the quadratic problem $F(x) = 0$ on the straight line through x_1, x_2 is defined by real eigenvalues of the matrix $J^{-1}(x_1)J(x_2)$. These singular points on the line can be found as $x_j = x_1 + \mu_j(x_2 - x_1)$, where μ_j are computed as $\mu_j = (1 - \lambda_j)^{-1}$ for all real eigenvalues $\lambda_j \neq 1$ of the matrix $J^{-1}(x_1)J(x_2)$.

Property 2. The maximum number of solutions of a quadratic equation $F(x) = 0$ on each straight line in the state space R^n_x is two.

Property 3. For quadratic mismatch functions $F(x)$, a variation of x along a straight line through a pair of distinct solutions of the problem $F(x) = 0$ results in variation of the mismatch vector $F(x)$ along a straight line in R^n_p.

Property 1 gives a background of the proposed Δ-plane method. Properties 2 and 3 provide helpful implementation for the method. Proofs of these properties are given in Appendix C.

4.5.2 Obtaining bifurcation curves on Δ-plane in R^n_x

The aim here is to develop a method for plotting an intersection of the power flow feasibility domain boundary by a plane in the space of dependent variables x. It is known that the boundary itself consists of points where $detJ(x) = 0$.

A plane in R^n_x can be defined by any three distinct points x_1, x_2 and x_3 provided that

$$x_3 \neq x_1 + \mu(x_2 - x_1) \tag{4.55}$$

is satisfied for any scalar parameter μ. Condition (4.55) means that the three points x_1, x_2 and x_3 do not lie on a single straight line in R^n_x. Once (4.55) is true, the points x_1, x_2 and x_3 form a triangular Δ which defines a plane in R^n_x and gives the name for the proposed method. Any point on the Δ-plane can be expressed by means of scalar parameters γ_1 and γ_2 as shown in Figure 4.10:

$$x(\gamma_1, \gamma_2) = x_1 + \gamma_1(x_2 - x_1) + \gamma_2(x_3 - x_1) \tag{4.56}$$

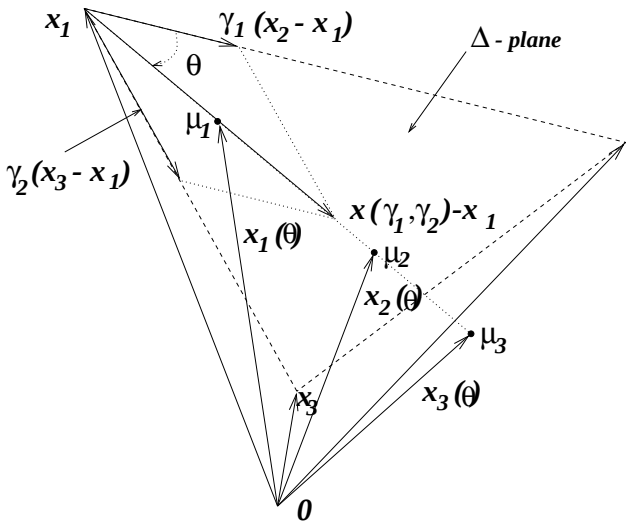

Figure 4.10: The Δ-plane in R_x^n

It is clear that $x(0,0) = x_1$, $x(1,0) = x_2$ and $x(0,1) = x_3$.

Suppose that at the point x_1, the matrix $J(x)$ is nonsingular, i.e.

$$detJ(x_1) \neq 0 \tag{4.57}$$

Then the following procedure can be used to find out all singularities of $J(x)$ in the Δ-plane. The idea consists in rotation of a vector $x(\gamma_1, \gamma_2) - x_1$ in the Δ-plane, and subsequent computations of all singularities of $J(x)$ on each line defined by this vector (see points μ_j in Figure 4.10). The following steps are to be used:

1. Take the angle $\theta = 0$
2. Compute $\gamma_1 = l\ cos\ \theta$ and $\gamma_2 = l\ sin\ \theta$, $l \gg 0$
3. Define a point $x = x(\gamma_1, \gamma_2)$ as in (4.56)
4. Find eigenvalues of the matrix $J^{-1}(x_1)J(x)$
5. Compute $\mu_j = (1 - \lambda_j)^{-1}$ for all real eigenvalues $\lambda_j \neq 1$ from the previous step
6. For each value of μ_j, define the corresponding point in the Δ-plane as

$$x_j(\theta) = x_1 + \mu_j[\gamma_1(x_2 - x_1) + \gamma_2(x_3 - x_1)] \tag{4.58}$$

7. Change $\theta = \theta + \Delta\theta$, where $\Delta\theta$ is an increment, and go to step 2 unless $\theta \geq \pi$.

The set of points $x_j(\theta)$ computed for different θ forms a cut-set of the feasibility domain boundary Σ by the Δ-plane. Note that the proposed procedure does not require an iterative solution except the eigenvalue problem. The reliable QR technique is recommended to be used in step 4.

4.5.3 The Δ-plane Shown in R_x^n

Although the bifurcation points $x_j(\theta)$ in (4.58) belong to the Δ-plane, they are vectors in the multidimensional space R_x^n. To get a visual representation for them, it is convenient to use a new two-dimensional coordinate system associated with the Δ-plane itself. For this purpose, we use the following oblique-angled coordinate system (Figure 4.11).

$$\begin{aligned} \tilde{x}_1 &= \begin{pmatrix} 0 \\ 0 \end{pmatrix} \\ \tilde{x}_2 &= \begin{pmatrix} \|x_2 - x_1\| \\ 0 \end{pmatrix} \\ \tilde{x}_3 &= \begin{pmatrix} \|x_3 - x_1\| \, cos\, \alpha_x \\ \|x_3 - x_1\| \, sin\, \alpha_x \end{pmatrix} \end{aligned} \tag{4.59}$$

where

$$\alpha_x = arccos \frac{(x_3 - x_1)^t (x_2 - x_1)}{\|x_3 - x_1\| \|x_2 - x_1\|}$$

In the new two-dimensional coordinate system, the expression for computing the power flow singular points is the following:

$$\tilde{x}_j(\theta) = \mu_j(\gamma_1 \tilde{x}_2 + \gamma_2 \tilde{x}_3) \tag{4.60}$$

4.5.4 Δ-plane Shown in R_p^n

Consider a particular case when the vectors x_1, x_2 and x_3 are distinct solutions of (4.54). It follows from Property 2 in Section 4.5.1, that those three points can not lie on a straight line in R_p^n. Property 3 in the same section 4.5.1 indicates that, by

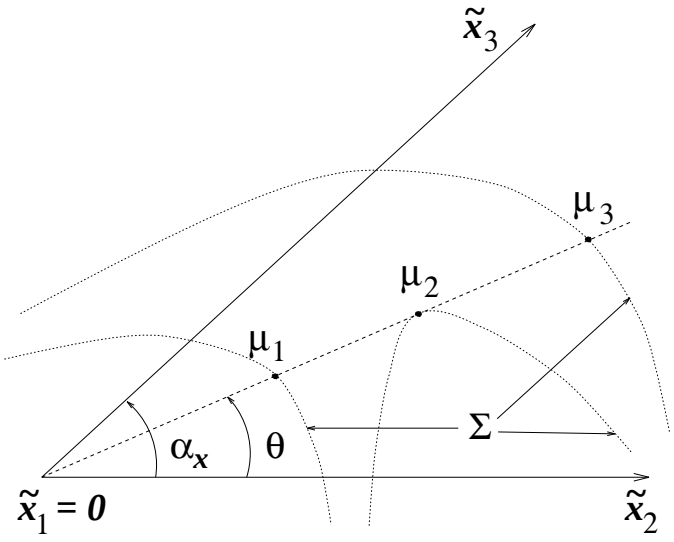

Figure 4.11: Visual representation of the Δ-plane

$y = -f(x)$, the straight lines

$$x(\gamma_1, 0) = x_1 + \gamma_1(x_2 - x_1) \tag{4.61}$$

$$x(0, \gamma_2) = x_1 + \gamma_2(x_3 - x_1) \tag{4.62}$$

in R_x^n are mapped in the straight lines

$$p_1 = p(\gamma_1, 0) = \gamma_1(\gamma_1 - 1)J(x_1)(x_2 - x_1) \tag{4.63}$$

$$p_2 = p(0, \gamma_2) = \gamma_2(\gamma_2 - 1)J(x_1)(x_3 - x_1) \tag{4.64}$$

in R_p^n respectively. The last two lines pass through a common point $-f(x_1)$, and they define a plane which we call the Δ-plane in R_p^n - see plane ABC in Figure 4.12.

4.5.5 Visualization of the Δ-plane in R_p^n

By $p = -f(x)$, all singular points computed along the lines (4.61) and (4.62) are mapped into points of the lines (4.63) and (4.64) respectively. So, they lie on Δ-plane in the space R_p^n. The rest of the points $y_j(\theta)$ do not normally belong to the plane as the plane Δ-plane in R_x^n is mapped by $p = -f(x)$ into a surface which is not a plane (Figure 4.12, surface $ABDC$). The only thing we can do here is to

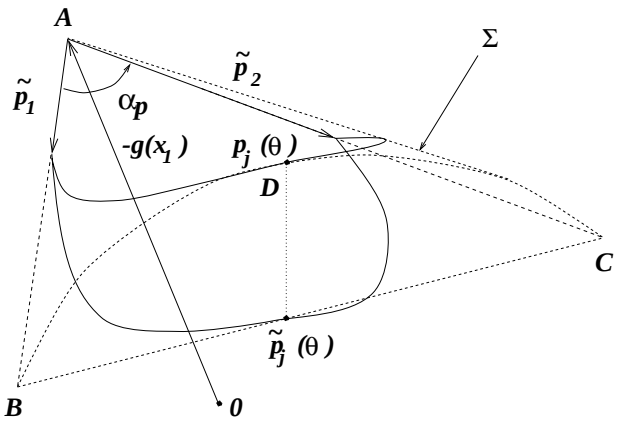

Figure 4.12: The Δ-plane in R_p^n

find the projections $\tilde{p}_j(\theta)$ on Δ-plane in the space R_p^n. The projection $\tilde{p}_j(\theta)$ can be found by the following way. Let

$$\tilde{p}_j(\theta) = \beta_1 \tilde{p}_1 + \beta_2 \tilde{p}_2 \tag{4.65}$$

where β_1 and β_2 are scalar parameters, and $\tilde{p}_1$, $\tilde{p}_2$ are defined as

$$\tilde{p}_1 = \begin{pmatrix} \|p_1\| \\ 0 \end{pmatrix} \tag{4.66}$$

$$\tilde{p}_2 = \begin{pmatrix} \|p_2\| \; cos \; \alpha_p \\ \|p_2\| \; sin \; \alpha_p \end{pmatrix} \tag{4.67}$$

where

$$\alpha_p = arccos \frac{(p_2)^t (p_1)}{\|p_2\| \|p_1\|}$$

The coefficients β_1 and β_2 can be found by solving the linear equation

$$\begin{pmatrix} \|p_1\|^2 & p_1^t p_2 \\ p_1^t p_2 & \|p_2\|^2 \end{pmatrix} \begin{pmatrix} \beta_1 \\ \beta_2 \end{pmatrix} = \begin{pmatrix} p_1 y_j(\theta) \\ p_2 y_j(\theta) \end{pmatrix} \tag{4.68}$$

They are used in (4.65) after that to get singular points in the two-dimensional oblique-angled coordinate system $(\tilde{p}_1, \tilde{p}_2)$.

As the singular points belong to a nonlinear surface (see the surface $ABDC$ in Figure 4.12), and only their projections on the Δ-plane are used, the resulting plot reflects only a qualitative representation of the singular boundary in R_p^n. Nevertheless, all singular points along the lines AB and AC are presented very accurately.

4.5.6 Δ-plane View of The New-England Test System

The proposed method has been tested for the New England Test System [16] as given in Figure 3.2. The system consists of 39 buses, 10 generators, and 18 loads. Bus number 31 is a slack bus. All other generators are simulated by means of constant active powers and terminal voltages. Loads have fixed active and reactive demands.

Three distinct load flow solutions x_1, x_2 and x_3 given in Table 4.1 are considered. These solutions were selected from a solution set obtained by the method for computing multiple solutions of quadratic algebraic problems given in [105, 109]. All three points are low voltage solutions. Solutions x_1, x_2 and x_3 define a Δ-plane in R_x^n shown in Figure 4.13. The orientation of the plane is do by setting x_1 correspond to zero point $(0, 0)$, and the vector $x_2 - x_1$ be directed along the horizontal axis.

Solution x_1 is taken as a fixed point for the plot, and all straight lines, along which the singularities are determined, belong to Δ-plane and pass through x_1. The cut-set of the feasibility domain boundary by Δ-plane is shown by dotted curves.

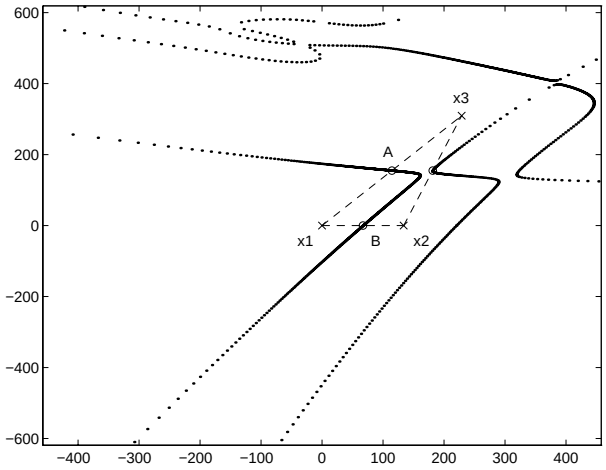

Figure 4.13: Δ-plane in R_x^n plane of nodal voltages (New England Test System)

A detailed consideration of the feasibility boundary topology is not the main purpose here. Nevertheless some observations can be made based on the Δ-plane:

- The singular points marked by small circles lie exactly in the middle of the

Bus	Solution x_1		Solution x_2		Solution x_3	
	V, kV	δ, grad	V, kV	δ, grad	V, kV	δ, grad
1	103.1	-25.2	0.0	-23.2	89.3	-42.4
2	101.7	-18.9	86.9	-11.0	64.1	-41.1
3	95.5	-20.8	92.0	-15.1	3.8	-125.2
4	84.2	-19.9	94.6	-15.7	44.5	-39.2
5	77.0	-16.8	96.6	-14.1	64.0	-29.0
6	78.7	-15.3	97.2	-13.1	67.7	-26.4
7	68.5	-19.5	96.0	-16.3	66.3	-32.7
8	64.1	-20.7	95.9	-17.3	66.5	-34.5
9	0.0	-21.1	100.8	-23.4	88.9	-40.2
10	88.2	-13.2	98.9	-10.8	73.5	-25.3
11	84.9	-13.9	98.2	-11.6	71.2	-25.7
12	84.6	-14.2	96.8	-11.7	67.6	-26.7
13	87.9	-14.4	98.2	-11.7	68.9	-27.5
14	87.9	-17.3	96.9	-13.6	59.0	-34.3
15	94.2	-19.1	97.5	-14.5	64.3	-45.0
16	98.6	-18.0	99.4	-13.1	69.5	-45.2
17	98.3	-19.4	97.2	-14.3	52.3	-49.7
18	97.1	-20.4	95.1	-15.1	32.0	-56.4
19	103.5	-13.2	103.8	-8.4	93.6	-39.1
20	98.3	-14.5	98.5	-9.7	92.6	-40.8
21	100.0	-15.4	100.6	-10.6	79.5	-41.2
22	103.4	-10.8	103.7	-6.0	92.5	-35.1
23	102.7	-11.0	103.1	-6.2	91.5	-35.3
24	99.5	-17.9	100.3	-13.0	73.0	-45.1
25	103.5	-17.6	93.9	-12.0	75.6	-45.8
26	102.4	-18.2	98.3	-12.9	73.4	-48.1
27	99.9	-20.0	97.2	-14.9	62.5	-51.7
29	103.6	-14.6	101.5	-9.2	88.8	-43.2
29	104.1	-11.8	102.7	-6.3	94.1	-39.9
30	104.8	-16.5	104.8	-8.3	104.8	-37.4
31	98.2	-0.3	98.2	0.0	98.2	0.0
32	98.3	-5.1	98.3	-3.7	98.3	-15.6
33	99.7	-8.7	99.7	-3.8	99.7	-34.4
35	101.2	-9.4	101.2	-4.6	101.2	-35.5
35	104.9	-6.0	104.9	-1.2	104.9	-29.7
36	106.4	-3.1	106.4	1.7	106.4	-26.52
37	102.8	-11.0	102.8	-4.9	102.8	-37.3
38	102.7	-5.1	102.7	0.5	102.7	-32.7
39	103.0	-28.9	103.0	-27.3	103.0	-42.5

Table 4.1: Three Distinct Load Flow Solutions Defining The Δ-Plane

dashed lines connecting the points x_1, x_2 and x_3. This fact is due to the quadratic load flow properties. Detailed explanation can be found in [105, 109] etc.

- The singular curves in Figure 4.13 have an open shape. This means that, by certain unrestricted variations of nodal powers p in R_p^n, voltages x in R_x^n may be indefinitely increased without reaching the power flow feasibility boundary. This paradoxical fact can be explained as follows. The singular boundary is considered without any limitations applied to parameters p. Therefore the generator terminal voltages and nodal powers in all buses can be varied arbitrarily. Obviously, by varying p, it is possible to get unrestricted voltage increase in some buses and provide unlimited power transfers. In real situations, the limitations for p, for example, equality constraints for generator terminal voltages and zero power injections in empty buses, must be taken into account.

Figure 4.14 shows the corresponding Δ-plane in R_p^n. Point 0 represents the operating condition $p_0 + g(x) = 0$ of the system. The singular boundary is plotted by using the map $p = -p_0 - g(x))$. Points A and B correspond to the points A and B in Figure 4.13. All singular points which belong to the straight lines defined by $0 - A$ and $0 - B$ are given accurately. All other points are obtained as projections of multidimensional singular curves on the Δ-plane in R_p^n.

As seen from the descriptions above, this new technique does not require an iterative solution of nonlinear equation sets. For quadratic problems, it produces all saddle node bifurcation points on a straight line in space of dependent variables (e.g. nodal voltages given in rectangular form) by solution of an eigenvalue problem. The method is useful for visualization and topological studies of the multiple solution and feasibility domain structures. However, since the boundaries produced by this method are rather complex, this clearly raises questions about their approximate solution in realistic power systems.

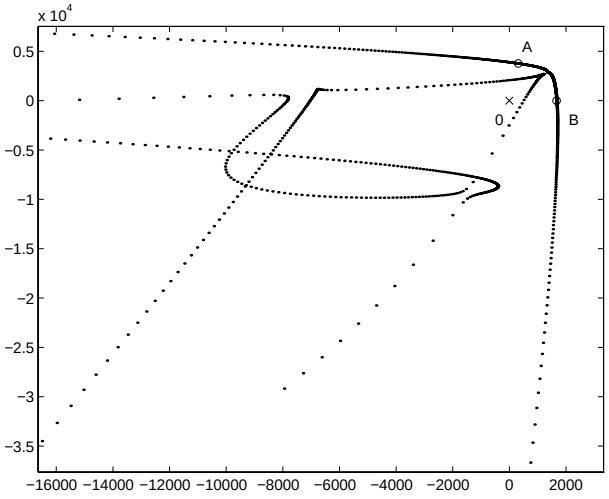

Figure 4.14: Δ-plane in R_p^n plane of nodal powers (New England Test System)

4.6 Continuation Method for Tracing the Aperiodic and Oscillatory Stability Boundaries

We now present a continuation method procedure for tracing the aperiodic and oscillatory stability boundaries.

Besides the traditional steady-state stability limit which is usually taken from the power flow feasibility limits, the aperiodic and oscillatory small-signal stability restrictions (saddle node and Hopf bifurcation boundaries) should also be considered as a characteristic of the network transfer capability. In open access grids, there is the likelihood of increasing numbers of stability limited transfers. We refer to the following well-known facts [77]:

- Economic incentives often require the open-access system to operate away from its nominal design conditions;
- The grid is subject to uncertain and significant changes in generation and load.

In longitudinal systems, for instance, this may lead to poorly damped inter-area oscillations which are difficult to eliminate by using the traditional approaches.

Bifurcation analysis is mainly used to indicate power system voltage collapse and instability in power systems. The assessment of the saddle node and Hopf bifurcation boundaries and corresponding stability margins in the space of system parameters would be helpful and maybe essential for monitoring transfer capability in open-access grids.

There are techniques locating these stability points along a given ray in the parameter space, which have been discussed in Chapter 3 and Sections 4.1-4.6 of this chapter. However the general solution system equations are rewritten here for completion,

$$f(x, p_0 + \tau\Delta p) = 0 \tag{4.69}$$

$${J_s}^t(x, p_0 + \tau\Delta p)l' + \omega l'' = 0 \tag{4.70}$$

$${J_s}^t(x, p_0 + \tau\Delta p)l'' - \omega l' = 0 \tag{4.71}$$

$$l_i' - 1 = 0 \tag{4.72}$$

$$l_i'' = 0 \tag{4.73}$$

Solutions of the system (4.69)-(4.73) correspond to either saddle node ($\omega = 0$) or Hopf ($\omega \neq 0$) bifurcations. Nevertheless the extreme load flow feasibility conditions (if they do not coincide with the saddle node bifurcations) can not be located by means of this system. They can be located by any of the techniques discussed before, e.g. direct method by substituting the load flow Jacobian with the state matrix, or Δ-plane method for their cut-set in the parameter space.

Before starting tracing the bifurcation boundaries, an initial solution of the bifurcation point is needed. This step has been discussed in section 3.4. Once the first solution had been found, implicit function based theorem can be used to follow the solution curves. The Davidenko -Newton -Raphson method was employed to fulfill the task [136]. The method can be explained as follows:

- At the equilibrium point, assume the bifurcation problem is formulated as $0 = f(x, \lambda)$, where x is the vector of state variables, and λ is the bifurcation parameter. When differentiating both sides of the equation, the result comes out as,

$$0 = df = f_x dx + f_\lambda d\lambda$$

$$dx/d\lambda = -(f_x)^{-1} f_\lambda$$

- Then given $x(\lambda_0) = x_0$, the equation above can be solved using any ordinary differential equation [ODE] solver such as R-K method to determine the dependence of x on λ.

- Subsequently, the solution of the last step will be taken as initial guessed value of solution for the next step and so on to trace the bifurcation boundary / solution curve.

Due to singularity or ill-conditioning of the Jacobian matrix, the tracing procedure may converge very slowly or not at all in some cases. To avoid this, as the first choice, a smaller step size for Δp can be used. In more complicated cases, the entire procedure should be repeated for different eigenvalues and initial loading directions. In view of complicated shape and possible loops in the bifurcation curve, it can be useful to relocate the point y_0 and change the loading direction Δp and parameter τ during the tracing procedure. The idea is to ensure a better position for the point p_0 with respect to the bifurcation boundary and to avoid cases where $\tau\Delta p$ is a tangent vector to this boundary. Note that the vectors p_0, Δp and parameter τ can be easily changed in coordination to preserve zero mismatches of power flow condition. To achieve this, the initial operating point $p_0 + \tau\Delta p$ is kept fixed through the process. The following correction procedure can be used:

- Compute the curventure radius and center of the boundary with the former solution points.

- Set a new point p_0 in the torsion center, change the direction Δp and bifurcation parameter τ to preserve the last obtained bifurcation point p_* .

- Continue with the tracing procedure.

Figure 4.15 illustrates the proposed correction procedure. Suppose that initially the vector $\tau\Delta p$ originates at point a, and that, as a result of its clockwise rotation, the point c is achieved. It is clear that further tracing of the bifurcation boundary in the clockwise direction is impossible. However by rotating the origin of $\tau\Delta p$ in the point b, which is the current curventure center of the curve, and changing the vector $\tau\Delta p$ correspondingly, clockwise tracing of the bifurcation boundary can be continued.

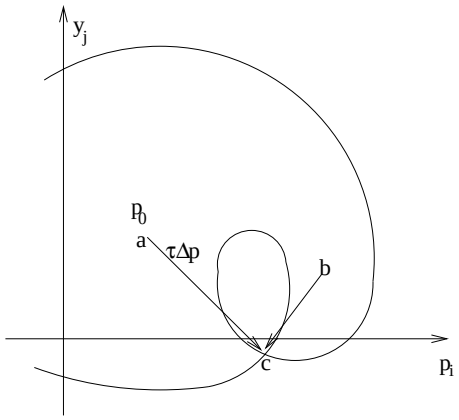

Figure 4.15: Continuation corrector method

Numerical Example Using the Technique

The tracing technique has been applied to the single machine infinite bus system with motor load [33] in Figure 3.6 and described by equations (3.68) –(3.71). The tracing results are given in Figures 3.13 -3.18. The feasibility and Hopf bifurcation boundaries are given in Figure 4.16, and all other figures are simulations aimed to verify the method. These figures have been given in Section 3.6.2. The figure

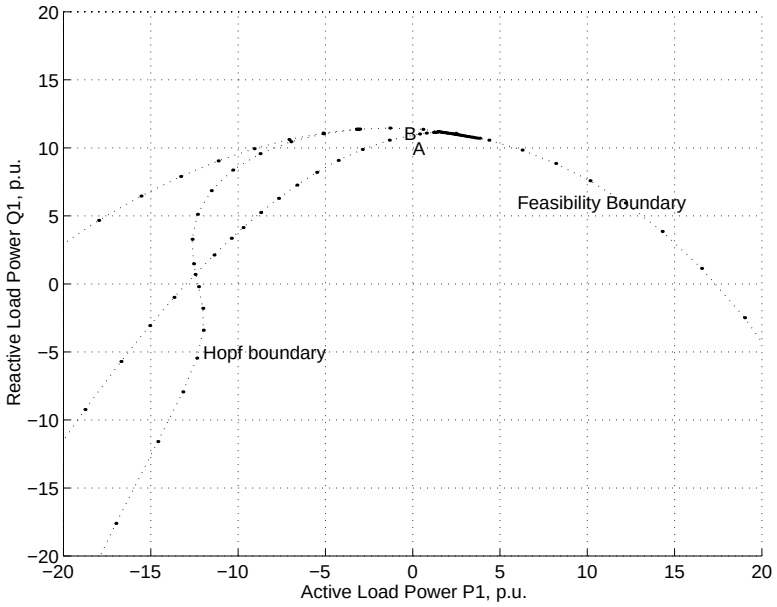

Figure 4.16: The Feasibility and Hopf Bifurcation Boundaries as A Result of Tracing

is obtained by two steps: (1) locating the initial bifurcation point by initial value approximation techniques given in Chapter 3, Section 3.4 - see Figure 3.1 - and (2)parameter continuation tracing techniques given in this section.

4.7 Conclusion

Two major techniques are addressed in this chapter: (1) visualizing the security boundary hyperplane defined by characteristic points; (2) a continuation method to trace the aperiodic and oscillatory instability boundaries. As compared with traditional approaches, the new techniques proposed here are superior in their capability to show the boundaries from point of view of computation efficiency and result accuracy. The potential usage of the results is greatly increased by the problems faced in modern open access systems.

In the next chapter, a powerful optimization tool, i.e. the Genetic Algorithm (GA) is to be discussed, which can overcome difficulties caused by non-convexity, and non-differentiable nature of some problems that need optimization.

Chapter 5

Genetic Algorithms for Small Signal Stability Analysis

5.1 Introduction

In this chapter, we address a new genetic optimization technique which can be used to compute the small signal stability boundaries and margins in the space of power system parameters of interest. The margins are determined as a set of critical [the shortest] and subcritical [closest to the shortest] distances from the system's state point to the load flow feasibility, aperiodic and oscillatory stability boundaries. The proposed technique is able to locate the distances quite robustly within one procedure. It is an important feature that the distances are computed for all of the different boundaries concurrently.

Recall the analytical techniques to locate power system small signal stability critical conditions discussed in Chapters 3,4. The problem we need to solve includes an initial guess of solution points, numerical methods to locate the critical solutions, as well as general methods to find all characteristic points in the parameter space. All these methods start from a ray in the parameter space, and obtain solution by solution along the direction defined by this ray. Also a problem arises when tracing a particular eigenvalue in the search procedures. Take for example the general method; the optimization procedure has to be repeated for every eigenvalue of interest in order to locate these stability characteristic points in one direction. In case the power systems to be studied are very large, the computation costs will increase greatly.

Once again, the result depends upon the initial guesses of variables and selected eigenvalues. The choice of these parameters is a complicated task. One can use some practical ideas regarding the most dangerous loading direction and critical eigenvalues [for example, corresponding to the inter-area oscillatory modes.]. Nevertheless, it looks quite difficult to get all of the critical and subcritical distances by these analytical approaches.

One of the most compelling difficulties in all the formerly mentioned procedures is computing the small signal characteristic points in view of breaks of smoothness in the objection function and constraints. For example, to take account of reactive power limits, different models in the constraint set will have to be used. A sudden change in the model causes severe problems for the optimization procedures. In fact, it can lead to an instant instability [42].

To summarize, the analytical approaches to the small signal stability analysis have many difficulties which can be hard to solve by traditional optimization techniques. For this reason, we are attempting to apply the genetic optimization procedures.

The structure of the chapter is as follows. A brief review of features of GAs is given. Then a black box model of the power system is used with inputs corresponding to parameters of interest and output as the fitness function. A fitness function is designed to reflect in influence of the critical eigenvalue and the distance to the stability boundary. The GA operates in the space of black box inputs. The solution of the problems of locating characteristic points and critical distances is demonstrated on two examples. Finally, a scheme for reactive power planning using GAs is presented.

5.2 Fundamentals of Genetic Algorithms (GAs)

Genetic Algorithms (GAs) [56] are heuristic probabilistic optimization techniques inspired by natural evolution processes. In genetic algorithms, the fitness function is used instead of objective function as in the traditional optimization procedures. Each concrete value of variables to be optimized is called as an individual. Then a current number of individuals compose the generation. In the process of GAs, individuals with better fitness survive and those with lower fitness die off, so finally the individual with the best fitness is located as the final solution. They are capable of locating the global optimum of a fitness function in a bounded search domain, provided a sufficient population size is given. The GA sharing function method is able to locate the multiple local maxima as well.

Genetic Algorithms (GAs) belong to class of the derivative-free optimization methods. They rely on repeated evaluations of the objective function, and the subsequent search direction after each evaluation follows certain heuristic guidelines [80]. GAs use reproduction, crossover and mutation as major operators to simulate natural evolution process. Based the evaluation of the objective functions, only the populations with highest fitness values can survive till we obtain the acceptable optimization point. GAs are suitable for noisy and discontinuous functions. They work with a set of parameters and probabilistic transition rules thus providing a robustness property for many optimization problems [56].

As compared with other search techniques, the features of Genetic Algorithms can be summarized as [56, 94]:

- Heuristic probabilistic algorithms for searching and optimization, which emulate natural evolution processes;
- Based on a set of encoded strings representing parameters (instead of these parameters themselves);
- Started from a set of individuals standing for a group of possible solutions of variables to be optimized instead of a single point, while traditional optimization techniques do start from a point;
- Inherently parallel;
- Capable of handling multimodal, nonlinear, non-convex problems;
- Optimization procedure does not require differentiation operations;
- Capable of locating global optimum and local optima within search domain.

The major genetic operators are:

Selection/Reproduction - which creates a new population from the old population biased towards the highest fitness. Selection is based on individual fitness of the current generation. Generally the selection scheme is Roulette Wheel Selection, which calculates the ratio of individual fitness to the sum of all fitnesses of the generation, $\frac{f_i}{\sum f_i}$. This ratio is the individual's probability of being selected. Once an individual is selected, it is copied exactly and put into a temporary mating pool for usage by other genetic operations. By this way, the higher the individual's fitness, the more possible it will survive by being copied of its gene into individuals of later generations.

Crossover/Mating - swaps chromosome parts between individuals. There are two steps of crossover operation. Firstly, a couple of individuals is selected from the mating pool produced during selection/reproduction. This selection is done with a certain probability. Then this two individuals are crossed over and a new couple of individuals are produced as a result. The crossover can be done on one point or two points on the string representing the mating individuals. In Figure 5.1

one-point and two-point crossover are performed on two sample mating individuals. A Genetic Algorithm achieves global optimization by reproduction and crossover to pass over and mating the information included in individual strings.

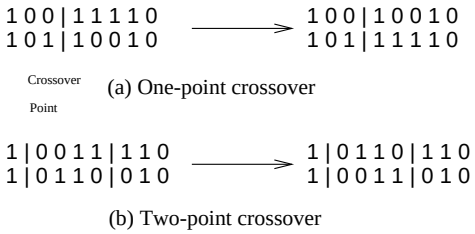

Figure 5.1: **Crossover/Mating** - swaps chromosome parts between individuals.

Mutation - changes a random part of the string, aimed to bring back any lost bit from selection and crossover. Mutation is usually taken as an auxiliary operator. Mutation is performed on single individuals by changing bits on individual chromosome with very small probability. By mutation, the differences among individuals are kept so to bring back bits with better fitness lost during former genetic operation. Mutation prevents the genetic algorithm from premature convergence toward local optima instead of global optima.

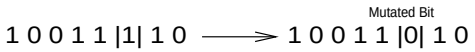

Figure 5.2: Mutation - changes a random part of the string, aimed to bring back lost bit from selection and crossover.

Corresponding to these operators are the probabilistic factors, P_s, P_c, and P_m which are selection probability, crossover probability and mutation probability. They usually take the values as $P_s \leq 1.0$, $P_c \approx 0.8$, and $P_m \approx 0.001 \sim 0.02$. Note that the mutation probability rate should be very small, otherwise the optimization process may fluctuate and takes longer time to converge. However, zero mutation rate may result in loss of the best fit chromosome during optimization. Note $P_m > 0.5$ will lead to random search regardless of crossover probability [56]. Generation size is also important for efficient genetic optimization procedure.

It can be seen that Genetic Algorithms are evolved from nature evolution process, and listed in Table 5.1 are the items of GA as compared with natural evolution.

However, Genetic Algorithms are usually not as fast as traditional methods, [71].

Terms for Natural Evolution	Terms for Genetic Algorithms
Chromosome	String
Gene	Characteristic
Gene type	Structure
Epistasis	Nonlinearity

Table 5.1: Terms of natural evolution as compared with GA terms.

For bulk power systems, population control is necessary to save computation costs. The idea of population control is that computation should start with large population size, then reduce it gradually in every generation that followed. Also resolution control will help with large size systems. Resolution control requires large step size in the beginning of the generations, till promising regions are reached; then it can be reduced to find more accurate results [71].

5.3 Genetic Optimization Procedures

The traditional algorithms for optimization sometimes fail to give the correct solution or can even give no solution at all if the problem lacks such properties as linearity, convexity and differentiability [134]. For all the analytical approaches to stability analysis, the optimization methods used are mainly Newton-Raphson like, which uses the Lagrange function method in equation (3.101) and the procedure shown in Figure 3.8. This method starts from one point and searches for the optimal solution based on differentiation information and a series of iteration procedures. It might stop at local optima and requires the objective function be continuous, differentiable and locally convex. Other methods can be used to locate the global optimum. For instance, the infinite search method, compares the objective function values based on many discrete points in the search domain to locate the best solution taken as the global optimal solution. However, it becomes impossible to use for a very large search domain. Another nonlinear optimization method is the Interior Point (IP) method, which is capable of handling large sets of equality and inequality constraints within the problem solution by using a Lagrangian function. The IP method has been used in determining power system loadability, collapse point,

and other feasibility limits. However, IP method still requires Newton's method to solve the modified objective function, which contains objectives and constraints [79]. Simulated Annealing (SA) and the Monte Carlo method are other kinds of heuristic probabilistic optimization methods. The SA mimics the annealing process by decreasing the temperature, which is represented by the objective function, to locate the point with minimum value. The normal SA method may stop at local optima and fail to find the global one. The Monte Carlo method often involves too much random information for practical processing [100]. An overview of optimization techniques being applied to the determination of power system feasibility regions can be found in [19].

The Genetic Algorithms compared with all these traditional optimization methods, are very robust in locating the global optima, and do not require the objective function to be continuous, differentiable, and convex.

Before the Genetic Algorithm can optimize a real optimization problem, the variables to be optimized will have to be encoded. Since GAs operate on chromosomes, or bits of strings representing the optimization variables, a suitable encoding scheme is essential to GA operation. Currently, the binary encoding scheme is the most popular one. The key aim of genetic optimization is achieved by searching for the best fitted individual as the solution in the search domain. The final result is usually a group of solution points with very close fitness clustered around the global optimal point. The Genetic optimization algorithm can be represented by

$$\begin{aligned} y &= F_{fitness}(x) \\ x_{optimal} &\subset \{x | y = max[F_{fitness}(x)]\}. \end{aligned}$$

Procedures involved in GA Optimization

1. Production of initial population: $P(0) = \{\xi_1(0), \xi_2(0), ..., \xi_\eta(0)\}$

2. Individual fitness evaluation: evaluation of the encoded individuals, $f(P(j)) = \{f(\xi_1(j)), f(\xi_2(j)), ..., f(\xi_\eta(j))\}$, where P stands for population, j stands for j-th generation, and ξ_i are the i-th individuals of the generation, there are totally η individuals in the generation.

3. Genetic operations

- Reproduction/Selection
- Crossover/Mating
- Mutation

4. Produce new generation.

5. Repeat from step 2 till some stopping criteria is met. This criteria may be the preset maximum number of generation being met, or stabilized population fitness measurement over several genetic operation iterations from steps 3, 4, 5 and 2.

The conventional Genetic Algorithm is illustrated in Figure 5.3 [93].

5.3.1 Genetic Algorithms Sharing Function Method

A Genetic Algorithm by itself is able to locate the global optimal solution in the search domain. This is very important in global optimization and search problems. However, this is not enough for power system analysis in certain cases. For example, to locate the shortest distance to instability in the parameter space, there are not only global shortest distances, but also many local shortest distances which may affect the power system safe operation as well. In such cases, an algorithm is expected to locate both global and local optima. The sharing function method [56, 57], is capable of fulfilling this task.

The sharing function method comes from the two-armed bandit payoff rule, where the number of players are allocated according to payoffs of each arm [57]. There are two important terms for the method; these are niche, which means a group of individuals within a certain distance under a similarity measure, and species, which is a generated stable subpopulation. For example, in the Bandit case, species are associated with the stable subpopulations behind each arm which is referred to as a niche. More generally, a niche can be understood as an domain of certain distance, in which individuals can reside. The method is achieved by degradation of individuals payoff via its fitness according to its distance to the neighboring individuals.

To sum up, The method decreases the fitnesses for similar individuals by the "niche count", $m'(i)$. For each individual ξ_i, the niche count is computed as a sum of

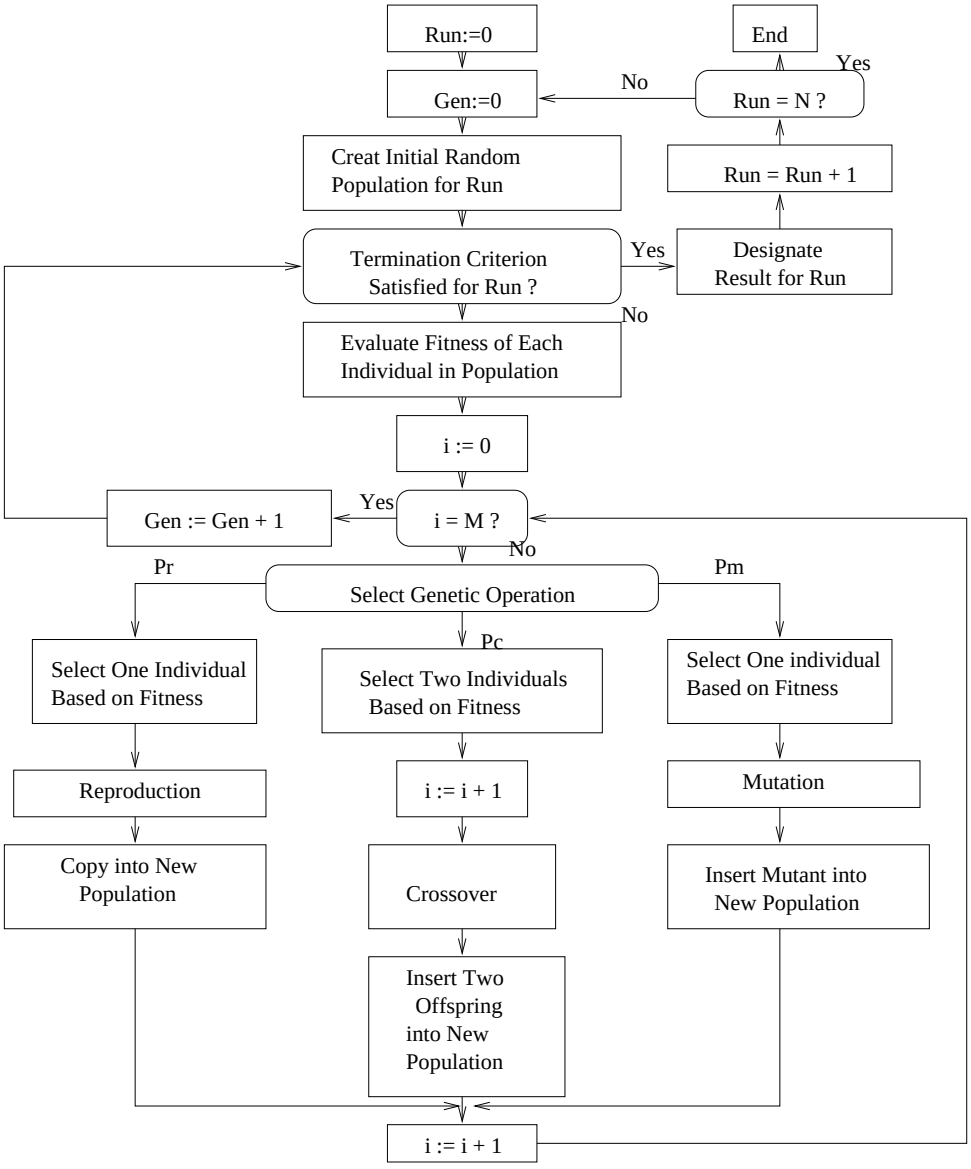

Figure 5.3: Genetic Algorithm Flowchart.

sharing function values between the individual and all individuals ξ_j generated - see equation (5.2) below. The similarity of individuals is evaluated by the distance, $d(i,j)$ from each other. The resulting shared fitness Φ' is changed through dividing the original fitness, Φ by the corresponding niche count (5.3), where the fitness Φ is defined depending on specific problem to be optimized [56, 57, 102]. These operations are represented as follows:

$$d(i,j) = d(x_i, x_j) \tag{5.1}$$

$$m'(i) = \sum_{j=1}^{n} sh[d(i,j)] \tag{5.2}$$

$$\Phi'(i) = \frac{\Phi(i)}{\sum_{j=1}^{n} sh[d(i,j)]} \tag{5.3}$$

The sharing function is defined so that it fulfills,

$$sh(d) = \begin{cases} 0 \leq sh(d) \leq 1 \\ sh(0) = 1 \\ \lim_{d\to\infty} sh(d) = 0 \end{cases} \tag{5.4}$$

For example, the sharing function can have the form,

$$sh(d) = \begin{cases} 1 - (\frac{d}{\sigma})^{\alpha}, & \text{if } d < \sigma \\ 0, & \text{otherwise} \end{cases} \tag{5.5}$$

where α is a constant, and σ is the given sharing factor.

By doing so, an individual receives its full fitness value if it is the only one in its own niche, otherwise its shared fitness decreases due to the number and closeness of the neighboring individuals.

In later sections, a Genetic Algorithm with sharing is applied to small signal stability analysis, where the optimization problem is highly non-linear and sometimes, non-differentiable.

Take for example the optimization problem of the multi (decreasing) peak function,

$$f(x) = sin^6(5.1\pi x + 0.5)e^{[-4x^2]} \tag{5.6}$$

The optimization result by using a normal genetic algorithm and GA with sharing function method are given in Figures 5.4. As indicated in the figures, after genetic optimization, the solution points are crowded at around the global optimal point without sharing. Otherwise the solutions are distributed around several local optima as well.

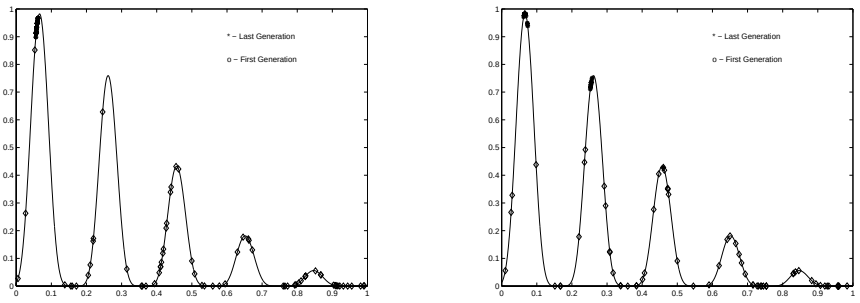

A B

Figure 5.4: A - Optimization Results without Sharing. B - Optimization Results with Sharing.

5.3.2 Fitness Function Formulation

In order to find the optimal solution to a problem, the objective function associated with that problem will have to be converted into the form of a fitness function for Genetic Algorithm optimization. There are several requirements in the conversion, among which the most important conditions are listed below:

- The fitness function must always be positive in the search domain;
- The fitness function is designed so that the optimal solution is obtained at the maximum value of the fitness, i.e. GAs are globally locating the maximum fitness.

Accordingly, in practical optimization problems, the fitness function itself often needs to be adjusted to obtain better genetic optimization results. The major need for fitness adjustment arises in cases when: (a) the minimization problem leads to a negative objective function; (b) premature termination of the search process because of reproduction of individuals is dominated by above average fitness at the beginning of genetic optimization; and (c) where bad convergence emerges from simple random reproduction caused by closely distributed fitnesses among individuals. There are several approaches to adjust fitness, namely, linear transformation, power law transformation, and exponential transformation. Normally, linear transformation is good enough for fitness adjustment [56].

For power system small signal stability assessment, the fitness function should be selected to reflect the influence of the critical eigenvalue and the critical distance to the small signal stability boundaries. For this problem, we suggest the following general form of the fitness function,

$$\Phi(\alpha, d) = \phi_1(d)\phi_2(\alpha) \tag{5.7}$$

where α is the real part of the system critical eigenvalue, and $d = ||\mu(p - p_0)||$ is the distance from the current operating point p_0. The diagonal matrix μ scales the power system parameters which may have different physical nature and range of variation. The first multiplier in equation (5.7) reflects the influence of distance, and the second one keeps the point y close to the small signal stability boundary. For example, the following expressions for ϕ_1 and ϕ_2 can be exploited,

$$\phi_1(d) = 1/d \tag{5.8}$$

$$\phi_2(\alpha) = e^{k\alpha^{-2}} \tag{5.9}$$

where k is the factor defining the range of critical values of α. The second multiplier acts as a filter. If k is very large, say about 1000 or more, then only those α which are very close to zero can pass the filter and survive during the genetic optimization process. The filter eliminates a large number of negative α, to force the GA to select individuals close to the small signal stability boundaries. The filter function takes the shape as shown in Figure 5.5, where the horizontal axis, α, is the real part

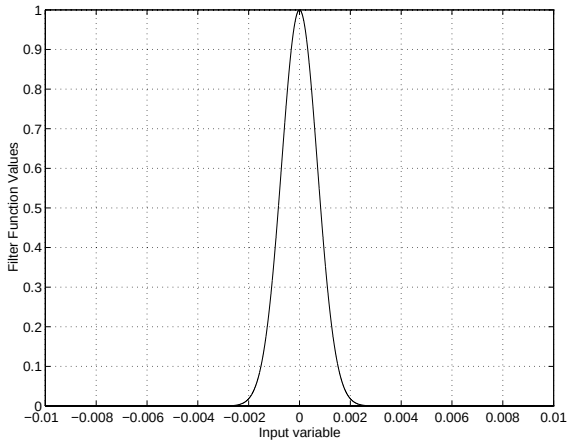

Figure 5.5: The Filter Function for the Fitness Function

of the power system Jacobian critical eigenvalue(s), and the filter function is close

to 1 only when the $\alpha \approx 0$, which corresponds to saddle node or Hopf bifurcations, and by proper modeling, can also correspond to load flow feasibility limits, and minimum /maximum damping conditions - see Section 5.4.1.

5.3.3 Population Size Control

The shape of power system small signal stability boundaries can be very complicated, and there are many niches existing. In order to ensure the GA locates the multiple maxima of the fitness function, and to avoid the noise induced by genetic drift, the sufficient population size should be considered. Different population size requires different genetic parameters in order to obtain better performance. For example, for population sizes of 20 to 40, either higher crossover probability (P_c) together with lower mutation probability (P_m), or lower P_c with higher P_m will give good results. However, the larger the population size, the less the probability of optimal crossover occurs, and the convergence period will be prolonged as well. Techniques for choosing the population size can be found in [102].

To enhance the GA search capability and speed up convergence, population size can be set at a large value in the beginning; then with the increasing number of generations as the generated individuals are being located into narrower search areas, the population size can be decreased. By doing so, the convergence will be achieved faster which still ensuring the global reliability of the final solution. However, the minimum level of population size should be chosen carefully so that the GA search process has enough searching diversity to avoid being trapped into some locally optimal regions.

5.3.4 Mutation Probability Control

Mutation probability is exponentially decreased with increase of generation numbers. The procedure is adopted from the concept of Simulated Annealing where the 'temperature' is decreased according to the increment of iteration numbers [147]. In this context, the mutation rate is set to be .28 in the beginning, then decreased close to zero after the tenth generation - see Figure 5.6. For better GA performance with not very large scale systems, adaptively adjusted mutation probability can be used [101]. Higher mutation probability in the beginning ensures individuals will be

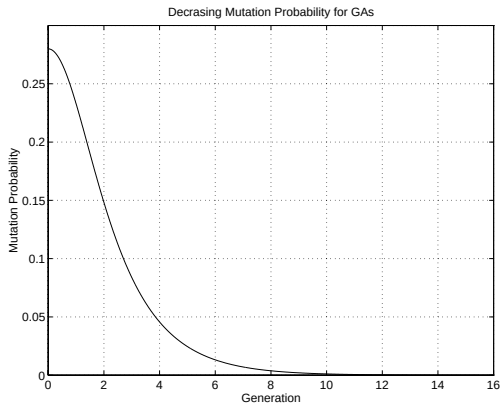

Figure 5.6: The decreasing trajectory of mutation probability

produced to be distributed all over the search domain instead of clustered into some small areas. As the search proceeds, more and more individuals are produced close to the global optimal solution points, so a lower mutation probability is adopted to prevent long convergence time. The process is summarized in Table 5.2.

	High P_m	Low P_m
Stage	Beginning	Close to End
Effects	Search diversity	Stable solution

Table 5.2: Mutation Probability Adjustment

5.3.5 Elitism - The Best Survival Technique

In reference [56], the Simple Genetic Algorithm (SGA) proposed includes all the operators of the GA optimization mechanism. However, the SGA cannot guarantee that the best fit solution survives throughout the optimization process. In other words, the best solution obtained from the SGA may not be included in the last generated solutions, which are clustered towards a solution spot. To overcome this problem, the elitism technique is used in the GA such that once an individual with highest fitness among the current generation is found, it will be kept unchanged and transferred into the next generation. By doing so, the chromosome contained in this individual is being copied to other individuals in the optimization that follows. Finally, the solution of the last generation will cluster close to it. But this approach

achieves its property by sacrificing one possible newly generated individual. This can be overcome by choosing a slightly higher population size.

5.3.6 Gene Duplication and Deletion

Gene duplication and gene deletion techniques can also be applied to enhance the search capability of a genetic algorithm. Biologically, gene duplication and deletion are considered as genetic disorders resulting in the formation of a slightly longer or shorter chromosome [56]. For gene duplication, a gene is duplicated and appended to the chromosome to form a longer chromosome. On the other hand, a gene is randomly deleted within the chromosome and results in a shorter chromosome. They can be used to reproduce chromosomes with different length as compared to the parents. All these operations are to bring diversity to the search process aimed to locate the global optima. Detailed description of these techniques can be found in references [29, 56].

5.4 GAs in Power System Small Signal Stability Analysis

As studied in the former chapters and sections, a power system is a highly nonlinear large scale system. Power system stability analysis requires optimization of complicated objective functions for different purposes. These objective functions can be nonlinear, non-differentiable, and non-convex, which makes traditional optimization methods struggle to find the optima. However, Genetic Algorithms can be applied to such problems to obtain approximate solutions which can be acceptably close to the global optima and several local optima as well with proper techniques.

In this section, novel approaches toward power system small signal stability analysis, and reactive power planning will be studied. A Genetic Algorithm with sharing function method gives more comprehensive solutions as compared with traditional optimization methods. This approach is based on a novel power system black box model, which is suitable for GA optimization for solving small signal stability problems. To solve the reactive power planning problem, a two stage planning technique is adopted to speed up the GA searching process.

5.4.1 Power System Black Box System Model for Genetic optimization

In the system model used in the analytical form of the small signal stability problem - see the Equations (1.1),(1.2) - we have a highly nonlinear, nonconvex optimization task. It is known that the traditional optimization methods meet serious difficulties with convergence while solving such problems. Besides this, the constraint sets, in equation (5.11) -(5.15) and (5.17 -(5.21) take account of only one eigenvalue during the optimization. To get the stability margin for all eigenvalues of interest, as well as the critical load flow feasibility conditions, it is necessary to vary the initial guesses and repeat the optimization. Additionally, the functions in equation (5.11) -(5.15) and (5.17 -(5.21) can have discontinuities due to the different limits applied to power system parameters. For example, the generator current limiters may cause sudden changes in the model, and consequently break in the constraint functions. This makes the analytical optimization problem even more complicated.

In the genetic optimization procedures, those difficulties can be overcome by using the black box power system model - see Figure 5.7 - described in the sequel.

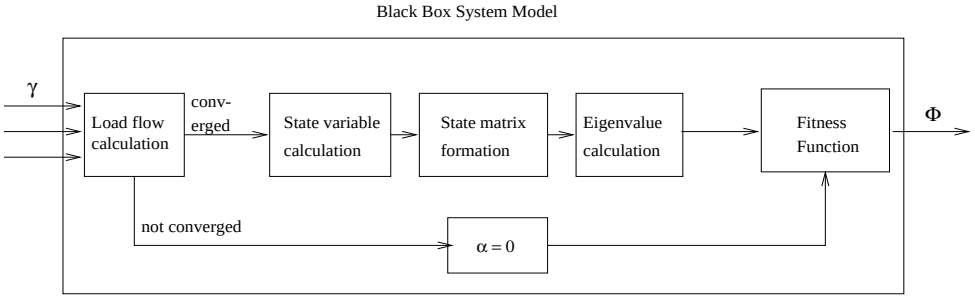

Figure 5.7: Black Box System Model for Optimization

The black box has control parameters γ as inputs, and the fitness function Φ as outputs. Inside the black box, we compute the load flow first. If it converges, then the state variables and matrix are computed, and then the eigenvalues of the state matrix are obtained. Thereafter, the critical (i.e. the most right) eigenvalue is chosen for analysis. The critical eigenvalue's real part is used to compute a particular value of the fitness function. If the load flow does not converge, which means that a load flow solution does not exist, we put the critical eigenvalue real part to zero. By such a way, the load flow feasibility points are treated in the same way as

the saddle node and Hopf bifurcation points. The fitness function Φ can be changed quite flexibly depending on the concrete task to be solved. For example, if the state matrix is unstable or the load flow procedure diverges, the fitness is taken to be large and it is decreased with the increase of distance. If the load flow procedure converges and the state matrix is stable, the fitness is then taken uniformly low. Finally, the last population is concentrated outside the stability domain [which is the intersection of the load flow feasibility and small signal stability domains] close to the critical and subcritical distance points.

To demonstrate the advantages of the black box model, consider the tasks of locating power system small signal stability characteristic points, and locating the closest distance toward instability. They have been studied in former chapters and the equations describing the problem are given below for reference. For the general method described in Section 3.6, we have the formulation (equations (5.10) –(5.15))

$$\alpha^2 \Rightarrow max/min \tag{5.10}$$

subject to

$$\begin{aligned} f(x, p_0 + \tau\Delta p) &= 0 && (5.11)\\ \tilde{J}^t(x, p_0 + \tau\Delta p)l' - \alpha l' + \omega l'' &= 0 && (5.12)\\ \tilde{J}^t(x, p_0 + \tau\Delta p)l'' - \alpha l'' - \omega l' &= 0 && (5.13)\\ l'_i - 1 &= 0 && (5.14)\\ l''_i &= 0 && (5.15) \end{aligned}$$

For closest distance problem, we have (equations (5.16) –(5.21)),

$$||p - p_0||^2 \Rightarrow min \tag{5.16}$$

subject to

$$\begin{aligned} f(x, p) &= 0 && (5.17)\\ \tilde{J}^t(x, p)l' - \alpha l' + \omega l'' &= 0 && (5.18)\\ \tilde{J}^t(x, p)l'' - \alpha l'' - \omega l' &= 0 && (5.19)\\ l'_i - 1 &= 0 && (5.20)\\ l''_i &= 0 && (5.21) \end{aligned}$$

Detailed notation of the variables in the equations can be found in former Sections 3.3.1 and 3.6.

To reveal all characteristic small signal stability points, such as maximum loadability, saddle and Hopf bifurcation and minimum and maximum damping points, along a given ray $p_0 + \tau\Delta p$ in the space of power system control parameters, p, the general small stability problem equation. (5.10) -(5.15) can be solved. If the above problem is solved by traditional optimization methods, the solution obtained depends on initial selection of the eigenvalue traced, and variables x. Moreover, even for one eigenvalue selected, it is not possible to get all the characteristic points in one optimization procedure. By applying the black box model and GA techniques all the problem characteristic points can be found within one optimization procedure. In this case, the input is the loading parameter, $\gamma = \tau$, and the fitness function is α^2 for maximization and $1/\alpha^2$ for maximization. To compute the function, the load flow is computed for a given value of τ. If the load flow converges, then the state matrix and its eigenvalues are computed, an eigenvalue of interest is selected (for example, the critical eigenvalue with the minimum real part), and used to get the fitness function. The black box model only has one input and one output, and is used in the standard GA optimization.

To find out all the critical distances to the load flow feasibility and bifurcation boundaries in the problem, equation. (5.16) -(5.21), the same black box system model can be used. In this case, the inputs are Δp and τ, and the fitness function is increased when the distance decreases and the critical eigenvalue real part tends to zero.

5.4.2 Global Optimal Direction to Avoid Instability

By using a GA with sharing function method, both critical and sub-critical distances can be obtained. More broadly, the distances computed can be any of the significant directions of operation in the space of any power system parameters of interest. For example, they can be associated with critical/subcritical distances, minimum damping conditions, saddle node or Hopf bifurcations, load flow feasibility boundaries etc. Upon obtaining these directions, the optimum operation direction can be defined thereafter. The approach can be visualized by Figure 5.8, where any two vectors, for example, the critical and subcritical distance vectors, in the parameter

space are located by GA sharing function method as $\vec{V_i}$, where $i = 1, 2, ...m$. They form a cutset in the space and define a new vector

$$\vec{V_o} = -\sum_{i=1}^{m}(k_{vi}\vec{V_i}) \tag{5.22}$$

where k_{vi} is the weighting factor depending on the influence of parameter sensitivity as well as differences between $||V_i||$s. For example, to reveal the influence of the critical and subcritical distances toward instability, they can be taken as

$$k_{vi} \propto \frac{1}{||\vec{V_i}||} \tag{5.23}$$

Or in the sense of parameter sensitivity, they can be,

$$k_{vi} = \frac{\partial V_i}{\partial p_i} \tag{5.24}$$

Then $\vec{V_o}$ gives the direction of optimum operation which enables, at least in the meaning of system parameters involved, safest operation direction. Stability problems of other kinds can be investigated accordingly.

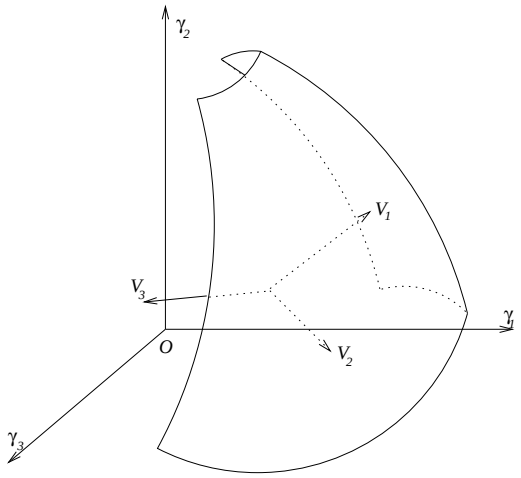

Figure 5.8: The Cutset of Power System Security Space

5.4.3 Power System Model Analysis Using Genetic Algorithms

Power system models exhibiting nonlinear small signal stability phenomena are studied here using GAs and the proposed black box system optimization model. In

the model test systems, the population size is selected in the range from 30 to 200. It has been discovered that this population size is sufficient to locate the maxima in the space of power system parameters.

Example 1. Single Machine Infinite Bus Model with Induction Motor Load

The model has been given in Figure 3.6, and the dynamic equations are described in equations (3.68)-(3.71) and the dynamic loads are modeled as (3.72)-(3.73).

As compared to the formerly obtained results, which is the solid line boundaries in Figure 5.9, the closest stability points to the boundaries were located by genetic algorithm with sharing function method in the same figure. Note that since GAs can only locate solutions near optimum, not all of the solutions marked with '$\times$' are located on the stability boundaries. As a result of the sharing function used, the solutions are grouped around different global and local optima from the operating point to the stability boundaries.

One of the genetic optimization fitness statistics is given in Figure 5.10.

Example 2. Three-Machine Nine-Bus Power System Model

The model system is given in Figure 2.8 with equations (3.102) -(3.107) describing its dynamic properties. The optimal operation direction is given by applying equation (5.22) after the sharing function method locates the critical and subcritical solutions - see Figure 5.11- where the critical directions are $\vec{Vec}_1$ and $\vec{Vec}_2$, and the optimal direction of operation is defined by vector $\vec{Vec}_3 := -k(\frac{\vec{Vec}_1}{||\vec{Vec}_1||} + \frac{\vec{Vec}_2}{||\vec{Vec}_2||})$.

5.5 Reactive Power Planning with Genetic Algorithm

Modern power systems are often affected by inadequate reactive power supply. Besides reduction of the voltage stability margin, insufficient reactive power can also have negative effect on voltage profiles, active and reactive losses and cause equipment overloads [48]. Reactive power control can significantly improve on these

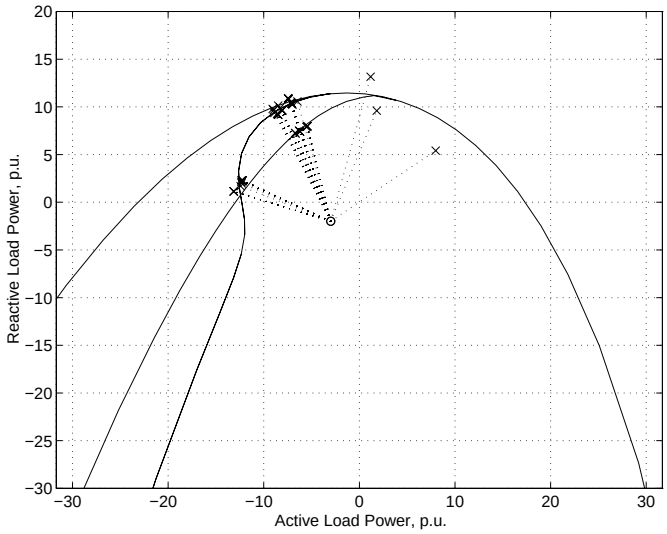

Figure 5.9: The Closest Stability Boundary Points

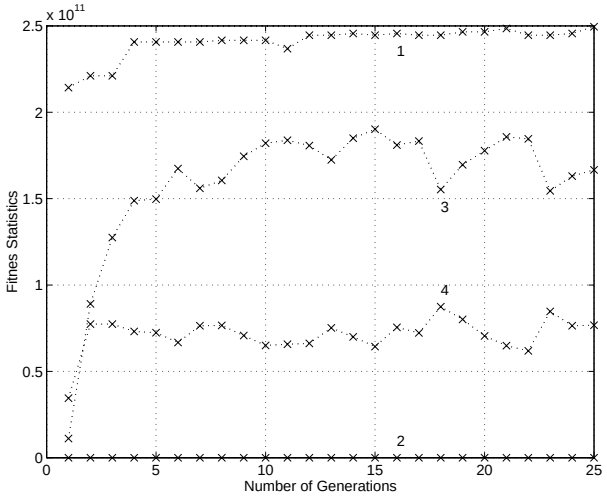

Figure 5.10: Genetic Optimization Statistics: 1 Maximum Fitness, 2 Minimum Fitness, 3 Mean of Fitness, $\bar{x} = \frac{1}{n}\sum_{i=1}^{n} x_i$, 4 Standard Division of Fitnesses which is $s = (\frac{1}{n-1}\sum_{i=1}^{n}(x_i - \bar{x})^2)^{\frac{1}{2}}$

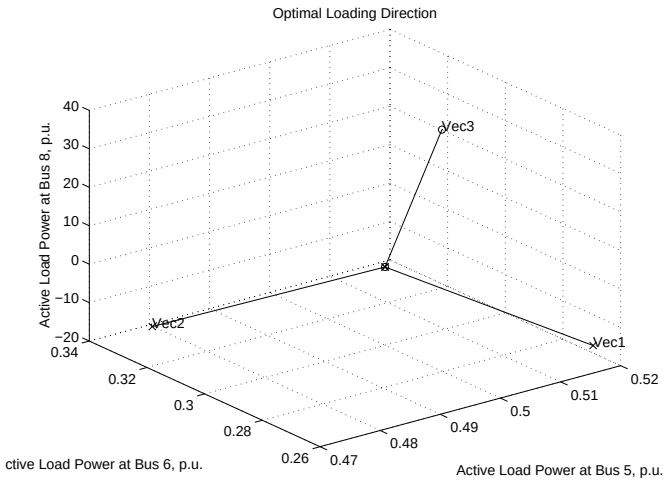

Figure 5.11: The Critical Directions $(\vec{Vec_1}, \vec{Vec_2})$ to Small Signal Stability Boundaries and its Corresponding Optimum Direction $(\vec{Vec_3})$, where $\vec{Vec_3} = -k(\frac{\vec{Vec_1}}{||\vec{Vec_1}||} + \frac{\vec{Vec_2}}{||\vec{Vec_2}||})$.

characteristics. It can be realized by several approaches, for instance, transformer tap control, generator voltage control, controllable and static VAR sources. Most of these controls are discrete and limited. The task is to provide an optimal reactive power supply with minimum cost. One of the options to provide VAR supply is installation of reactive power sources such as Static VAR Conpensators (SVCs), series compensation capacitors at appropriate buses. The major concern of optimal placement of reactive devices are [70]:

- locations of VAR devices;
- type and sizes of VAR devices to be installed;
- settings of VAR devices in different system operational conditions

The task of finding the optimal location and size of VAR devices in the grid is an important topic for power utilities.

The core of a VAR planning problem is proper selection of the objective function and the optimization techniques used. The objectives can be more specifically expressed as follows [28, 70, 83, 113]:

- Maximize reactive demand margin of the system, Q_M;

- Retain voltage stability of the system;
- Minimize the expenditure including purchase, installation, maintenance, and energy cost;
- Provide desired voltage magnitudes by minimizing voltage deviations;
- Minimize line flow deviations;
- Support buses most vulnerable to voltage collapse.

The technique of placing reactive power sources should be able to achieve the best locations and the best stability enhancements under the most economical cost. Therefore, this is a multi-objective optimization problem. The problem is expressed by an objective function subject to equality and non-equality constraints. These functions and constraints are partially discrete, non-differentiable, nonlinear functions, which may cause solution difficulties with traditional optimization methods. Many methods including linear [41] and nonlinear programming [126], expert systems [83], neural networks [128], and others have been employed to cope with the problem. More recently, the simulated annealing and genetic algorithms approaches were used [28, 48, 70, 83, 101, 113, 128, 138].

Despite the robustness of genetic algorithms, they take a substantial computational time for large power systems. The computational cost also increases if all buses are considered for VAR source installation. In practice, it is not necessary; many buses can be eliminated from consideration.

To reduce the computational cost, a preliminary screening should be done to minimize the number of alternative locations. Here, bus participation factors are used to select the candidate buses for the subsequent VAR source placement. The buses with higher participation factors are selected first, and they are considered in the second stage where the genetic algorithm technique is employed to optimize the location, size and type of VAR sources.

5.5.1 Preliminary Screening of Possible Locations

The bus participation factors of the power flow Jacobian matrix are used to determine the critical modes of voltage instability [113, 115]. The computation is

performed to find the critical eigenvalues, eigenvectors and corresponding participation factors based on the solution of the load flow problem close to the voltage collapse point. To find out the voltage collapse point, a loading procedure is implemented. Several critical bus participation factors [53] are computed based on the critical eigenvalues. Then the buses with largest participation factors are assumed to contribute most to voltage instability, and thus VAR devices should be placed at those buses. The procedure is summarized below:

- Increase the system nodal power loads in the predicted load increase direction till load flow does not converge.
- Calculation the load flow Jacobian based on the last convened load flow solutions.
- Reduce the load flow Jacobian by, $\Delta Q = J_R \Delta V$ where

$$J_R = -\frac{\partial Q}{\partial \delta}\frac{\partial P}{\partial \delta}^{-1}\frac{\partial P}{\partial V} + \frac{\partial Q}{\partial V} \tag{5.25}$$

- Find the participation factor by eigenvalue and left/right eigenvector calculation. For the $k-th$ bus, the participation factor of the $i-th$ mode is $p_{i,k} = \xi_{ki}\eta_{ik}$, where ξ and η are the left and right eigenvectors of matrix J_R respectively. The bus participation factor $p_{i,k}$ stands for the contribution of the $i-th$ eigenvalue to the $V-Q$ sensitivity at the $k-th$ bus [53].
- Buses with higher participation factors are more prone to voltage instability, and they are selected as candidates for VAR compensation.
- VAR planning based on the candidate buses aimed to provide voltage stability, while considering economic dispatches.

Since the approach was only an approximation of the $\Delta Q/\Delta V$ assuming $\Delta P = 0$, those buses with higher than average or higher than a preset value of participation factor should be selected as candidate buses. Besides the buses linked with higher participation factors, those associated with lower than average voltages are also considered as candidate buses for VAR installation. Upon obtaining these candidate buses, a Genetic Algorithm based optimizer is used to distribute VAR sources among these candidate buses within pre-set VAR limits to meet the desired voltage levels,

reduced real power loss as well as minimized installation and maintenance costs for VAR devices.

To supplement this screening procedure, several contingency cases should also be considered to find the buses with higher participation factors to be included in the candidate buses. Also, in this stage, discrete factors as tap changer transfer taps, VAR units, etc are considered in detail for optimization purposes.

5.5.2 Objective Functions for VAR Planning

The VAR optimal planning aimed to improve the system performance, and enhance voltage stability as well as reduce the system operational cost. To achieve the best performance under minimum costs, the objective function plays the key role. Here the objective function takes consideration of the following factors: (1) active power loss reduction, (2) voltage deviation referring to the desired voltage levels, (3) reactive power deviation referring to the desired reactive power level, and (4) economic consideration including installation costs, and maintenance expenditures. The function is given in the equations below [83, 138]:

$$\begin{aligned} F_{obj} &= w_0 \Delta P_{loss} + w_1 f_1(V, V^d) + \\ &\quad + w_2 f_2(Q, Q^d) + w_3 f_c(S) \end{aligned} \tag{5.26}$$

where $w_i, i = 0, 1, ..., 3$ are weighting factors; ΔP_{loss} is the reactive power loss reduction as compared with the original system without new VAR sources, $(P_{loss}^{(0)})$; function $f_1(V, V^d)$ is the voltage deviation function with respect to the desired voltage level V^d; and $f_2(Q, Q^d)$ is the deviation function for reactive power; $f_c(S)$ is the function including cost of installation and maintenance of VAR devices to be installed. These functions are expressed as follows:

$$\begin{aligned} P_{loss} &= \sum_{k=1}^{nl} G_{ij}^{(k)} (V_i^2 + \\ &\quad + V_j^2 - 2 V_i V_j cos(\theta_i - \theta_j)) \end{aligned} \tag{5.27}$$

$$\Delta P_{loss} = ||P_{loss} - P_{loss}^{(0)}||^2 \tag{5.28}$$

$$f_1(V, V^d) = \sum_{i=1}^{ns} k_1(i) ||V_i - V_i^d||^2 \tag{5.29}$$

$$f_2(Q, Q^d) = \sum_{i=1}^{ns} k_2(i) ||Q_i - Q_i^d||^2 \tag{5.30}$$

$$f_c(S) = \sum_{i=1}^{nc} g_i^c * S_i^{cap} + \sum_{i=1}^{ni} g_i^i * S_i^{ind} \quad (5.31)$$

where V_i stands for voltage at bus number i, θ_i is the voltage angle at $i-th$ bus, V^d, Q^d are the desired level of voltage and reactive power respectively, S stands for the value of VAR devices, which can be capacitive, given by ^{cap}, or inductive, given as ^{ind}. The constraints are the load flow equations, system component operating limits, and other pre-set VAR installation limits [101] expressed as:

$$0 = P_i - V_i \sum_{j=1}^{Ni} V_j(G_{ij}cos\theta_{ij} + B_{ij}sin\theta_{ij}), \quad (5.32)$$
$$i = 1, 2, ..., N_B - 1$$
$$0 = Q_i - V_i \sum_{j=1}^{Ni} V_j(G_{ij}sin\theta_{ij} - B_{ij}cos\theta_{ij}). \quad (5.33)$$
$$i = 1, 2, ..., N_{PQ}$$

$$Q_{ci}^{min} \leq Q_{ci} \leq Q_{ci}^{max} \quad (5.34)$$
$$Q_{gi}^{min} \leq Q_{gi} \leq Q_{gi}^{max} \quad (5.35)$$
$$T_i^{min} \leq T_i \leq T_i^{max} \quad (5.36)$$
$$V_i^{min} \leq V_i \leq V_i^{max} \quad (5.37)$$
$$f_c \leq f_c^{max} \quad (5.38)$$

where N_B is the bus number, N_{PQ} is the P-Q bus number, P_i and Q_i are active and reactive injected powers, G_i and B_i are self conductance and susceptance of bus i, and T_i stands for the tap change transferrer tap position at bus i, f_c is the total cost, ^{min} and ^{max} stands for the lower and upper limits of these variables.

To summarize, the problem is to minimize the objectives, (5.26), (5.27) –(5.31), subject to the set of equality and inequality constrains, (5.32) –(5.38).

5.5.3 Power System Example of VAR Planning

A 16 machine 68 bus system which represents the simplified U.S. Northeastern and Ontario system [36] is studied using the algorithm as shown in Figure 5.12

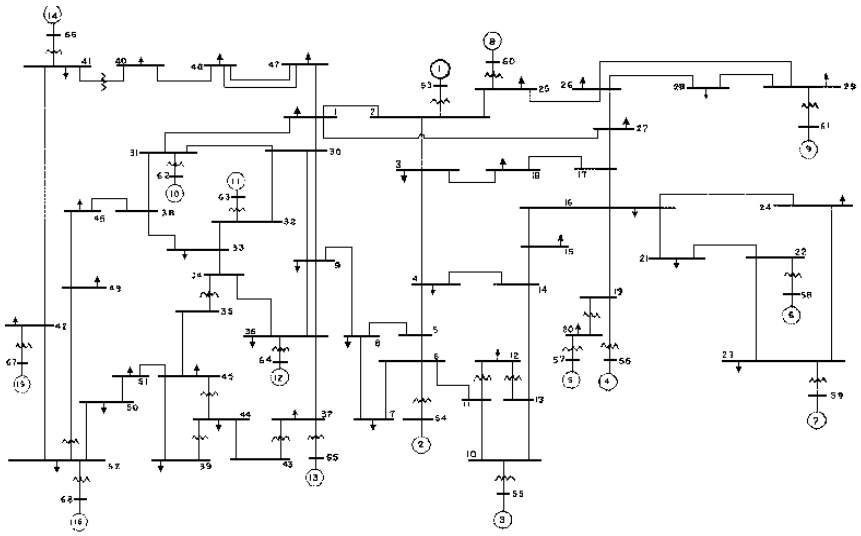

Figure 5.12: 16-Machine 68-Bus System

The weighting factors in the objective function decides which item needs more consideration for system planning. Therefore, different weighting factors gives different planning results. Here two cases are studied, (1) consider all the stated objectives with evenly distributed weight factors - see Table 5.3; (2) more emphasis is given to voltage deviation, cost and active power losses - see Table 5.4.

Bus No.	VAR size	Bus No.	VAR size
7	8.30	24	-13.12
8	-1.65	25	-6.84
9	5.61	26	7.45
10	-25.50	28	-3.43
11	-7.15	33	-6.47
17	13.48	37	-25.53
19	-41.73		

Table 5.3: 16 Machine System VAR Planning (Case 1).

As shown in these tables, VAR sources are placed to enhance the system voltage profile and reduce active power loss. Clearly, different emphasizes of the objectives produces different results in the VAR allocation.

For the Case 1 study, the results are represented in the bar plot as shown in Figure5.13. Buses 7, 9, 17 and 26 are shown positive in VAR value, which means

Bus No.	VAR size	Bus No.	VAR size
1	-3.02	39	-0.23
7	-2.11	40	1.10
8	-6.20	43	-1.20
9	-6.03	44	-1.65
30	-2.80	50	1.31
35	-1.51	52	1.09
37	-16.20		

Table 5.4: 16 Machine System VAR Planning (Case 2).

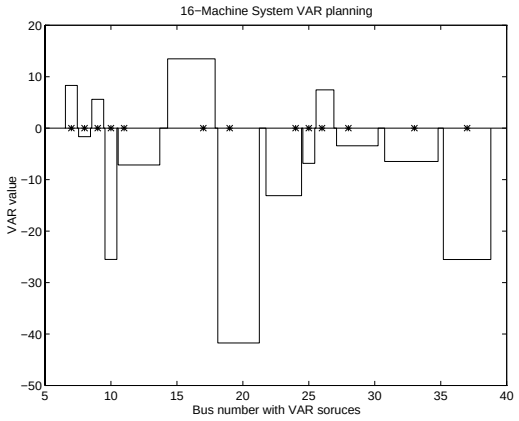

Figure 5.13: VAR Planning Result for the 16-Machine 68-Bus System

the VAR sources to be installed should be operating in inductive mode. While all others are capacitive VAR sources. This combination of inductive and capacitive resources is to be expected because the objective to be achieved is partially composed of voltage deviation minimization. For example, some bus voltages may be higher then the preferred value as a result of installation of capacitive VAR sources at other buses, and require inductive VAR sources to step down the voltage level in order to meet the preferred level. Unless some stability index is considered in the objective function, planning results considering only savings and voltage levels might actually move the system closer to collapse.

For Case 2 study, as compared with the original system, the power losses are listed in table 5.5. where P_{loss} is the total active power loss in the network, average V is the average voltage of all buses in per unit, lowest V is the lowest voltage among all the buses of the system, $\Delta\ V$ is the voltage deviation.

	Normal	Contingency	Compensated
P_{loss}	1.7472	5.9821	3.6529
Average V	1.0279	0.9443	1.0311
Lowest V	0.98	0.8000	0.9800
Δ V	0	-0.0835	0.0032

Table 5.5: Objectives of 16 Machine System VAR Device Optimal Placement

The installation of VAR devices has positive effects on system behavior in view of voltage levels, as shown in Figure 5.14:

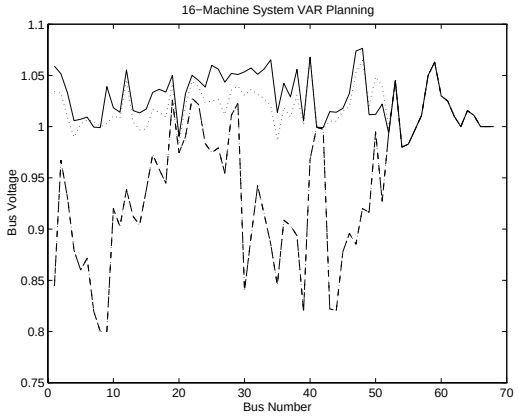

Figure 5.14: Voltage Profile of the System: Solid Line: Normal; Dotted Line: Planned; Dashed Line: Contingency.

The genetic algorithm used here considers elitism and mutation probability control. The optimization process is quite fast and the result can be improved consistently with the optimal solution from the former solution as a seed and put into the genetic algorithm with elitism for further improvement. The statistics as shown in the best fitness are given in Figure 5.15. As shown in the figure, within 10 generations, the GA has already located a solution which is quite close to the final solution. Then the search process terminates after further optimization without evident improvement (first figure). The remaining figures show the incremental improvement of the best fitness using the elitism technique. The negligible increment in the best fitness values indicates that, the result obtained is a close estimation of the exact global solution.

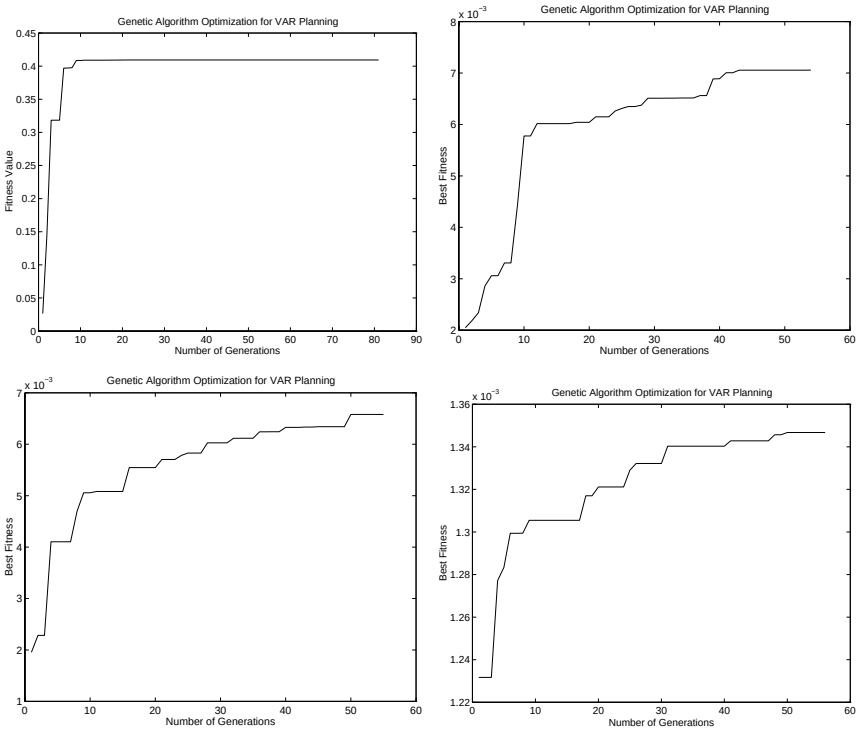

Figure 5.15: The Genetic Optimization Process of VAR Optimal Placement

5.6 Conclusion

The genetic optimization technique proposed here has been applied to solve problems in small signal stability analysis and power system planning. As compared with traditional optimization methods, more comprehensive results can be obtained for small signal stability analysis using GA. All the system eigenvalues can be considered for optimization instead by comparison only one of them can be traced by traditional methods. GAs are especially suitable for use in the power system planning problem. In the proposed reactive power planning approach, a two stage solution technique is developed to narrow down the search area for GA aimed at better convergence. At the same time, the first stage ensures that all the buses which have critical influence on voltage stability are selected for consideration. Overall, the procedure combines reliability and computation efficiency.

Chapter 6

Small Signal Stability Toolbox

6.1 Introduction

In this chapter, we describe a software toolbox which is aimed to provide a comprehensive analytical tool for system stability assessment and enhancement purposes. The essential functionalities combine several aspects of previous chapters to fulfill the aims of the toolbox. They are: (1) power system small signal stability assessment by computing the stability critical conditions and boundaries; (2) power system optimal VAR planning to reduce the line losses as well as considering other economic and security issues; (3) power load flow feasibility boundaries computation in the space of power system parameters; (4) Genetic Algorithm approach to locating the critical and subcritical stability conditions for optimal control actions; (5) load ranking analysis to reveal loads having the biggest influence on power system stabilities; and (6) other common power system analysis requirements, such as load flow, transient simulations.

6.2 The Toolbox Structure

The toolbox incorporates many research outcomes related to power system stability assessment and enhancement algorithms and methods from the Dynamical Systems and Control research group of the School of Electrical and Information Engineering at Sydney University under the supervision of Professor David J. Hill. The toolbox is in a preliminary version only, which means most algorithms are coded as they were from the research projects performed during recent years. However, there are several new modules developed directly for the toolbox; for example, the VAR planning module is new. Visual Basic, due to its flexibility in interface design and file I/O functionalities is chosen as overall interface development language. Excel and C++ are also used in addition to the MATLAB for major algorithms. The MATLAB only version is available for both PC and UNIX environments, and the combined VB/Excel/C++/MATLAB version is for PC only.

6.2.1 Programming Languages

There are three major programming languages used for the toolbox, namely, Matlab, Visual Basic, Excel and C++. They all have their own specific particular usages in the toolbox development. Matlab modules provide most of the algorithms for analytical purposes. Visual Basic and Excel build up the overall interfaces and link all applications under a Windows(R) environment. C++ provides fast computation for some of the algorithms such as Genetic Algorithms and system identification for future development.

We now examine each language for important features in modern power system computation.

Matlab

It is well-known that MATLAB provides high flexibility and numerous functions which make it ideal for software package modular development. MATLAB programming, which starts from the scripts in the form of m-files, has useful features, in particular:

- It provides high-level complete software development environment.
- It has the ability to develop Graphic User Interface (GUI) applications.
- It has most commonly used numerical methods as build in functions including sparse matrix operations, optimization methods, etc.
- With proper supplementary toolbox and packages, MATLAB can produce dynamically linked Fortran or C subroutines in the form of MEX-files. They may speed up the computation speed as compared with the equivalent MATLAB m-files.
- MATLAB is especially powerful in matrix manipulation, thus makes eigenvalue and eigenvector analysis for small signal stability analysis easy to achieve.

Besides those stated above, MATLAB offers file I/O functionalities, so the computation results can be shared by other programs. The GUI functions are easily to build using MATLAB's graphic objects handling capabilities. Matlab itself can be

used to build a complete package for power system computations [34, 103]. MATLAB is used for most of the computation algorithms in the package, also a complete package completely in MATLAB has been developed for the UNIX version.

C++

C++ is an object-oriented language with static binding rather than dynamic binding, which makes it is superior to other dynamic binding languages in case of implementation of embedded systems with stringent performance and memory requirements. C++ has several useful features, including: (1) it provides flexible data type controls; (2) it offers strong memory management; (3) it implements object oriented programming through inheritance and dynamic binding mechanisms; (4) it supports template functions and classes [99]; (5) the recent Visual C++ development platform makes the graphical user interface design easy to implement. What's more important, C++ allows use of abstract methods, which is a method name specification without actually defining the method. This fits the situation in software development when some algorithms, functions, variables or parameters have been defined as classes with programming methods associated, and are supposed to be defined by the user later [10].

In this toolbox, C++ in quickwin mode is used for one of the Genetic Algorithm approaches. It is designed that C++ should be the primary programming language for further toolbox design and implementation.

Visual Basic

Visual Basic (VB) is an object-based programming language. It is a useful tool to create applications for Microsoft Windows(R). Visual Basic includes a method used to create a graphical user interface(GUI) instead of writing lengthy lines of codes describing all of the properties, locations and appearances of interface elements. Besides, it uses the BASIC language and is implemented with many functions, keywords related directly with Windows GUI. Since it is Microsoft product, the Visual Basic programming language can also be used for Microsoft Excel and Microsoft Access, as well as other Windows based programs [144]. As the new Visual Basic edition emerges, Internet programming is included as a subset of the VB package,

which makes the applications accessible via Internet.

6.2.2 Package Structure

The over all structure of the toolbox includes data loading and storage, file I/O operations, basic power system computation tasks, as well as advanced stability assessment and enhancement analysis. The results can be visualized by Windows(R) based program such as Excel/ Visual Basic interfaces or by MATLAB routines. The major algorithms of the analysis are:

- Basic power system computation including power flow and transient simulations
- Advanced Stability Analysis:
  - Load flow feasibility boundaries computation and visualization.
  - Power system small signal stability boundaries computation and visualization.
  - Power system reactive power planning analysis
  - Power system load ranking analysis to indicate the most influential loads toward instability.
- Genetic Algorithm as compared to classic optimization and searching methods.

The program flow chart is given in Figure 6.1

6.3 Overall Interface Design and Functionality

To incorporate all the functionalities into one user friendly package, Microsoft Visual Basic is used to build the over all interface for the toolbox PC version. As mentioned in Section 6.2.1, Visual Basic provides an easy way to build the GUI and incorporate other programs. Therefore, it is selected as a programming language for the toolbox package to create the over all interfaces. Upon activation of the package, the user is prompted to answer a few questions to set up the path information of other

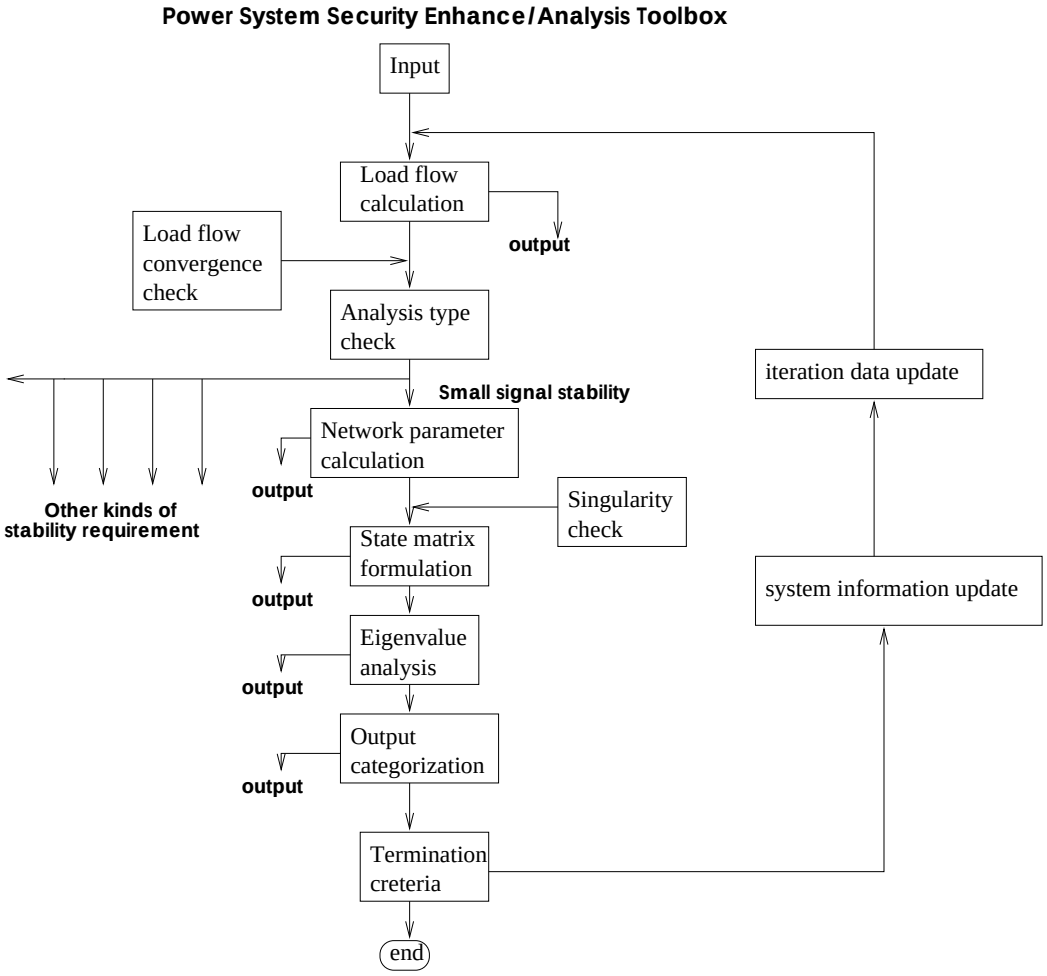

Figure 6.1: The Program Flow Structure of the Toolbox

applications, such as MATLAB, for later usage. Currently most of the algorithms are written in MATLAB and some in C/C++, and Fortran, they are left in their original codes for the trial version. As for later development, they may be converted into a uniform code such as C++ for faster executing performance.

There are several choices the user may make in the steps towards a case study:

- Programmable media
  The user can choose among MATLAB, Excel, Visual Basic or C++ for case study.

- Systems
  The user can either select to run the program for a new study or to visualize

the existing data.

- Study Models
  Several power system models are available for the user to choose for case study.
- Study Algorithms
  In this step, several algorithms /techniques are available for the user to choose from. They include the Δ-plane method, the general method, different genetic algorithms, and reactive power planning problems. In the mean time, the user can try different algorithms for the same problem to compare the results and performances.
- Computation speed
  The user can choose lower, higher standard computation speed for case study.

One of the interfaces with Visual Basic is given in Figure 6.2

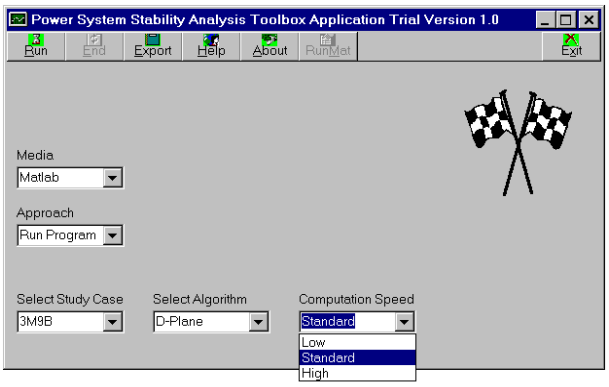

Figure 6.2: The main toolbox GUI

6.4 Algorithms

The major algorithms and techniques are described in the following sections.

6.4.1 Δ-Plane Method

The Δ-plane method of locating the power system loadflow feasibility boundaries is included in the package. The theoretical aspects of the method and power system

example have been discussed in Section 4.5.

Δ-plain Method Interface Design

In a Matlab environment, upon starting the procedure of the toolbox Δ-plane method analysis, the user will be asked to choose whether or not to use graphic user interface. If the selection is yes, the graphic user interface will appear to guide the user through the Δ-plain calculation for different study cases. Alternatively, the user can choose using command prompt to bypass the graphic interface to save calculation time. Upon selection of GUI usage, the following main Δ-plane window appears, Following the main window, the user can choose one of the study cases

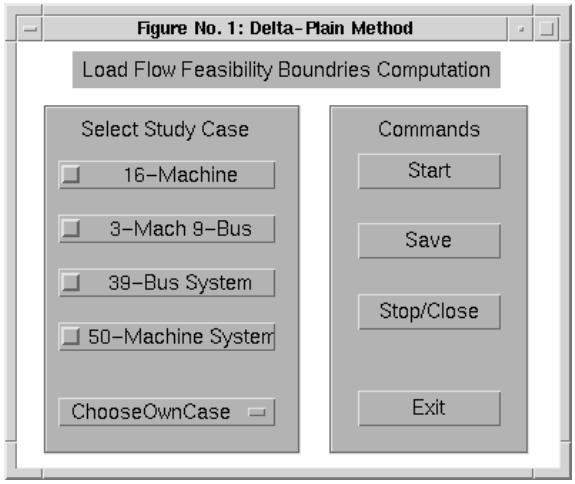

Figure 6.3: The main GUI for D-plain usage

from among,

- 16-machine system;
- 3-machine 9-bus system;
- New england test system;
- 50-machine system;
- User defined system.

For each study case, there is an associated GUI window for that case. For example, the 16-machine case prompts the following GUI window,

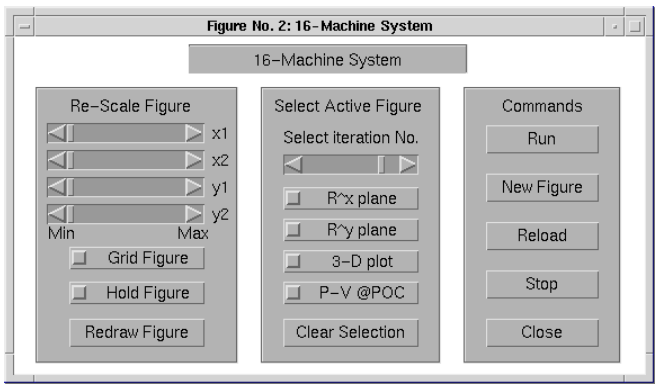

Figure 6.4: The GUI for D-plain application to 16-machine system

6.4.2 Small Signal Stability Conditions

Power system small signal stability computation, especially using the general method to reveal all characteristic points, is also included in the package for usage. Theoretical foundations and application examples are given in Section 3.6.

6.4.3 Optimal VAR Planning with Genetic Algorithms

The reactive power planning problem is an important system operation and planning consideration. The principles of reactive power planning have been discussed in Section 5.5. We recall that the major concern of optimal placement of reactive devices are:

- locations of VAR devices;
- type and sizes of VAR devices to be installed;
- settings of VAR devices in different system operational conditions

These concerns are more specifically expressed in the case of SVCs - see Section 5.5 - and can be categorized as:

- Maximize reactive demand margin of the system, $Q_M = \sum_i \Delta Q_i$, where ΔQ_i is the VAR increment of node-i.;
- Retain voltage stability of the system;

- Minimize the expenditure incurred, including SVC purchase cost, installation & maintenance cost, energy costs;
- Obtain desired voltage values by minimization of voltage deviation;
- Minimize line flow deviation;
- Enhance buses most vulnerable to voltage collapse.

The technique of placing SVCs should be able to acquire the best available locations of SVCs, best stability enhancement effects under most economical costs. Genetic algorithms and bus participation factors are used to obtain optimal VAR planning results for voltage stability enhancement.

The toolbox incorporated several approaches for SVC placement to obtain the most effective solution schemes. Depending on the concrete purpose and system situation, users can choose their own schemes for SVC placement, e.g. based on economic considerations, which emphasizes more on savings as a result of VAR planning, or voltage stability, which puts more weighting on voltage levels after planning, and other user defined weightings for different purposes of planning.

Toolbox User Interface for VAR Planning

The graphical user interface enables the users to choose their own initial system configurations, such as total amount of expenditures, total/max number of SVCs to be installed, min/max bus voltage limits. as well as different study cases and calculation algorithms. There are also interface windows available for Genetic Algorithm parameter settings, and helpful information displays as shown in Figures 6.5, and 6.6. On clicking on the command buttons, the functions can be activated to perform optimization of VAR planning for selected cases and algorithms under the parameter values set by default or user definition.

6.5 Further Development

Upon installation, users can choose to study power system small signal stability, load flow feasibility boundaries, reactive power planning, as well as other common power

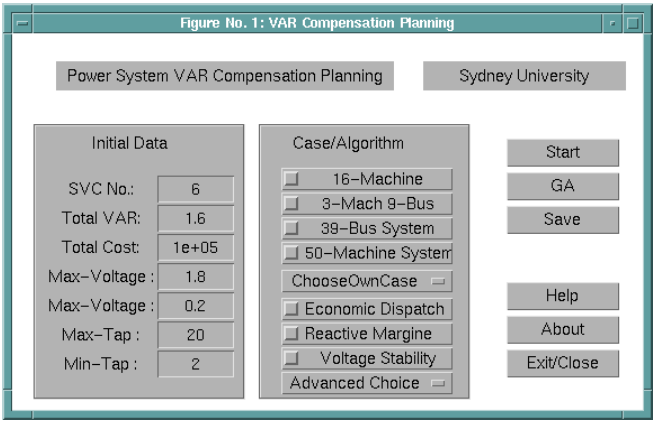

Figure 6.5: The main GUI for VAR planning (UNIX version)

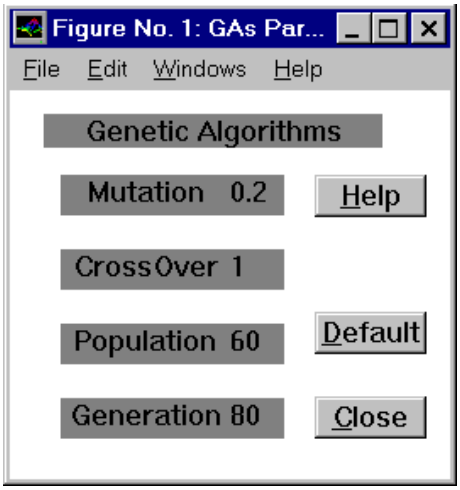

Figure 6.6: The GUI for Genetic Algorithm Parameter Settings (PC version)

system computations. However, because the major algorithm is based on MATLAB programs, the computation speed is currently not adequate for large systems. Also, more power system data are needed. The on-line help documentation need to be implemented so to provide more detailed help on using the toolbox as well as providing deeper understanding of the algorithms used for research references.

An important issue for future development is toward Internet based programs. There are emerging categories of applications being developed are based on Internet and designed for end users. Network centered applications are stored on a central server and are downloaded to the client on demand. This enables multiple versions of the same application. In the United States, OASIS (open access same-time

information system) which is a Federal Energy Regulatory Commission (FERC) mandated system, provides real-time information from a network bulletin board. It permits display of utilities' current available transmission capacity(ATC), as well as offers for the capacity to be received, processed and posted. The accompanying OASISNet as a simulator can be used to study different aspects of an OASIS network [140]. Similarly, with Visual Basic's Internet functionalities, the toolbox will be built capable of on-line execution through World Wide Web(WWW) browsers. Currently, a database for speeding up the application are being built which can be used in future Internet accessible versions.

To summarize, the future trends of the toolbox can be listed as:

- Converting codes into uniform code for optimal performance in computation speed, reliability and system software/hardware requirement.
- Incorporating more algorithms and methods for analysis.
- Including more power system examples and facilities which provide a user with more flexibility to build their own power systems for analysis.
- Develop Internet based application version to meet the open access trend.
- Build complete on line help documentation as well as software development documentation.
- Optimize the codes and GUIs for better user friendly purposes and robust performance.

Chapter 7

Conclusions and Future Developments

7.1 Conclusions of Thesis

In this thesis several numerical techniques dealing with power system stability analysis have been studied. The emphasis has been on providing accurate determination of boundaries and margins of stability.

The results are based on the opinion that under open access conditions, power system stability will become a more complex problem combining both angle stability and voltage stability. Some important terms and definitions for power system small signal stability were reviewed at the beginning of the thesis, there being no uniformly accepted definitions for stability. Existing numerical techniques, especially noting less known contributions in the Russian literature, are reviewed in Chapter 1 and as appropriate throughout the thesis.

Power system modeling is important for stability studies. Relevant power system modeling was briefly reviewed leading to a generic differential-algebraic equation structure with parametric influences explicitly shown. Based on the appropriate power system models, small signal stability can be applied to study the system's stability properties using eigenanalysis and model linearization. Somewhat more emphasis is given to load modeling since the importance to stability properties is less developed in general practice.

Mathematical definitions and known techniques for computing different stability characteristic points, such as saddle node and/or Hopf bifurcations, are reviewed. Normally, only critical stability characteristic points are of interest. There are direct and indirect methods to locate such points. These correspond to "one shot" solution of bifurcation equations and so-called continuation methods respectively. These approaches are mainly based on eigenvalue conditions derived from the load flow Jacobian or state matrices where the real parts of the eigenvalues are put to zero. The imaginary parts are put to zero as well in the case of load flow feasibility and saddle node bifurcation boundaries.

In this thesis, the first major contribution is a comprehensive general optimization method which is capable of locating all the characteristic points on a ray defined by a certain parameter variation direction within one approach. This compares with previous traditional approaches, where only one kind of characteristic point can typically be located for each optimization approach. These characteristic points

include load flow feasibility points, singularity induced bifurcations, saddle and/or Hopf bifurcations, and minimum and/or maximum damping conditions. By variation of the ray in the parameter space, power system stability characteristic points can be located in all directions in the parameter space. The method was tested and validated by numerical simulations, comparison with the previous results obtained for the test systems, and by transient simulations conducted at the characteristic points.

Besides these individual characteristic points in certain directions, the hypersurface containing all these characteristic points is useful to study for power system operation and control.

The second major contribution given is a robust method to visualize the stability boundaries in the parameter space in a specified cutplane - called the Δ-plane method in the thesis. This method does not require iterative solutions of the set of nonlinear equations as normally required by most solution techniques developed in recent years. It is based on the quadratic properties of the load flow problem by solution of an eigenvalue of the matrix $J^{-1}(x_1)J(x_2)$. Results of the method are presented in the space of dependent variables (e.g. nodal voltages given in rectangular form). It is useful for both visualization and topological studies of the multiple solution and feasibility domain structures.

Another contribution aimed at visualization of these boundaries, is a parameter continuation method using the Implicit Function Theorem. This can be used to trace the bifurcation and load flow feasibility boundaries. These methods combine an eigenvalue sensitivity approach and special techniques over any discontinuity in the bifurcation boundaries.

Optimization plays a key role in application of all the technique presented. Because of the complexity of power systems, traditional optimization techniques may encounter difficulties in solving the stability problems due to nonlinearity, nonconvexity, and /or non-differentiable properties of the problem. To overcome such solution difficulties, Genetic Algorithms (GAs) are explored in the thesis. GAs are heuristic optimization techniques, which do not require derivatives of the problem to be optimized. From the evolutionary process of optimization, GAs are capable of locating the global optima in the search domain. With the sharing function, GAs can be applied to locate both the global and local optimal solutions of power

system small signal stability problem. In this thesis, a black box system model suitable for GA optimization is developed and applied to locate the globally and locally closest stability characteristic points in the parameter space. This approach considers all system eigenvalues during optimization, instead of only one of them as for traditional optimization approaches.

GAs are also suitable for power system planning problem. In the thesis, a two stage optimization technique is proposed for power system reactive power planning problem aimed to enhance voltage profiles. This technique narrows down the search area for the GA at the first stage in order to allow speed up of GA optimization convergence. Besides solving this multi-objective problem more efficiently, it also ensures that all the buses which are vulnerable to voltage problems are considered for reactive power source installation.

The final contribution is a prototype level software toolbox combining the techniques of the thesis with selected others. This toolbox has been designed to handle many power system small signal stability problems: stability assessment, enhancement, simulation and control.

7.2 Future Development

From the research carried on within the thesis, there are several directions for further development.

The numerical methods in Section 3.3 about the special problem formulation and matrix determinant minimization techniques for critical distance assessment can be furthered for wider application.

The thesis has considered various algorithms: direct vs indirect, analytic vs evolutionary and linear vs high order corrections. More comparisons could be done to explore which choices work best for certain classes of systems. More promising for further deeper research is exploration of system structure. We have seen simplifications in investigations involving parametric dependence (Section 3.3.1, Section 4.3.1) and quadratic power flow (Section 4.5.1).

There are also related basic questions to explore. Conventionally, the power system feasibility region is assumed to be convex; however, as indicated in Section 4.4.1,

a nonconvex power system feasibility boundary was observed with a simple power system addressed by the authors of [69]. Possibilities exists for infeasible areas inside the main feasibility domain (for large line impedance R/X ratios). There are also high-sensitivity areas. Another important subject is the limit-induced bifurcations, where instability occurs suddenly, without an eigenvalue passing the imaginary axis. Also, how singularity induced bifurcations present themselves in the space of nodal powers is a promising research area.

Following the investigation of Genetic Algorithms in Chapter 5, it is evident that GAs are not limited to stability and planning problems only. They have been used by researchers to solve various optimization problems. In deregulated power system operation situations, GAs have been used in electricity market pricing, renewable energy integration, and many other areas. In many cases, especially in the case of non-convex problems, GAs are the best choice over classic optimization methods which may fail to provide an adequate solution. This comparison is likely to need a more conventional level of investigation.

For power system small signal stability problems, GAs are relatively slower than classic optimization methods, especially when sharing function methods are used, so it is necessary to find a way to speed up the computation. One possible approach to this issue relies on algorithms used for eigenvalue computation. In case the problem consists of a very large state matrix, the eigenvalue computation will be very time consuming. New techniques are being exploited to avoid eigenvalue computation required for each individual's fitness in the black box system model. When such techniques are available, the whole computation can be speeded up for large power system small signal stability analysis.

It appears that fast and more reliable GAs are required to supplement the optimization of power system small signal stability problems. Other Evolutionary Algorithms like Evolutionary Programming (EP) reported in [119] are also very promising in solving such problems.

Currently, if the problem is simple, differentiable or of reasonable scale, which needs to be judged depending on the exact Genetic Algorithm adopted, a classical optimization method should be used to locate the stability conditions to save computation costs and get more accurate solutions. Otherwise, in case the analytical optimization approaches fails or apparently fails to converge, Genetic Algorithm

could be used to obtain the best available solution. One promising line of research appears to be development of a global optimization strategy which combines traditional and genetic/evolutionary techniques. For instance, a GA stage could be used to roughly locate critical distances followed by conventional optimization with the initial condition provided.

More robust and fast computational algorithms are needed to make the proposed techniques more applicable for practical usages.

Bibliography

[1] E. Abed and P. Varaiya, "Nonlinear Oscillations in Power Systems", *International Journal of Electric Power and Energy Systems*, Vol. 6, 1984, pp. 37 –43.

[2] V. Ajjarapu and B. Lee, "Bibliography on Voltage Stability," Iowa State University, see WWW site *http://www.ee.iastate.edu/~venkatar/VoltageStabilityBib*.

[3] V. Ajjarapu and B. Lee, "Bifurcation Theory and its Application to Nonlinear Dynamical Phenomena in an Electrical Power system", *IEEE Trans. on Power Systems*, Vol. 7, No. 1, Feb. 1992, pp. 424–431.

[4] F. Alvarado, I. Dobson and X. Hu, "Computation of Closest Bifurcations in Power Systems", *IEEE/PES 1993 Summer Meeting 93 SM 484-6 PWRS*, Vancouver,B.C., Canada, July 18-22, 1993.

[5] F. L. Alvarado and T. H. Jung, "Direct Detection of Voltage Collapse Conditions", *Proceedings: Bulk Power System Phenomena - Voltage Stability and Security*, EPRI Report EL-6183, Potosi, Missouri, January 1989, pp. 5.23 –5.38.

[6] P. M. Anderson and A. A. Fouad, *Power System Control and Stability*, Iowa State University Press, Ames, IA. 1977.

[7] G. Angelidis and A. Semlyen, "Improved Methodology for the Calculation of Critical Eigenvalues in Small Signal Stability Analysis", *IEEE Trans. on Power Systems*, Vol. 11, No. 3, August 1996, pp. 1209 –1217.

[8] S. Arabi, G. J. Rogers, D. Y. Wong, P. Kundur and M. G. Lauby, "Small Signal Stability Program Analysis of SVC and HVDC in AC Power Systems", *IEEE/PES 1991 Winter Meeting*, paper *91 WM 217-0 PWRS*, Ny. NY. February 3 -7, 1991.

[9] B. Avramovic and L. H. Fink, "Energy Management Systems and Control of FACTS", in M. D. Ilić edt. *Flexible AC Transmission Systems(FACTS) Special Issue, Electrical Power & Energy Systems*, Vol. 17, No. 3, June 1995, pp. 195 –198.

[10] R. Bacher, "Autogenerated Power Applications - Software Coding Approaches for the Future", *Future Needs and Trends in Power system Computing*, *PICA97* Tutorial, May 1997.

[11] J. Barquín and T. Gómez, "Determination of Voltage Collapse Areas Through Generalized Singular Value Analysis", *3rd Bulk Power System Voltage Phenomena, Seminar* August 1994.

[12] J. Barquín, T. Gómez and F. L. Pagola, "Hopf Limit Cycles Estimation in Power Systems", *Proc. Stockholm Power Tech* June 1995.

[13] J. Barquín, T. Gómez and F. L. Pagola, "Estimating The Loading Limit Margin Taking Into Account Voltage Collapse Areas", *Proc. IEEE/PES Winter Meeting* paper No. 95WM 183-4 PWRS, January 1995.

[14] A. R. Bergen, *Power System Analysis*, Prentice-Hall, Englewood Cliffs, New Jersey, 1986.

[15] K. Bhattacharya, J. Nanda and M. L. Kothari, "Optimization and Performance Analysis of Conventional Power System Stabilizers", *Electrical Power & Energy systems*, Vol. 19, No. 7, pp. 449 –458, 1997.

[16] R. T. Byerly, D. E. Sherman and R. J. Bennon, "Frequency Domain Analysis of Low-Frequency Oscillations in Large Electric Power Systems", *EPRI EL-726, RP744-1 Interim Report*, Palo Alto, California, April 1978.

[17] J. M. Campagnolo, N. Martins and J. L. R. Pereira, "Fast Small-Signal Stability Assessment Using Parllel Processing", *IEEE/PES 93 Summer Power Meeting*, paper No. 93 SM 481-2 PWRS, July 18-22,1993, Vancouver, Canada.

[18] J. M. Campagnolo, N. Martins and D. M. Falcão, "Refactored Bi-Iteration: A High Performance Eigensolution Method for Large Power System Matrices", *IEEE/PES* Paper 95 SM509-0 PWRS, IEEE Summer Meeting, Portland, Oregon July 1995.

[19] C. A. Cañizares, "Applications of Optimization to Voltage Collapse Analysis", *Panel Session: "Optimization Techniques in Voltage Collapse Analysis"*, IEEE/PES Summer Meeting, San Diego, July 14, 1998.

[20] C. A. Cañizares, W. Rosehart, "Bifurcation Analysis of Induction Motor Loads for Voltage Collapse Studies", *Proc. North American Power Symposium(NAPS)*, MIT, Nov. 96, pp. 559 –565.

[21] C. A. Cañizares, "Conditions for Saddle-Node Bifurcations in AC/DC Power Systems", *Electrical Power & Energy Systems*, Vol. 17, No. 1, pp. 61 –68, 1995.

[22] C. A. Cañizares, "On Bifurcation, Voltage Collapse and Load Modeling", *IEEE/PES summer meeting*, paper 94 SM 512-4 PWRS.

[23] C. A. Cañizares and S. Hranilovic, "Transcritical and Hopf Bifurcations in AC/DC Systems", *Proc. Bulk Power System Voltage Phenomena-III Seminar*, Davos, Switzerland, August 1994, pp. 105 –114.

[24] C. A. Cañizares, A. Z. de Souza and V. H. Quintana, "Improving Continuation Methods for Tracing Bifurcation Diagrams in Power Systems", *Proc. Bulk Power System Voltage Phenomena III. Voltage Stability, Security, and Control.* Davos, Switzerland, 22 -26 August 1994, pp. 349 –358.

[25] C. A. Cañizares, F. L. Alvarado, C. L. DeMarco, I. Dobson and W. F. Long, "Point of Collapse Methods Applied to AC/DC Power Systems", *IEEE Trans. on Power Systems*, Vol. 7, No. 2, May 1992, pp.673 –683.

[26] C. A. Cañizares and F. L. Alvarado, "Point of Collapse and Continuation Methods for Large AC/DC Systems", *IEEE/PES 1992 Winter Meeting*, paper # 92 WM 103-2 PWRS, New York, N.Y. January 26-30, 1992.

[27] C. L. Chang, Ah-Ching Liu and C. T. Huang, "Oscillatory stability analysis using real-time measured data", *IEEE Trans. on Power Systems*, Vol. 8, No. 3, August 1993, pp. 823 –828.

[28] C. S. Chang and J. S. Huang, "Optimal SVC Placement for Voltage Stability Reinforcement", *Electric Power Systems Research* 42 (1997) pp. 165 –172.

[29] C. S. Chang and S. S. Sim, "Optimizing Train Movements Through Coast Control Using Genetic Algorithms", *IEE Proc.-Electr.Power Appl.*, Vol. 144, No. 1, January 1997.

[30] CIGRÉ Paper 37-87, "The Power System Failure on July 23, 1987 in Tokyo", 1987.

[31] CIGRÉ Paper 38-11, "Voltage Stability - Fundamental Concepts and Comparison of Practical Criteria", 1984.

[32] H. -D. Chiang, C. W. Liu, P. Varaiya, F. F. Wu and M. G. Lauby, "Chaos in a Simple Power System", *IEEE Trans. on Power Systems*, Vol. 8, 1993, pp. 1407 –1414.

[33] H. -D. Chiang, I. Dobson, et al. "On Voltage Collapse in Electric Power Systems," *IEEE Trans. Power Systems,* Vol. 5, No. 2, May 1990.

[34] J. H. Chow and K. W. Cheung, "A Toolbox for Power System Dynamics and Control Engineering Education and Research", *IEEE/PES Trans. on Power Systems*, Vol. 7, No. 4, November 1992.

[35] J. H. Chow and A. Gebreselassie, "Dynamic Voltage Stability Analysis of a Single Machine Constant Power Load System", *Proc. 29th Conference on Decision and Control*, Honolulu Hawaii, December 1990, pp. 3057 –3062.

[36] J. H. Chow, editor, *Time-Scale Modeling of Dynamic Networks with Applications to Power Systems,* Springer-Verlag, Berlin, 1982.

[37] J. H. Chow and J. Hale, *Methods of Bifurcation Theory*, Springer-Verlag, N.Y. 1982.

[38] M. L. Crow and J. G. Chen, "The Multirate Simulation of FACTS Devices in Power System Dynamics", *IEEE Trans. on Power Systems*, Vol. 11, No. 1, Feb. 1996, pp. 376 –382.

[39] T. Van Custem and C. D. Vournas, "Voltage Stability Analysis in Transient and Mid-term Time Scales", *IEEE Trans. on Power Systems*, Vol. 11, No. 1, February 1996, pp. 146 –154.

[40] T. Van Custem, "A Method to Compute Reactive Power Margins with Respect to Voltage Collapse", *IEEE Transactions on Power Systems*, Vol. 6, No. 1, February 1991, pp. 145 –156.

[41] N. Deeb and S.M. Shahidehpour, "Linear Reactive Power Optimization in a Large Power Network Using the Decomposition Approach", *IEEE/PES Summer Meeting*, paper No. 89SM 695-8 PWRS, 1989.

[42] I. Dobson, "Computing a Closest Bifurcation Instability in Multidimensional Parameter Space", *Journal of Nonlinear Science*, Vol. 3, 1993, pp. 307-327.

[43] I. Dobson and L. Lu, "Computing an Optimum Direction in Control Space to Avoid Saddle Node Bifurcation and Voltage Collapse in Electric Power Systems", *IEEE Trans. on Automatic Control*, Vol. 37, No. 10, October 1992, pp.1616-1620.

[44] I. Dobson, "Observations on the Geometry of Saddle Node Bifurcation and Voltage Collapse in Electrical Power Systems", *IEEE Trans. on Circuits and Syst.-I: Fundamental Theory and Applications*, Vol. 39, No. 3, March 1992, pp. 240 –243.

[45] I. Dobson, H. -D. Chiang, et al., "A model of Voltage Collapse in Electric Power Systems", *IEEE Proceedings of the 27th Conference on Decision and Control*, Austin, Texas, December 1988, pp. 2104 –2109.

[46] I. Dobson and H. D. Chiang, "Towards a Theory of Voltage Collapse in Electric Power Systems", *System and Control Letters*, Vol. 13, pp. 253 –262, September 1989.

[47] I. Dobson, "An Iterative Method to Compute a Closest Saddle Node or Hopf Bifurcation Instability in Multidimensional Parameter Space", *Proceedings of the IEEE International Symposium on Circuits and Systems*, San Diego, CA, May 1992, pp. 2513–2516.

[48] M. A. El-Sharkawi, R. J. Makrs II and S. Weerasooriya, "Neural Networks and Their Application to Power Engineering", *Control and Dynamic Systems*, Vol. 41, 1991, pp.359-461.

[49] *EPRI TR-100834*, "Bifurcation and Chaos in Power Systems: A Survey", Prepare by University of California, Berkeley, *EPRI* Final Report, August 1992.

[50] D. K. Fadeev and V. N. Fadeeva, *Computational Methods of Linear Algebra*, W.H. Freeman and Co., 1963.

[51] F. D. Galiana and X. Lee, "On the Steady State Stability of Power Systems", *Proc. 1977 Power Industry Computer Applications Conference*, pp. 201 –210.

[52] F. D. Galiana and J. Jarjis, "Feasibility constraints in Power Systems", *Proc. IEEE PES Summer Meeting*, paper A 78 560-5, Los Angeles, 1978.

[53] B. Gao, G. K. Morison and P. Kundur, "Voltage Stability Evaluation Using Modal Analysis", *IEEE Trans. on Power Systems*, Vol. 7, No. 4, November 1992, pp. 1529 – 1542.

[54] C.B. Garcia and W.I. Zangwill, *Pathways to Solutions, Fixed Points, and Equilibria*, Prentice-Hall, Englewood Cliffs, New Jersey, 1981.

[55] P. E. Gill, W. Murray and M. H. Wright, *Practical Optimization*, Academic Press, 1981.

[56] David E. Goldberg, *Genetic Algorithms in Search, Optimization, and Machine Learning*, Addison-Wesley Publishing Company, INC. 1989.

[57] D. E. Goldberg and J. Richardson, "Genetic Algorithms with Sharing for Multimodal Function Optimization", *Genetic Algorithms and Their Applications: Proc. of the 2nd international Conference on GAs*, July 28-31, 1987, MIT, pp. 41 –49.

[58] A. Grace, "Optimization TOOLBOX User's Guide," The MathWorks, Inc. October 1994.

[59] I. A. Gruzdev, E. L. Toroptzev and S. M. Ustinov, "Optimization of Automatic Control Devices Tuning for a Variety of Power System Operating Conditions", *Elektrichestvo,* no. 4, 1986, pp. 11 –15 (in Russian).

[60] I. A. Gruzdev, V. A. Maslennikov and S. M. Ustinov, "Development of Methods and Software for Analysis of Steady-State Stability and Damping of Bulk Power Systems", *Issue: Methods and Software for Power System Oscillatory Stability Computations*, Publishing House of the Federation of Power and Electro-technical Societies, St.Petersburg, Russia, 1992, pp. 66 –88 (in Russian).

[61] J. Guckenheimer and P. Holmes, *Nonlinear Oscillations, Dynamical Systems, and Bifurcation of Vector Fields*, Springer -Verlag, 1983.

[62] B. D. Hasard, N. D. Kazarinoff and Y. -H. Wan, "Theory and Applications of Hopf Bifurcation", *London Math. Soc. Lect. Note Series*, No. 41, Cambridge university Press, UK (1981).

[63] D. J. Hill, ed., "Nonlinear Phenomena in Power Systems: Theory and Practical Implications", *Special Issue of Proceedings of IEEE*, The University of Sydney, November 1995.

[64] D. J. Hill and I. A. Hiskens, "Modelling, Stability and Control of Voltage Behaviour in Power Supply Systems", Invited paper, *IV Symposium of Specialists in Electric Operational and Expansion Planning*, Foz do Iguacu, Brazil, May 1994.

[65] D. J. Hill and I. A. Hiskens, "On Definitions for Power System Stability", Technical Report EE9229, Department of Electrical and Computer Engineering, The university of Newcastle, Australia, August 1992.

[66] D. J. Hill, V. A. Maslennikov, S. M. Ustinov, Y. V. Makarov, A. Manglick, B. Elliott, N. Rotenko and D. Conroy, "Advanced Small Disturbance Stability Analysis Techniques and MATLAB Algorithms" A final Report of the work *"Collaborative Research Project Advanced System Analysis Techniques" with the New South Wales*

Electricity Transmission Authority and The Department of Electrical Engineering, The University of Sydney", April 1996.

[67] I. A. Hiskens and R. J. Davy, "A Technique for Exploring the Power Flow Solution Space Boundary", *Proc. of the International Symposium on Electric Power Engineering Stockholm Power Tech*, Vol. Power Systems, Stockholm, Sweden, June 18-22, 1995, pp. 478 –483.

[68] D. J. Hill, I. A. Hiskens and D. H. Popovic, "Load Recovery in Voltage Stability Analysis and Control", *Proc. International Seminar on Bulk Power System Voltage Phenomena - III Voltage Stability, Security and Control*, Davos, Switzerland, August 1994, pp. 579–595.

[69] I. A. Hiskens and Y. V. Makarov, "Calculation of Power System Critical Loading Conditions", *Electrical Engineering Congress*, Sydney, 24-30 November 1994, pp. 185 – 190.

[70] Y. -T. Hsiao, H. -D. Chiang, C. -C. Liu and Y. -L. Chen, "A Computer Package for Optimal Multi-objective VAR Planning in Large Scale Power Systems", *IEEE Trans. Power Systems*, Vol. 9, No. 2, May 1994, pp. 668 –676.

[71] K. Iba, "Reactive Power optimization by Genetic Algorithm", *Proc. of 1993 Power Industry Computer Application Conference*, Phoenix, Arizona, May 4-7, 1993, pp. 195 –201.

[72] IEEE Committee Report, "Computer Representation of Excitation Systems", IEEE Trans. on Power Apparatus and Systems, Vol. PAS-87, June, 1968, pp. 1460 –1464.

[73] IEEE Committee Report, "Excitation System Models for Power System Stability Studies", *IEEE Trans. on Power Apparatus and Systems*, Vol. PAS-100, No. 2, February 1981, pp. 494 –509.

[74] IEEE Task Force on Load Representation for Dynamic Performance, "Bibliography on Load Models for Power Flow and Dynamic Performance Simulation", *IEEE Trans. on Power Systems*, Vol. 10, No. 1, February 1995, pp. 523 –538.

[75] IEEE Power System Engineering Committee, System Dynamic Performance Subcommittee, "Voltage Stability of Power Systems: Concepts, Analytical Tools, and Industry Experience", *IEEE Special Publication*, No. 90 TH0358-2-PWR, pp. 2.

[76] IEEE Special Publication, 90TH0358-2-PWR, "Voltage Stability of Power Systems: Concepts, Analytical Tools, and Industry Experience", 1990.

[77] M. D. Ilić, "Fundamental Engineering Problems and Opportunities in Operating Power Transmission Grids of the Future", *Electrical Power and Energy Systems*, Vol. 17, No. 3, 1995, pp. 207 –214.

[78] M. D. Ilić, edt. "Editorial", *Flexible AC Transmission Systems(FACTS) Special Issue, Electrical Power & Energy Systems*, Vol. 17, No. 3, June 1995, pp. 163 –164.

[79] G. D. Irisarri, X. Wang, J. Tong and S. Mokhtari, "Maximum Loadability of Power Systems using Interior Point Non-Linear Optimization Method", *IEEE/PES* Winter Meeting, paper 96 WM 207-1 PWRS, Baltimore, MD. January 21-25, 1996.

[80] J. -S. R. Jang, C. -T. Sun, and E. Mizutani, *Neuro-Fuzzy and Soft Computing, A Computational Approach to Learning and Machine Intelligence*, Prentice-Hall international, Inc.

[81] J. Jarjis and F. D. Galiana, "Quantitative Analysis of Steady State Stability in Power Networks", *IEEE Trans. on Power App. and Syst.*, Vol. PAS-100, no. 1, January 1981, pp. 318 –326.

[82] P. Ju, E. Handschin, Z. N. Wei and U. Schlückling, "Sequential Parameter Estimation of a Simplified Induction Motor Load Model", *1995 IEEE Power Industry Computer Application Conference*, Salt Lake City, Utah, May 7-12, 1995, pp. 206 –211.

[83] W. -S. Jwo, C. -W. Liu, C. -C. Liu and Y. -T. Hsiao, "Hybrid expert system and simulated annealing approach to optimal reactive power planning", *IEE Proc. -Gener. Transm. Distrib.*, Vol. 142, No. 4, July 1995, pp. 381 –385.

[84] D. Karlsson and D. J. Hill, "Modeling and Identification of Nonlinear Dynamic Loads in Power Systems", *IEEE Trans. on Power Systems*, Vol. 9, No. 1, 1994, pp. 157 –166.

[85] A. M. Kontorovich, "A Direction of Investigations of The Load Flow Problem", *Trudy LPI*, No. 406, 1985, pp. 18 –25 (in Russian).

[86] A. M. Kontorovich and N. P. Dunaeva, "Investigation of Load Flow Methods Based on The Taylor Expansion of A Solution", Issue: *Primenenie matematicheskih metodov pri upravlenii regimami i razvitiem elektricheskih sistem*, Irkutsk, pp. 65 –74, 1978 (in Russian).

[87] A. M. Kontorovich and A. V. Krukov, "Definition of Power Flow Limit Conditions by the Permanent Loading Method", *Trudy LPI (Proc. of the Leningrad Polytechnic Institute)*, Vol. 380, 1981, pp. 104 –108 (in Russian).

[88] A. M. Kontorovich and A. V. Krukov, *Critical Power Flows in Power Systems (Fundamentals of Theory and Computational Methods)*, Publishing House of the Irkursk State University, Irkutsk - Ulan-Ude, 1985 (in Russian).

[89] A. M. Kontorovich, A. V. Krukov, Y. V. Makarov, et. al., *Computer Methods for Stability Analysis in Complicated Power Systems*, Publishing House of the Irkursk State University, Irkutsk, 1988 (in Russian).

[90] A. M. Kontorovich and Y. V. Makarov, "Methods of Load Flow Computations Using High Order Terms of Taylor Series Expansions", *Technical Report EE9426*, Department of Electrical and Computer Engineering, The University of Newcastle, Australia, July 1994.

[91] A. M. Kontorovich, Y. V. Makarov and A. A. Tarakanov, "Improved Permanent Loading Methods for Computations of the Power System Load Flow Steady-State Stability Limits", *Trudy LPI (Proc. of the Leningrad Polytechnic Institute)*, No. 385, Leningrad, 1982 (in Russian).

[92] G. A. Korn and T. M. Korn, *Mathematical Handbook for Scientists and Engineers*, McGraw-Hill Book Company, New York, 1968.

[93] J. R. Koza, *Genetic Programming II, Automatic Discovery of Reusable Programs*, The MIT Press, 1994.

[94] K. Kristinsson and G. A. Dumont, "System Identification and Control Using Genetic Algorithms", *IEEE Trans. on System, Man, and Cybernetics*, No. 22, Vol. 5, September/October 1992, pp.1033 –1046.

[95] P. Kundur, *Power System Stability and Control*, New York: McGraw-Hill, Inc. 1994.

[96] H. G. Kwatny, R. F. Fischl and C. Nwankpa, "Local Bifurcation in Power Systems: Theory, Computation and Application", D. J. Hill (ed), *Special Issue on Nonlinear Phenomena in Power Systems: Theory and Practical Implications, IEEE Proceedings,* Vol. 83, No. 11, November, 1995, pp. 1456 –1483.

[97] K. T. Law, D. J. Hill and N. R. Godfrey, "Robust Co-ordinated AVR-PSS Design", *IEEE Trans. on Power Systems*, Vol. 9, No. 3, pp. 1218 –1225, August 1994.

[98] B. Lee and V. Ajjarapu, "Bifurcation Flow: A Tool to Study Both Static and Dynamic Aspects of Voltage Stability", *Proceedings of the Bulk Power System Voltage Phenomena III. Voltage Stability, Security and Control*, Davos, Switzerland, August 22-26, 1994, pp. 305–324.

[99] S. B. Lippma, *C++ Primer*, 2nd edition, Addison-Wesley, 1991.

[100] H. N. Liu, "Study on Fundamental Theory of Genetic Algorithms and its Application in System Identification", MScEE Thesis, Tianjin University, March 1997 [in Chinese].

[101] J. T. Ma and L. L. Lai, "Improved Genetic Algorithm for Reactive Power Planning", *Proc. 12th Power Systems Computation Conference*, Dresden, Sweden, August 19-23, 1996, pp. 499 –505.

[102] S. W. Mahfoud, "Population Size and Genetic Drift in Fitness Sharing", L. D. Whitile and M. D. Vose edt. *Foundations of Genetic Algorithms • 3*, Morgan Kaufmann Publishing, Inc. 1995, pp. 185–223.

[103] J. Mahseredjian and F. Alvarado, "MATLAB, Fortran and Objected Oriented Languages for Power System Application Development", in *Future Needs and Trends in Power System Computing*, *PICA97* Tutorial.

[104] Y. V. Makarov, *Load Flow Calculation Methods for Information and Control Systems (ICS) Used in Power System Control*, PhD thesis, The Leningrad Polytechnic Institute, Leningrad, 1984 (in Russian).

[105] Y. V. Makarov, D. J. Hill and I. A. Hiskens, "Study of Multi-Solution Quadratic Load Flow Problems and Applied Newton -Raphson Like Methods", *Proc. of the IEEE International Symposium on Circuits and Syst.*, Seattle, Washington, USA, April 29 - May 3, 1995.

[106] Y. V. Makarov, D. J. Hill and I. A. Hiskens, "Properties of Quadratic Equations and Their Application to Power System Analysis", submitted to *International Journal of Electrical Power Systems.*

[107] Y. V. Makarov, D. J. Hill and J. V. Milanovic, "Effect of Load Uncertainty on Small Disturbance Stability Margins in Open-Access Power Systems", *Proc. Hawaii International Conference on System Sciences HICSS-30*, Kihei, Maui, Hawaii, January 7-10, 1997, Vol. 5, pp. 648 –657.

[108] Y. V. Makarov and I. A. Hiskens, "A Continuation Method Approach to Finding the Closest Saddle Node Bifurcation Point", *Proceedings of NSF/ECC Workshop on Bulk Power System Voltage Phenomena III*, Davos, Switzerland, August 1994.

[109] Y. V. Makarov, A. M. Kontorovich, D. J. Hill and I. A. Hiskens, "Solution Characteristics of Quadratic Power Flow Problems", *Proc. 12-th Power System Computation Conference,* Vol. 1, Dresden, Germany, August 19 –23 , 1996, pp. 460 –467.

[110] Y. V. Makarov, V. A. Maslennikov and D. J. Hill, "Calculation of Oscillatory Stability Margins in the Space of Power System Controlled Parameters", *Proc. of the International Symposium on Electric Power Engineering, Stockholm Power Tech*, Vol. Power Systems, Stockholm, Sweden, June 18 -22, 1995, pp. 416 –422.

[111] N. Martins and L. T. G. Lima, "Eigenvalue and Frequency Domain Analysis of Small Signal Electromechanical Stability Problems", *Eigenanalysis and Frequency domain Methods for system Dynamic Performance*, IEEE publication 90TH0292-3-PWR.

[112] Y. Mansour (ed.), *Voltage Stability of Power Systems: Concept, Analytical Tools, and Industry Experience*, IEEE Task Force Report, Publication 90 TH 0358-2-PWR, 1990.

[113] Y. Mansour, W. Xu, F. Alvarado and C. Rinzin, "SVC Placement Using Critical Modes of Voltage Instability", *Proc. 1993 Power Industry Computer Application Conference, IEEE PICA'93*, Phoenix, Arizona, May 4 -7, 1993, pp.131 –137.

[114] Y. Mansour and P. G. Harrington, "Voltage Instability - B. C. Hydro's Practice and Experience", Panel Session on voltage Instability, *1987 IEEE/PES Summer Meeting*, San Francisco, CA.

[115] Y. Mansour and P. Kundur, "Voltage Collapse: Industry Practices", in *Control and Dynamic Systems*, Vol. 42, Academic Press, Inc. pp. 111 –161, 1991.

[116] V. A. Maslennikov and S. M. Ustinov, "The Optimization Method for Coordinated Tuning of Power System Regulators", *Proc. 12th Power System Computation Conference*, Dresden, 19-23 August, 1996.

[117] J. V. Milanović, *The Influence of Loads on Power System Electromechanical Oscillations*, PhD thesis, The University of Newcastle, NSW. Australia, February, 1996.

[118] J. V. Milanović, I. A. Hiskens, "Effects of Dynamic Load Model Parameters on Damping of Oscillations in Power Systems", *Electric Power Systems Research*, Vol. 33, pp.53 –61, 1995.

[119] V. Miranda, D. Srinivasan, and L. M. Proenca, "Evolutionary Computing in Power Systems", *Proc. of the 12th Power System Computation Conference*, Dresden, Sweden, August 19-23, 1996, pp. 25 –40.

[120] S. L. Nilsson, "Security Aspects of Flexible AC Transmission System Controller Applications", in M. D. Ilić edt. *Flexible AC Transmission Systems(FACTS) Special Issue, Electrical Power & Energy Systems*, Vol. 17, No. 3, June 1995, pp. 173 –179.

[121] M. K. Pal, "Voltage Stability Analysis Needs, Modeling Requirement, and Modeling Adequacy," *IEE Proceedings of Part C.*, Vol. 140, pp. 279 –286, July 1993.

[122] M. A. Pai "Structural Stability in Power Systems," J. H.Chow, P. V. Kokotovic and R. J. Thomas edit, in *Systems and Control Theory for Power Systems*, Springer-Verlag, 1995, pp. 259 –281.

[123] M. A. Pai, C. D. Vournas, A. N. Michel and H. Ye, "Application of Interval Matrices in Power System Stabilizer Design", *Electrical Power & Energy Systems*, Vol. 19, No. 3, pp. 179 –184, 1997.

[124] G. B. Price, "A Generalized Circle Diagram Approach for Global Analysis of Transmission System Performance", *IEEE Trans. on Power App. and Syst.*, Vol. PAS-103, no. 10, October 1984, pp. 2881 –2890.

[125] C. Rajagopalan, P. W. Sauer and M. A. Pai, "Analysis of Voltage Control Systems Exhibiting Hopf Bifurcation", *Proceedings of the 28th Conference on Decision and Control*, Tampa, Florida, December 1989, pp. 332 –335.

[126] S.S. Sachdeva and R. Billinton, "Optimum Network VAR Planning by Nonlinear Programming", *IEEE Trans. on Power Apparatus and Systems*, Vol.PAS-92, 1973, pp.1217-1225.

[127] G. Shackshaft, O. C. Symons and J.G. Hadwick, "General-purpose Model of Power-system Loads", *Proc. IEEE*, Vol. 124, No. 8, August 1977.

[128] N. I. Santoso and O. T. Tan, "Neural Net Based Real-Time control of Capacitors Installed on Distribution Systems", *IEEE/PES Summer Meeting*, 89SM 768-3 PWRD, Long Beach, California, 1989.

[129] P. W. Sauer, B. C. Lesieutre and M. A. Pai, "Maximum Loadability and Voltage Stability in Power Systems," *International Journal of Electrical Power and Energy Systems*, Vol. 15, pp. 145 –154, June 1993.

[130] P. W. Sauer and B. C. Lesieutre, "Power System Load Modeling," J. H.Chow, P. V. Kokotovic and R. J. Thomas edit, in *Systems and Control Theory for Power Systems*, Springer-Verlag, 1995, pp. 283 –313.

[131] P. W. Sauer and M. A. Pai, "Modeling and Simulation of Multimachine Power System Dynamics", *Control and Dynamic Systems*, Vol. 43, pp. 1 –99, 1991.

[132] P. W. Sauer and M. A. Pai, "Power System Steady-State Stability and the Load-Flow Jacobian", *IEEE Trans. on Power Systems*, Vol. 5, No. 4, November 1990, pp. 1374 –1383.

[133] R. A. Schleuter, et al, "Methods for determining proximity to voltage collapse", *IEEE Trans. Power Systems*, Vol.6, No.1, pp.285-292.

[134] M. Schoenauer and S. Xanthakis, "Constrained GA Optimization", *Proc. of the 5th International Conference on GAs*, 1993, pp. 573 –580.

[135] H. Seifi and K. Imhof, "Voltage Stability Analysis in an Energy Management System", *Proc. of the 12th Power Systems Computation Conference*, Dresden, August 19-23, 1996, pp. 988 –994.

[136] R. Seydel, *From Equilibrium to Chaos, Practical Bifurcation and Stability Analysis*, 2nd edition, N.Y. Springer-Verlag, 1994.

[137] P. Smith, P. Wright and W. Grainger, "The New South Wales-Queensland Interconnection: Extending the Eastern States Electricity Network", *Electrical Engineering Congress,* Sydney, 24-30 November 1994, pp. 83 –89.

[138] K. S. Swarup, M. Yoshimi, S. Shimano and Y. Izui, "Optimization Methods using Genetic Algorithms for Reactive Power Planning in Power Systems", *Proc. 12th Power systems Computation Conference*, Dresden, Sweden, August 19-23, 1996, pp.483 –491.

[139] C. -W. Tan, M. Varghese, P. Varaiya and F. F. Wu, "Bifurcation, Chaos and Voltage Collapse in Power Systems", D.J. Hill (ed), *Special Issue on Nonlinear Phenomena in Power Systems: Theory and Practical Implications, IEEE Proceedings*, Vol. 83, No. 11, November, 1995, pp. 1484 –1496.

[140] R. Thomas, The Internet, Java, and Objects for Network-Centered Computing and Communications with Applications for Power Systems", in *Future Needs and Trends in Power system Computing*, *PICA97* tutorial, May, 1997.

[141] V. P. Vasin, *Power Flow Feasibility Regions of Electrical Systems*, Publishing House of the Moscow Power Engineering Institute, Moscow, 1982 (in Russian).

[142] V. Venkatasubramanian, H. Schättler and J. Zaborszky, "Dynamics of Large Constrained Nonlinear Systems -A Taxonomy Theory", D. J. Hill (ed), *Special Issue on Nonlinear Phenomena in Power Systems: Theory and Practical Implications, IEEE Proceedings,* Vol. 83, No. 11, November, 1995, pp. 1530 –1561.

[143] V. A. Venikov, V. A. Stroev, V. I. Idelchik and V. I. Tarasov, "Estimation of Electric Power System Steady-State Stability in Load Flow Calculation," *IEEE Trans. on Power Apparatus and Systems*, Vol. PAS-94, May-June 1975, pp. 1034 –1041.

[144] *Visual Basic Books On Line*, Microsoft Visual Basic software.

[145] H. O. Wang, E. H. Abed and A. M. A. Hamdan, "Bifurcations, Chaos, and Crises in Voltage Collapse of a Model Power System", *IEEE Trans. on Circuits and Systems-I: Fundamental Theory and Applications*, Vol. 41, No. 3, March 1994, pp. 294 –302.

[146] L. Wang and A. Semlyen, "Application of Sparse eigenvalue Techniques to the Small Signal Stability analysis of Large Power Systems", *IEEE Trans. On Power Systems*, PICA89, Vol. 5, No. 2, 1990, pp. 635 –642.

[147] K. P. Wong, and Y. W. Wong, "Genetic and Genetic/Simulated-Annealing Approaches to Economic Dispatch", *IEE Proc. C.* 1994, 141, (5), pp. 685 –692.

[148] F. F. Wu and P. Varaiya, *Coordinated Multilateral Trades for Electric Power Networks: Theory and Implementation*, Department of Electrical Engineering and Computer Sciences, University of California, Berkeley, August 1995.

[149] W. Xu and Y. Mansour, "Voltage Stability Analysis using Generic Dynamic Load Models", *IEEE/PES 1993 Winter Meeting*, paper 93 WM 185-9 PWRS, Columbus , OH, January 27 1992.

[150] W. Zhu, R. R. Mohler, R. Spee, W. A. Mittelstadt and D. Maratuklam, "Hopf Bifurcation in a SMIB Power System with SSR", *IEEE Trans. on Power Systems*, Vol. 11, No. 3, August 1996, pp 1579 –1584.

Appendix A

Matrix Analysis Fundamentals

A.1 Eigenvalues and Eigenvectors

The Lyapunov stability first method is the fundamental analytical basis for power system small signal stability assessment. It is based on eigenvalue analysis. The properties of eigenvalues and eigenvectors for stability study are listed here. A power system or any other dynamic system can be represented by a state variable model after linearization as:

$$\dot{x} = Ax + Bu \tag{A.1}$$

$$y = Cx + Du \tag{A.2}$$

where A is the state matrix, x is vector of state variables, u is vector of control variables, and y is vector of output variables. The process of finding the state matrix's eigenvalues corresponds to finding nontrivial solutions of,

$$AV = \Lambda V \Leftrightarrow Av_i = \lambda_i v_i \tag{A.3}$$

where, if A is $n \times n$ matrix, V is a $n \times n$ matrix, whose columns are v_j, $j = 1, ..., n$, and $\Lambda = diag\{\lambda_i\}$ is a $n \times n$ diagonal matrix. Λ and V satisfying the equation are vector of eigenvalues and matrix of *right eigenvectors* of A respectively. It can be solved by,

$$\det(A - \Lambda I) = 0 \tag{A.4}$$

where Λ is the vector of eigenvalues of A. The *left eigenvectors* can be calculated by solving,

$$WA = \Lambda A \Leftrightarrow w_i^T A = \lambda_i w_i^T \tag{A.5}$$

where w_i are the i-th *left eigenvectors* of A corresponding to the i-th eigenvalue λ_i. Note that W^T is a matrix with left eigenvectors as its rows, and V is the matrix with right eigenvectors as its columns.

The left and right eigenvectors are orthogonal and as used in the techniques, are normalized, i.e. they satisfy,

$$w_i^T v_j = \begin{cases} 0, & \text{if} \quad i \neq j \\ 1, & \text{if} \quad i = j \end{cases} \tag{A.6}$$

A.2 Participation Factors

The participation factors are defined using the information provided by the right and left eigenvalues,

$$p_{ij} = w_{ji}^T v_{ij} \tag{A.7}$$

The participation factor p_{ij} represents the net participation of the i-th state in the j-th mode. As followed from the orthogonality property of the right and left eigenvectors, the sum of the participation factors for one state is one.

Appendix B

Numerical Methods in Optimization

B.1 The High Order Numerical Solution Technique

A numerical technique, which is proposed in [85, 86, 91, 104], exploits high order information to improve convergence of solution of algebraic equations. This is useful in application to the stages of refinement of initial values, and numerical solution of the critical point algorithm. This technique is also useful in continuation approach to locate the closest saddle node bifurcations as described in Chapter 4.

B.1.1 Solution Motion and Its Taylor Series Expansion

Consider a general set of smooth nonlinear equations given by,

$$g(z, \beta) = \beta \Delta g + \underline{g}(z) = 0 \tag{B.1}$$

where z is a vector of dependent variables, β is a scalar parameter, and Δg is a vector of increments.

If $\frac{\partial g}{\partial z}$ is nonsingular, then the function $g(z, \beta)$ can be considered as an implicit

function which defines the dependence $z(\beta)$. Differentiation of (B.1) yields

$$(\frac{\partial g}{\partial z})(\frac{dz}{d\beta}) + (\frac{dg}{d\beta}) = (\frac{\partial \underline{g}}{\partial z})(\frac{dz}{d\beta}) + \Delta g = 0 \tag{B.2}$$

If the Jacobian matrix $\frac{\partial \underline{g}}{\partial z}$ is nonsingular, we get the differential equation

$$\frac{dz}{d\beta} = -[\frac{\partial \underline{g}}{\partial z}]^{-1}\Delta g \tag{B.3}$$

The equation (B.3) defines motion of a solution of (B.1) as the parameter β varies. A solution of (B.3) can be represented as the Taylor series expansion [92]

$$z(\beta) = z^0 + \sum_{k=1}^{\infty}(k!)^{-1}(\frac{d^k z}{d\beta^k})(\beta - \beta^0)^k, \tag{B.4}$$

where $\beta = \beta^0$, $z = z^0$ is a nominal solution of (B.1). Substituting $\alpha = (\beta^0 - \beta)$ gives

$$z(\alpha) = z^0 + \sum_{k=1}^{\infty}(\frac{\alpha^k}{k!})\Delta z_k \tag{B.5}$$

where

$$\Delta z_k = \frac{d^k z}{d\alpha^k}|_{\alpha=0, z=z^0} \tag{B.6}$$

The expansion (B.5) represents the solution function $z(\alpha)$ as a polynomial of the scalar parameter α.

If $\beta^0 = 1$, and Δg is thought of as a mismatch vector of (B.1) at the point $z = z^0$, then if the series expansion (B.5) converges for $\alpha = 1$, it will give a solution of the problem $\underline{g}(z) = 0$.

Due to the impracticality of computing a large number of Δz_k, the summation (B.5) must be restricted to a finite number of terms K. Accordingly, (B.5) becomes an iterative procedure

$$z_{i+1} = z_i + \sum_{k=1}^{K}(\frac{\alpha_i^k}{k!})\Delta z_{k,i} \tag{B.7}$$

where i is the iteration number and $\Delta z_{k,i}$ is the k-th correction vector. The α_i has sense of a *correction coefficient* which influences convergence reliability. It can be easily shown that for $K = 1$, (B.7) corresponds to the Newton-Raphson method with an optimal multiplier. If $K > 1$, then (B.7) becomes a generalization of the Newton-Raphson method which takes into account nonlinear terms of the Taylor series expansion. The linear approximation of $\underline{g}(z)$ that is used in the Newton-Raphson method is replaced by an approximation that is nonlinear.

B.1.2 Computation of the correction vectors Δz_k

Expressions for correction vectors Δz_k can be obtained by successive differentiation of (B.2) with respect to β. We set $\alpha = (\beta^0 - \beta) = 1$ in (B.1) and express $\underline{g}(z)$ as a Taylor series, so giving

$$(1-\beta^0)\Delta g = \underline{g}(z) = \underline{g}(z^0) + J_g(z^0)\Delta z + \sum_{l=2}^{\infty} \frac{1}{l!} W_l(\underbrace{\Delta z, .., \Delta z}_{l}) \tag{B.8}$$

where $J_g(\cdot)$ is the Jacobian matrix, and $W_l(\cdot)$ is the l-th order term of the Taylor series. It is shown in [90, 104] that by substituting $\Delta z = \sum_{k=1}^{K}(\frac{\Delta z_k}{k!})$ into (B.8), the following expressions can be obtained

$$\begin{aligned}
\Delta z_1 = &\quad -J_g^{-1}(z^0)[(\beta^0 - 1)\Delta g + \underline{g}(z^0)] = J_g^{-1}(z^0)\Delta g \\
\Delta z_2 = &\quad -J_g^{-1}(z^0)[W_2(\Delta z_1, \Delta z_1)] \\
\Delta z_3 = &\quad -J_g^{-1}(z^0)[3W_2(\Delta z_1, \Delta z_2) + W_3(\Delta z_1, \Delta z_1, \Delta z_1)] \\
\Delta z_i = &\quad -i! J_g^{-1}(z^0) \sum_{l=2}^{i} \sum_{\left[\begin{smallmatrix} s_1, s_2, \cdots, s_K = 0, .., l \\ s_1 + s_2 + \cdots + s_K = l \\ s_1 + 2s_2 + \cdots K s_K = i \end{smallmatrix}\right]} \\
&\qquad \prod_{k=1}^{K} (k!)^{-s_k} (s_k!)^{-1} W_l(\underbrace{\Delta z_1, .., \Delta z_1}_{s_1}, .., \underbrace{\Delta z_K, .., \Delta z_K}_{s_K})
\end{aligned} \tag{B.9}$$

The high order terms $W_l(\cdot)$ in (B.9) can be expressed through values of the function $\underline{g}(z)$. For example, if (B.1) was a set of quadratic equations, then for $K = 5$, the following recurrent equalities can be obtained,

$$\begin{aligned}
\Delta z_1 &= -J_g^{-1}(z^0)[(\beta^0 - 1)\Delta g + \underline{g}(z^0)] = J_g^{-1}(z^0)\Delta g \\
\Delta z_2 &= -J_g^{-1}(z^0)[W_2(\Delta z_1, \Delta z_1)] \\
\Delta z_3 &= -J_g^{-1}(z^0)[3W_2(\Delta z_1, \Delta z_2)] \\
\Delta z_4 &= -J_g^{-1}(z^0)[3W_2(\Delta z_2, \Delta z_2) + 4W_2(\Delta z_1, \Delta z_3)] \\
\Delta z_5 &= -J_g^{-1}(z^0)[5W_2(\Delta z_1, \Delta z_4) + 10W_2(\Delta z_2, \Delta z_3)]
\end{aligned} \tag{B.10}$$

where

$$W_2(\Delta z_i, \Delta z_j) = \underline{g}(\Delta z_i + \Delta z_j) - \underline{g}(\Delta z_i) - \underline{g}(\Delta z_j) + \underline{g}(0) \tag{B.11}$$

The expressions (B.10),(B.11) are used at each iteration (B.7) of the method.

B.1.3 Correction coefficients

To provide reliable convergence of the method, it is necessary to use appropriate values of the correction coefficients α_i in (B.7). The correct choice of α_i gives direct motion in the space of parameters g. It can be shown that the deviation of the method from the direct line $(\beta^0 - \beta)\Delta g$ is evaluated by the norm

$$\|(\beta^0 - \alpha)\Delta g + \underline{g}(z^0 + \sum_{k=1}^{K} \frac{\alpha^k}{k!}\Delta z_k)\| \leq \epsilon_g \tag{B.12}$$

It is clear that for $\alpha = 0$ the norm (B.12) is equal to zero. Increasing α results in the method taking larger steps, but the deviation (B.12) can also increase. However, having calculated the correction vectors $z_{k,i}$ at the i-th iteration, and knowing the specified maximum deviation ϵ_g, it is not difficult to obtain the corresponding value of α_i which keeps the deviation (B.12) within the desired accuracy ϵ_g. If the value of ϵ_g is small enough, the method will converge up to a singular point of (B.1) [104].

Appendix C

Proof of Quadratic Properties of Load Flow $\triangle$-plane Problem

Proofs are given of Properties 1-3 in Section 4.5.1, they are taken from [106].

C.1 Proof of Property 1

Property 1. For any two points $x_1 \neq x_2$ and $detJ(x_1) \neq 0$, the number and location of singularities of the quadratic problem $f(x) = 0$ on the straight line through x_1, x_2 is defined by real eigenvalues of the matrix $J^{-1}(x_1)J(x_2)$. These singular points on the line can be found as $x_j = x_1 + \mu_j(x_2 - x_1)$, where μ_j are computed as $\mu_j = (1 - \lambda_j)^{-1}$ for all real eigenvalues $\lambda_j \neq 1$ of the matrix $J^{-1}(x_1)J(x_2)$.

Proof: Define the line through x_1, x_2 as

$$x = x_1 + \mu(x_2 - x_1) = x_1 + \mu\Delta x_{21}, \tag{C.1}$$

For a quadratic function $f(x)$, its Jacobian matrix $J(x)$ consists of elements which are linear functions of x. So, it can be represented as

$$J(x) = \sum_{i=1}^{n} A_i x_i + J(0), \tag{C.2}$$

where A_i, $J(0)$ are $(n \times n)$ constant matrices of Jacobian coefficients, and x_i is i-th element of x.

Using (C.2), it is easy to show that

$$J[x_1 + \mu(x_2 - x_1)] = (1 - \mu)J(x_1) + \mu J(x_2). \tag{C.3}$$

As x_1 is a nonsingular point, for $\mu \neq 0$, expression (C.3) can be written as

$$J(x) = \mu J(x_1)\left[J^{-1}(x_1)J(x_2) - (\mu - 1)\mu^{-1}I\right], \tag{C.4}$$

where I is the identity matrix. For $\mu \neq 0$, the determinant of $J(x)$ is equal to zero if and only if

$$det\left[J^{-1}(x_1)J(x_2) - \lambda I\right] = 0 \tag{C.5}$$

where $\lambda = (\mu - 1)\mu^{-1}$. It is clear that all singular points on the line (C.1) can be computed in terms of real eigenvalues $\lambda_i \neq 1$ of the matrix $J^{-1}(x_1)J(x_2)$:

$$\mu_i = (1 - \lambda_i)^{-1} \tag{C.6}$$

□

C.2 Proof of Property 2

Property 2. The maximum number of solutions of a quadratic equation $f(x) = 0$ on each straight line in the state space R_x^n is two.

Proof: Take the function

$$\phi(\mu) = f^t(x + \mu\Delta x)f(x + \mu\Delta x) \tag{C.7}$$

For a quadratic mismatch function $f(x)$,

$$f(x + \mu\Delta x) = f(x) + \mu J(x)\Delta x + 0.5\mu^2 W(\Delta x) \tag{C.8}$$

where $W(\Delta x)$ is a quadratic term of expansion (C.8). So,

$$\begin{aligned}\phi(\mu) = \quad & \|f(x) + \mu J(x)\Delta x + 0.5\mu^2 W(\Delta x)\|^2 = \\ & = \|f(x)\|^2 + \|\mu J(x)\Delta x\|^2 + \\ & + \|0.5\mu^2 W(\Delta x)\|^2 + 2\mu f^t(x)J(x)\Delta x + \\ & + \mu^3 W^t(x)J(x)\Delta x + \mu^2 f^t(x)W(\Delta x).\end{aligned}$$

Function $\phi(\mu)$ equals to zero if and only if $f(x + \mu\Delta x) = 0$. At a solution point $x = x_*$, $f(x_*) = 0$, and function (C.7) is

$$\begin{aligned}\phi_*(\mu) = \ & \tfrac{1}{4}\mu^4\|W(\Delta x)\|^2 + \mu^3 W^t(\Delta x)J(x)\Delta x + \\ & +\mu^2\|J(x)\Delta x\|^2 = (a\mu^2 + b\mu + c)\mu^2.\end{aligned}$$

For any fixed direction $\Delta x \neq 0$, $\phi_*(\mu)$ equals to zero in the two following cases

(a) $\mu = 0$;

(b) $a\mu^2 + b\mu + c = 0$.

The first case gives us the original solution point $x = x_*$. The second case may correspond to solutions $x \neq x_*$ on the straight line directed by Δx. But as it is clear from (C.7), the function (C.7) can not be negative. Thus $a\mu^2 + b\mu + c \geq 0$, and in the case (b) it is possible to have only one additional solution except x_*, but not two or more. So, on the line we get one original root $x = x_*$, and we can have only one additional root corresponding to condition (b). □

C.3 Proof of Property 3

Property 3. For quadratic mismatch functions $f(x)$, a variation of x along a straight line through a pair of distinct solutions of the problem $f(x) = 0$ results in variation of the mismatch vector $f(x)$ along a straight line in R^n_y.

Proof: Let x be a point on the straight line connecting two distinct solutions x_1, x_2:

$$x = x_1 + \mu(x_2 - x_1) = x_1 + \mu\Delta x_{21}, \tag{C.9}$$

where μ - is a parameter, and $\Delta x_{21} = x_2 - x_1$. For quadratic mismatch functions,

$$f(x)=f(x_1)+\mu J(x_1)\Delta x_{21}+0.5\mu^2 W(\Delta x_{21}), \tag{C.10}$$

$$f(x_2) = f(x_1) + J(x_1)\Delta x_{21} + 0.5W(\Delta x_{21}), \tag{C.11}$$

where $0.5W(\Delta x_{21})$ is the quadratic term of the Taylor series expansion (C.11). At points x_1, x_2, we have $f(x_1) = f(x_2) = 0$. So, from (C.11),

$$0.5W(\Delta x_{21}) = -J(x_1)\Delta x_{21}. \tag{C.12}$$

Using (C.12), equation (C.10) transforms to

$$f(x_1 + \mu\Delta x_{21}) = \mu(1-\mu)J(x_1)\Delta x_{21} = \beta\Phi, \tag{C.13}$$

where $\beta = \mu(1-\mu)$, $\Phi = J(x_1)\Delta x_{21}$. Thus mismatch function $f(x_1 + \mu\Delta x_{21})$ varies along the straight line $\beta\Phi$ in R_y^n. □

Appendix D

Publications Arising from The Thesis

- Y. V. Makarov, D. J. Hill and Z. Y. Dong, "Computation of Bifurcation Boundaries for Power Systems: A New Delta-Plane Method", accepted for publication in *IEEE Trans. on Circuits and Systems.*

- Y. V. Makarov and Z. Y. Dong "Eigenvalues and Eigenfunctions", Vol. Computational Science & Engineering, *Encyclopedia of Electrical and Electronics Engineering*, John Wiley & Sons.

- Z. Y. Dong, Y. V. Makarov and D. J. Hill, "Power System Small Signal Stability Analysis Using Genetic Optimization Techniques", *Electric Power Systems Research*, to appear.

- Y. V. Makarov, Z. Y. Dong and D. J. Hill, "A General Method for Small Signal Stability Analysis", *IEEE Transaction on Power Systems* (to appear).

- H. N. Liu, Z. Y. Dong, et al, "An Improved Genetic Algorithm in System identification", submitted to *Systems Research and Information Science.*

- Y. V. Makarov, D. J. Hill and Z. Y. Dong, "A New Robust Method to Explore the Load Flow Feasibility Boundaries", *Proc. of the Australian Universities Power Engineering Conference AUPEC'96*, Vol. 1, Melbourne, Australia, October 2-4, 1996, pp. 137-142.

- Z. Y. Dong, Y. V. Makarov and D. J. Hill, "Computing the Aperiodic and Oscillatory Small Signal Stability Boundaries in Modern Power Grids", *Proc. International Conference on System Sciences* - 30, Kihei, Maui, Hawaii, January 7-10, 1997.

- Y. V. Makarov, Z. Y. Dong and D. J. Hill, "A General Method for Small Signal Stability Analysis", *Proc. Power Industry Computer Applications Conference PICA'97*, Columbus, Ohio, USA, May 11-16, 1997, pp.280–286.

- Y. V. Makarov, Z. Y. Dong, D. J. Hill, D. H. Popovic, and Q. Wu, "On Provision of Steady-State Voltage Security", *Proc. International Conference on Advances in Power System Control, Operation and Management APSCOM'97*, Wanchai, Hong Kong, November 11-14, 1997, Vol.1. pp.248–253.

- Z. Y. Dong, Y. V. Makarov and D. J. Hill, "Genetic Algorithms in Power System Small Signal Stability Analysis", *Proc. International Conference on Advances in Power System Control, Operation and Management APSCOM'97*, Wanchai, Hong Kong, November 11-14, 1997, Vol.1. pp. 342 - 347.

- Z. Y. Dong, Y .V. Makarov and D. J. Hill, "Genetic Algorithm Application in Power System Small Signal Stability Analysis of Power System with FACTS Devices", submitted to *the Australian Universities Power Engineering Conference AUPEC'97*, September 29 - October 1, 1997, UNSW, Australia.

- Z. Y. Dong, D. J. Hill and Y. V. Makarov, "Power System VAR Planning using Improved Genetic Algorithm", Proc. *Workshop on Emerging Issues and Methods in The Restructuring of the electric Power Industry.* University of Western Australia, Perth, Western Australia, 20-22 July, 1998.

- Y. V. Makarov, D. J. Hill and Z. Y. Dong, "Exploring the Power System Load Flow Feasibility Boundaries in the Parameter Space" *Proc. The 13th Power Systems Computation Conference: PSCC'99*, Trondheim, Norway, June 28 - July 2, 1999. [to appear]

- Z. Y. Dong, D. J. Hill and Y. V. Makarov, "Advanced Reactive Power Planning by a Genetic Algorithm", *Proc. The 13th Power Systems Computation Conference: PSCC'99*, Trondheim, Norway, June 28 - July 2, 1999. [to appear]

- Z. Y. Dong, Y. Wang, D. J. Hill and Y. V. Makarov, "Voltage Stability Enhancement by Reactive Power Control Using a Genetic Algorithm", submitted to *The International Power Engineering Conference IPEC'99*, Singapore, 24-26 May 1999.

- W. Q. Liu, Z. Y. Dong, C. S. Zhang and D. J. Hill, "Minimum Order Stable Linear Predictor Design via Genetic Algorithm Approach", submitted to *International Journal of Signal Processing*.